Charge exchange in ion-atom collusions relevant to fusion plasma diagnostics

Peter George Davies

Charge Exchange in Ion-Atom Collisions Relevant to Fusion Plasma Diagnostics

by

Peter George Davies M.Sc

A thesis submitted to the University of Durham in candidature for the degree of Doctor of Philosophy

January 1998

Abstract

Total charge exchange and excitation cross-sections are presented for collisions between He^{2+} ions and helium atoms, the laboratory frame collision energy being in the range 16-800keV. Cross-sections from the helium ground state and the $He(1s2s^1S)$ and $He(1s2s^3S)$ metastable states are calculated.

The calculations were performed using the semiclassical impact parameter model where wave-functions are expressed as an expansion of two-electron atomic basis states. Transfer channels included plane-wave translation factors.

The transition $He^+(n = 4) \longrightarrow He^+(n = 3)$ results in the emission of visible light (468.5nm) which is observed in the JET fusion device. Helium beam injection into the JET device introduces some of the atoms in initially excited states. Even a small fraction of metastable helium effects the observed 468.5nm spectrum significantly because of the very large charge exchange cross-sections. Accurate charge exchange cross-sections to the $He^+(n = 4)$ states are required to analyse the spectroscopic data used in the diagnosis of the plasma. The cross-sections produced are therefore also presented in a form suitable for direct inclusion into the plasma analysis database.

Where possible the current results are compared to previous calculations. Total charge exchange cross-sections from the $He(1s2s^1S)$ state are in good agreement with the previous one-electron calculation. Charge exchange cross-sections from the triplet state are found to differ with those from the singlet.

The results are discussed in the context of their usefulness in the diagnosis of fusion plasmas. Suggestions for further work are made.

Acknowledgements

I would like to thank my supervisor, Prof. D.R. Flower for all his help and encouragement during the work carried out for this thesis. I am also indebted to Dr. Henk Slim and Dr. Lydia Heck for their time and assistance.

I would also like to thank Dr. P.R. Thomas, Dr. M.G. von Hellermann and Prof. H.P. Summers for awarding me a CASE studentship and for their hospitality while I was at JET Joint Undertaking.

I would like to thank my many research student colleagues; Chris Caron, Hilary Davies, Henry Day, Brian Jackson, Andrew Fearnside, Emine Mese, Alex Ng and Richard Whitehead for their friendship during my time at Durham. Extra thanks also go to my very good friends, bridge partners and drinking companions; Jason Wilde and Dr. Henry '*the hog*' Day.

I would like to acknowledge the financial support of the Engineering and Physical Sciences Research Council (EPSRC) and of JET Joint Undertaking through order number JP5/11832.

Finally, I express my greatest gratitude to Joanne Kennedy, my best friend and partner for her love, support and patience throughout.

'An old rule of thumb among US fusion researchers holds that the funding for the field almost always parallels the average price of oil, delayed by about a year' [2]

Declaration

I declare that the work contained in this thesis has not previously been submitted for a degree, either at this university or at any other. All the work presented herein was conducted by the author, unless explicitly stated otherwise.

Peter Davies, January 1998

Contents

Acknowledgments i

Declaration iii

1 Introduction 1

1.1 Ion-Atom Collisions 1

1.1.1 Cross-Sections 2

1.1.2 Classical Scattering 3

1.1.3 Atomic Units 4

1.1.4 Collision Energy Regimes 4

1.2 Atomic Data and Fusion 6

1.3 The He^{2+} – He Collision System 7

2 The Semiclassical Close-Coupling Method 9

2.1 Introduction 9

2.1.1 Approximations 11

2.1.2 Co-ordinate Systems 11

2.1.3 Real Spherical Harmonics 13

2.1.4 Electronic Translation Factors 14

2.2 Types of Basis Functions 15

2.2.1 Slater Basis Functions 15

2.2.2 Sturmian Basis Functions 16

2.2.3 Gaussian Basis Functions 17

2.3 Two-electron Wave-functions 17

2.3.1 Introduction 17

2.3.2 Diagonalizing a Two-Electron Basis 18

2.3.3 Choice of One-Electron Functions for Diagonalization . . . 21
2.4 Calculation of Matrix Elements . . . 23
2.4.1 Overview . . . 23
2.4.2 Charge Exchange Matrix Elements . . . 26
2.4.3 Prolate Spheroidal Co-ordinates . . . 26
2.4.4 One-Electron Exchange . . . 27
2.4.5 Two-Electron Exchange Matrix Elements . . . 30
2.4.6 Electron-Electron Repulsion Exchange Integrals . . . 31
2.5 Choosing an atomic basis set . . . 35

3 Computational Method **38**
3.1 Parallelization . . . 38
3.1.1 Introduction . . . 38
3.1.2 General Parallel Concepts . . . 39
3.1.3 Parallel Virtual Machine . . . 41
3.1.4 Close-Coupling Code Parallelization . . . 42
3.2 Numerical Evaluation of Exchange Integrals . . . 44
3.3 Matrix Element Interpolation . . . 45
3.3.1 Chebyshev Interpolation . . . 46
3.4 Propagation of Occupation Amplitudes . . . 47
3.5 The Integration of Final Occupation Amplitudes . . . 48
3.5.1 The Gill-Miller Algorithm . . . 48

4 Charge Transfer as a Fusion Diagnostic **50**
4.1 Introduction . . . 50
4.1.1 Thermonuclear Fusion . . . 50
4.1.2 Plasmas . . . 52
4.1.3 Methods of Plasma Confinement . . . 55
4.1.4 Lawson Criterion . . . 56
4.1.5 Ignition . . . 57
4.1.6 Plasma Heating . . . 57
4.2 JET Joint Undertaking . . . 58
4.2.1 Tokamak Architecture . . . 58

4.2.2 The Divertor Region 60
4.2.3 ITER 62
4.3 Plasma Diagnostics 62
4.3.1 Overview 62
4.3.2 Neutral Beam Injection 65
4.3.3 The ADAS Database 71
4.4 Concluding Remarks 72

5 Results and Discussion **74**
5.1 Introduction 74
5.2 Charge-Transfer from $He(1s1s^1S)$ to H^+ 75
5.3 Charge-Transfer in the He^{2+} – He System 77
5.3.1 Introduction 77
5.3.2 Basis Functions 77
5.3.3 Matrix Elements 80
5.3.4 Convergence of Cross-Sections 87
5.3.5 Charge-Transfer from $He(1s1s^1S)$ to He^{2+} 90
5.3.6 Occupation Amplitudes 94
5.3.7 Charge-Transfer from the Singlet-State: $He(1s2s^1S)$ 97
5.3.8 Charge-Transfer from the Triplet-State $He(1s2s^3S)$ 100
5.4 468.5nm Emission 102

6 Conclusion **105**

A Results in ADF01 format **108**
A.1 ADF01 files for the ADAS Database 108
A.1.1 ADF01 File for Transfer from $He(1s2s^1S)$ 109
A.1.2 ADF01 File for transfer from $He(1s2s^3S)$ 110

Index **111**

Bibliography **114**

Chapter 1

Introduction

1.1 Ion-Atom Collisions

When an ion and an atom collide various processes can take place. Consider a system involving only one electron in which a bare projectile nucleus B^{Z_B+} is in collision with the target $(A^{Z_A+} + e^-)$. What follows is an outline of the relevant electron processes.

(i)	$B^{Z_B+} + (A^{Z_A+} + e^-) \longrightarrow B^{Z_B+} + (A^{Z_A+} + e^-)$	elastic collision
(ii)	$B^{Z_B+} + (A^{Z_A+} + e^-) \longrightarrow B^{Z_B+} + (A^{Z_A+} + e^-)^*$	direct excitation
(iii)	$B^{Z_B+} + (A^{Z_A+} + e^-) \longrightarrow (B^{Z_B+} + e^-) + A^{Z_A+}$	capture
(iv)	$B^{Z_B+} + (A^{Z_A+} + e^-) \longrightarrow B^{Z_B+} + A^{Z_A+} + e^-$	ionization

Process (i) is an elastic process whereas all the others are inelastic. Inelastic processes involve an exchange between kinetic and internal energies. In process (iii) the electron may be captured into the ground or an excited state of the resulting ion. These capture processes are also known as *charge exchange* or as *rearrangement collisions.*

If both nuclei are the same $(A = B)$ then the system is said to be symmetric. In symmetric systems there are always processes which have initial and final states with the same internal energy. These processes are said to be *resonant* e.g.

$$\mathrm{H}^+ + \mathrm{H(1s)} \longrightarrow \mathrm{H(1s)} + \mathrm{H}^+ \tag{1.1}$$

In non-symmetric systems there may exist some (accidental) resonances e.g.

$$He^{2+} + H(1s) \longrightarrow He^{+}(2s) + H^{+} \qquad (1.2)$$

When more than one electron is involved in an ion-atom collision various combinations of the processes outlined above can occur e.g. transfer-excitation, multiple transfer etc.

The type and rate of occurence of these processes depends on various factors: projectile/target charge, collision energy, initial state of the electron and the distance of closest approach of the nuclei. The effect of the collision energy is discussed in section 1.1.4.

1.1.1 Cross-Sections

Cross-Sections are used as a measure of the likelihood of an event in atomic collisions. A cross-section is defined as the number of scattering events per scatterer per unit flux of the incident particle per unit time. The flux of the incident particles is defined as the number of particles passing through a unit area perpendicular to the direction of the beam per unit time. From this definition it is clear that cross-sections have the dimensions of area. Equation (1.3) defines the rate N_C of production of C from the impact of A (with flux $\mathcal{N}_A$) on n_B target B atoms in terms of the cross-section (σ).

$$N_C(s^{-1}) = \mathcal{N}_A(s^{-1}m^{-2}) \times n_B \times \sigma_{[A+B\rightarrow C]}(m^2) \qquad (1.3)$$

It is possible to define a differential cross-section as the cross-section for an event in a particular scattering direction. The total cross-section is the differential cross-section integrated over all scattering angles (1.4).

$$\sigma_{tot} = \int_0^{2\pi} \int_0^{\pi} \left[\frac{d\sigma}{d\Omega}(\theta,\phi)\right] \sin(\theta) d\theta d\phi \qquad (1.4)$$

1.1.2 Classical Scattering

For an atomic collision event to be represented adequately by a classical approximation the wavelength associated with each of the particles must be suitably localized so that they can be treated as classical. The size of this wave-packet must be significantly smaller than the interaction region. It must also be the case that the uncertainty in the angle of scattering is very small compared to the actual angle of scattering.

Rutherford interpreted the results from experiments on the collisions of alpha-particles with atoms using equation (1.5). He was able to conclude that atoms contained a very small positively charged centre: the nucleus. The effect of the electrons in these experiments within the atom can be neglected because their mass is insignificant compared to that of the positively charged nuclei and alpha-particles. The equation given here is for the differential cross-section in the collision between any two positive charges.

$$\frac{d\sigma}{d\Omega} = \frac{(Z_A Z_B)^2}{(4\pi\epsilon_0)^2} \frac{e^2}{4\mu^2 v^4 \sin^4(\frac{1}{2}\theta)} \tag{1.5}$$

Here μ is the reduced mass given by equation (1.6), v is the initial velocity and θ is the angle of scattering. The values Z_A and Z_B are the charges of the two particles in atomic units. Atomic units will be used throughout unless otherwise stated and are defined in the following section.

$$\mu = \frac{M_A M_B}{M_A + M_B} \tag{1.6}$$

It is a peculiar feature of the Coulomb potential that exactly the same result is obtained for the differential cross-section when a full quantum mechanical treatment is used.

1.1.3 Atomic Units

Atomic units are defined by assigning $e = m = \hbar = 1$, where e is the charge of an electron, m is its rest-mass and $\hbar$ is Planck's constant divided by 2π. These quantities are given below in standard units, along with the atomic unit of length a_0 (the Bohr radius).

$$\begin{aligned} e &= 1.602 \times 10^{-19}\text{C} \\ m &= 9.110 \times 10^{-31}\text{kg} \\ \hbar &= 1.055 \times 10^{-34}\text{Js} \\ a_0 &= 5.292 \times 10^{-11}\text{m} \end{aligned}$$

1.1.4 Collision Energy Regimes

The outcome of an ion-atom collision is dependent on, among other things, the collision energy. The collision energy may be roughly divided into three regimes.

The types of processes expected for each regime are discussed in the following sections. A brief description of the methods used to model the ion-atom collisions is also given.

High Energy

In this regime the projectile velocity is much larger than the orbital velocity associated with the active electrons ($v_{coll} \gg v_e$). It is possible to calculate excitation cross-sections using the first Born approximation at these energies. The calculation of charge exchange cross-sections would require at least a second order approximation. Charge exchange cross-sections are usually very small at these energies and the the use of the Born approximation would be inaccurate.

At high collision energy various classical models may be valid. A full classical model assumes that both the nuclei and electron are point particles, for example the classical trajectory Monte Carlo method[7]. A semiclassical model assumes

the motion of the nuclei is classical whereas the electrons are treated quantum mechanically.

Relativistic effects

The need to include relativistic effects when describing ion-atom collisions can come about in two ways. If the ionic charge is large then a bound electron may have an associated orbital velocity near to the speed of light. Also relativistic kinematics must be taken into account when the velocity of the incoming projectile approaches the speed of light. If an electron is attached to this projectile then it must also be treated relativistically. Any wave-function representing a relativistic electron must satisfy the Dirac equation[6].

Intermediate Energy

This is where the projectile velocity is approximately the same as the orbital velocity associated with the active electrons ($v_{coll} \sim v_e$). At these energies, direct and rearrangement processes usually have equal importance. The *semiclassical close-coupling method* is valid across a large range of energies but is particularly useful in this difficult regime. The semiclassical close-coupling method was used for the calculations performed for this thesis; the method will be discussed fully in chapter 2.

Low Energy

In this regime the projectile velocity is much smaller than the orbital velocity associated with the active electrons ($v_{coll} \ll v_e$). A natural way to describe such a system is to treat it as a molecule in which the internuclear separation is varying very slowly. Since the changes in electronic energy during the collision are comparable to the nuclear kinetic energy, the nuclear motion is effected by the motion of the electrons. The *perturbed stationary state model*[38] is used.

1.2 Atomic Data and Fusion

Theoretically calculated cross-sections are needed in various areas of physics. They are used both as a check on experimentally measured values and when experiment is not possible. Plasma physics is perhaps the most demanding area, because of the numerous ion-atom and electronic processes that occur in a plasma.

Fusion plasmas consist mainly of fully ionized atoms and electrons at very high temperatures. Measurements cannot be performed on such plasmas using material probes. The edge region of a fusion plasma is cool enough for some electronic bound states to exist. Spectroscopic analysis of line emissions from transitions between such states is possible. The characteristic linewidths and shifts give insight into the plasma properties. The hot central region of a fusion plasma is not so easily diagnosed since the degree of ionization is very high. The continuous spectrum of bremsstrahlung radiation yields electron properties. Ionic behaviour is of greater interest since it is the ions that we would like to fuse. The location, temperature and density of fuel and impurity ionic species is desired.

Neutral beam injection is a method used to probe the central region of a plasma. The beam of neutral atoms can pass into the magnetically confined plasma since it is undeflected by the fields. As it enters the plasma it loses its electrons through ionization or charge exchange with other ions. Electrons may be exchanged to excited states of plasma ions in the central region. Any subsequent radiative decay can be measured spectroscopically. Fusion plasma diagnostics are covered fully in chapter 4.

Data are needed for all relevant atomic species in the plasma to analyse these spectroscopic measurements. The relevant species include mainly the light elements; hydrogen, deuterium, tritium, helium, beryllium, carbon, nitrogen and oxygen. Deuterium and tritium are the fuels, helium is the ash impurity resulting from the burning of the fuels and the remainder are impurities, produced by sput-

tering or from the incompleteness of the vacuum when the chamber is pumped down.

Helium is of special interest because its presence would eventually hinder further fusion in a running reactor; helium ash needs to be exhausted. Helium is injected into the JET[1] device at present. This is because tritium is only used sparingly, and fusion reactions are infrequent. The He^{2+} – He collision system is of particular interest. Thermalized helium nuclei are in collision with the atoms of the neutral beam. Charge exchange leads to population of the state $He^{+}(n = 4)$, which subsequently decays radiatively to $He^{+}(n = 3)$ with the emission of blue visible light (468.5nm). The helium beam consists of some atoms in metastable states, from which electron capture into the $He^{+}(n = 4)$ level is almost resonant[12]. Accurate theoretical cross-sections are needed if the spectrum around 468.5nm is to be analysed correctly.

1.3 The He^{2+} – He Collision System

The He^{2+} – He collision system has been studied a great deal as it is the obvious first choice of an ion-atom collision involving two electrons. Unfortunately the symmetry of the system leads to complications. Folkerts *et al*[11] noted that one electron transfer below a laboratory frame energy of about 40keV resulted in either the projectile or the target ending in an excited state with approximately the same frequency. It was also noted that below 40keV resonant two-electron capture into the ground state of the projectile was the most significant process.

The system of single and double electron transfer in this system was studied by Gramlich *et al*[23] using Gaussian orbitals at low collision energies (8-300keV). More recent results from Fritsch[16] show good agreement. At collision energies above 400keV single and double ionization processes become more significant in

[1]**J**oint **E**uropean **T**orus: The European fusion device based near Abingdon, Oxfordshire

this system. These have been studied using the independent event model by Marshall *et al*[37].

Almost all previous $He^{2+} - He$ studies assumes the helium atom to be initially in the ground state. Only Fritsch[16] has addressed charge transfer from the state $He(1s2s^1S)$. He used a model where only one electron is assumed to be active. The other electron is represented by modifying the target nuclear potential. Fritsch showed that the charge transfer cross-sections are much larger from the initially excited state. At a collision energy of 40keV, the transfer cross-section is 100 times that from the ground state and the difference increases at lower energies. Also the proportion of capture into the excited $He^+(n = 4)$ states is larger because of the similarity in initial and final binding energies.

In this thesis a two-electron model is used to verify the one-electron calculations of Fritsch for the $He^{2+} - He(1s2s^1S)$ collision system. It is also desirable to study charge transfer from the longer lived $He(1s2s^3S)$ state, for which there are no previous calculations. The results are presented and discussed in chapter 5.

Chapter 2

The Semiclassical Close-Coupling Method

2.1 Introduction

The total wave-function of an ion-atom collision system must be known in order to model all electronic processes that occur. This wave-function should be known at all times during the collision so that the initial, final and any possible intermediate states are represented. The total time dependent wave-function can be written as an expansion (2.1) of the product of carefully chosen basis functions and the so called *time dependent occupation amplitudes*[17].

$$\Psi = \sum_k a_k(t)\psi_k(\vec{r},t) \tag{2.1}$$

The choice of the basis functions $\psi_k(\vec{r},t)$ is both system and collision energy dependent. The choice of basis will be discussed in section 2.5. If more than one electron is involved then the total wave-function Ψ must represent all electrons and be properly symmetrized. Only one-electron systems will be considered at present in order to keep notation to a minimum. The extensions needed for two-electron systems are covered in section 2.3.

Once a suitably large basis is chosen, one requires that each of the basis func-

tions satisfy the time dependent Schrödinger equation within the basis i.e.

$$\left\langle \psi_k \left| \hat{H} - i\frac{\partial}{\partial t} \right| \Psi \right\rangle = 0 \qquad \text{for all } k \tag{2.2}$$

Substitution of (2.1) into (2.2) yields

$$i\sum_{k=1}^{N} O_{jk}\dot{a}_k = \sum_{k=1}^{N} H_{jk}a_k \qquad \text{for all } j \tag{2.3}$$

where O_{jk} are the elements of the two-dimensional overlap matrix $\mathbf{O}$ and H_{jk} are the elements of the coupling matrix $\mathbf{H}$. The vector $\mathbf{a}$ has a_k as its elements. The methods used for the calculation of these matrix elements are outlined in section 2.4.

$$\begin{aligned} O_{jk} &= \langle \psi_j \mid \psi_k \rangle \\ H_{jk} &= \left\langle \psi_j \left| \hat{H} - i\frac{\partial}{\partial t} \right| \psi_k \right\rangle \end{aligned} \tag{2.4}$$

Once the matrix elements are known it is simply a matter of integrating the occupation amplitudes with respect to time, from time $t = -\infty$ to $t = +\infty$.

$$i\dot{\mathbf{a}} = \left[\mathbf{O}^{-1}\mathbf{H}\right]\mathbf{a} \tag{2.5}$$

$$a_k(-\infty) = \delta_{ik} \qquad \text{with } i \text{ the initial channel} \tag{2.6}$$

This is an initial value problem for a system of coupled first-order differential equations. The method used for the solution of this problem will be discussed in section 3.4 of chapter 3.

The cross-section for a final state f is calculated by integrating the square of the magnitude of the associated occupation amplitude a_f evaluated at time $t = +\infty$ over the impact parameter b.

$$\sigma_f = \int_0^{\infty} 2\pi b \left| a_f(+\infty) \right|^2 db \tag{2.7}$$

If no further approximations are made it can be shown that both unitarity (2.8) and detailed balance are respected (2.9)[26].

$$\frac{\partial}{\partial t}\langle \Psi \mid \Psi \rangle = 0 \tag{2.8}$$

$$a_f(i;+\infty) = a_i(f;+\infty) \tag{2.9}$$

In equation (2.9), $a_f(i;+\infty)$ denotes the amplitude observed for the occupation of a final state f after the collision, following initial occupation of state i.

2.1.1 Approximations

To demand that the associated de Broglie wavelengths of the nuclei are much smaller than atomic dimensions requires the collision energy to be greater than about 1eV (2.10). When this is the case, the nuclear motion during a collision may be considered to be classical.

$$\begin{aligned} \lambda \simeq \frac{h}{p} &\lesssim \mathrm{a_0} \\ \mathrm{E_{collision}} &\gtrsim \mathrm{1eV} \end{aligned} \tag{2.10}$$

Internal energy changes due to electronic excitation or rearrangement are of the order of a few electron volts. If the kinetic energy of the incoming projectile nucleus is significantly larger than any internal energy changes, the nuclear motion may be considered to be uncoupled from the electronic motion. This is usually the case when the projectile energy is greater than about 100eV.

If the velocity of the projectile is large enough so that its trajectory is undeflected by either the electrons or the target nucleus then the impact parameter approximation holds[40]. At very low energies it may be appropriate to use curved trajectories[14] when the internuclear potential has a significant effect on the projectile motion.

2.1.2 Co-ordinate Systems

In the laboratory frame of an ion-atom collision the target nucleus is at rest while the projectile moves along a straight line trajectory at a speed v. It is useful to employ a centre of mass co-ordinate system to describe the collision; see figure 2.1. The projectile **B** is at a position $\vec{R}(b,t)$ with respect to the target nucleus **A**

and the electron is at a position $\vec{r}$ with respect to the origin. The parameter q determines the position of the origin along the internuclear axis and is defined in equations (2.11).

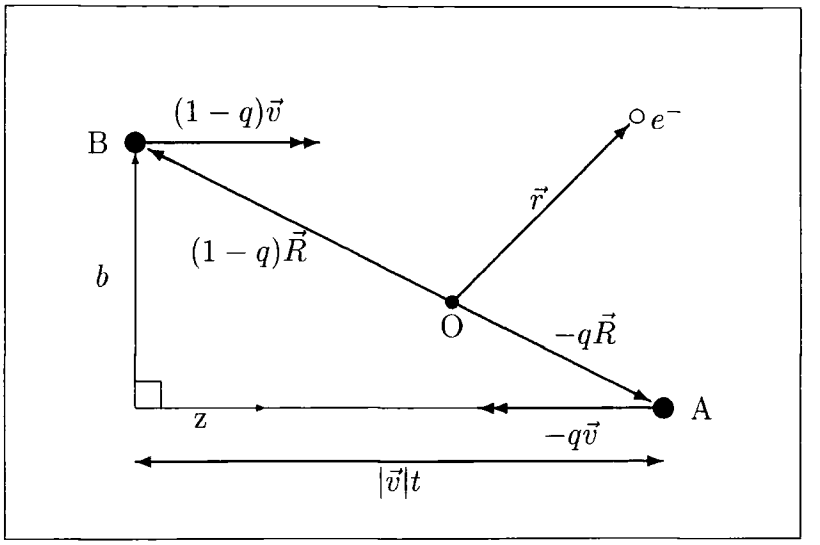

Figure 2.1: Collision co-ordinate system

In the centre of mass co-ordinates the two nuclei move parallel to the z-axis in opposite directions. The projectile and target velocities are given in equations (2.12). The impact parameter (b) lies along the x-axis and is the distance of closest approach, which is reached at time $t = 0$.

$$q = \frac{M_B}{M_A + M_B} \qquad 0 \leq q \leq 1 \tag{2.11}$$

$$\vec{v_A} = (1-q)\vec{v} \qquad \vec{v_B} = -q\vec{v} \tag{2.12}$$

The vectors $\vec{r_A}$ and $\vec{r_B}$ give the position of the electron relative to each centre. The relationships between $\vec{r_A}$, $\vec{r_B}$, $\vec{R}$, $\vec{r}$ and t are given below.

$$\vec{r_A} = \vec{r} + q\vec{R} \tag{2.13}$$

$$\vec{r_B} = \vec{r} - (1-q)\vec{R} \tag{2.14}$$

$$\vec{R} = |\vec{v}|t\hat{z} + b\hat{b} \tag{2.15}$$

In a homonuclear system **O** lies at the mid-point of **AB** and $q = \frac{1}{2}$. The space-fixed quantization axis lies along the z-axis as in figure 2.1. The body-fixed quantization axis lies along the line connecting the nuclei, in the direction of **A** from **B**. If space-fixed co-ordinates are defined as $\vec{r}(x, y, z)$ and the body-fixed co-ordinates are defined as $\vec{r'}(x', y', z')$ the relationships between the two frames are given in equations (2.16), where β is the angle between the space-fixed z-axis and the internuclear axis.

$$\begin{aligned} x' &= x\cos\beta + z\sin\beta \\ y' &= y \\ z' &= z\cos\beta - x\sin\beta \end{aligned} \tag{2.16}$$

2.1.3 Real Spherical Harmonics

The use of real spherical harmonics greatly simplifies much of the algebra used in the calculation of matrix elements. They are defined as follows:

$$\overline{Y}_{\ell m} = N_m\left(Y_{\ell m} + Y^*_{\ell m}\right) \tag{2.17}$$

Where N_m is a normalization factor given by

$$N_m = \begin{cases} \frac{1}{2} & m = 0 \\ \frac{1}{\sqrt{2}} & m \neq 0 \end{cases} \tag{2.18}$$

The use of real spherical harmonics is valid because of the choice of quantization axis and the symmetry of the collision system. Here the spherical harmonics are in the body-fixed frame. The body-fixed quantization axis lies in the collision plane, along the internuclear axis. The collision system is symmetric under reflection through this plane and rotation about the internuclear axis (or equivalently the quantization axis). No physics is lost by projecting spherical harmonics onto the real axis. The imaginary part of a spherical harmonic only distinguishes the space at one side of the collision plane from the other.

The real spherical harmonics can be expressed in terms of normalised associated Legendre polynomials[6].

$$\overline{Y}_{\ell m} = \frac{2}{\sqrt{2\pi}} N_m (-1)^m P_\ell^m(\cos\theta)\cos(m\phi) \tag{2.19}$$

Matrix elements evaluated in the body-fixed frame may be transformed into space-fixed co-ordinates. The spherical harmonics are transformed using rotation matrices[39]. These rotation matrices are calculated using the identities (2.16) and representations of the spherical harmonics in terms of cartesian co-ordinates, using:

$$\begin{aligned} \cos\theta &= \frac{z}{r} \\ \sin\theta\sin\phi &= \frac{y}{r} \\ \sin\theta\cos\phi &= \frac{x}{r} \end{aligned} \tag{2.20}$$

2.1.4 Electronic Translation Factors

If an electron is transferred from the target nucleus onto a moving projectile the kinetic energy and linear momentum of the electron changes. These changes must appear in the wave-function if the travelling state is to be represented properly. In the centre of mass co-ordinate system both nuclei are in motion and therefore electronic states on both nuclei must include these so called *translation factors*[4].

$$\begin{aligned} \phi_i^A(\vec{r},t) &= \chi_i^A(\vec{r_A}) exp\left\{-iq\vec{v}.\vec{r} - i\int\left[\epsilon_i + \frac{1}{2}q^2v^2\right]dt\right\} \\ \phi_j^B(\vec{r},t) &= \chi_j^B(\vec{r_B}) exp\left\{i(1-q)\vec{v}.\vec{r} - i\int\left[\epsilon_j + \frac{1}{2}(1-q)^2v^2\right]dt\right\} \end{aligned} \tag{2.21}$$

The vectors $\vec{v}$, $\vec{r}$, $\vec{r_A}$ and $\vec{r_B}$ and parameter q were defined in section 2.1.2. The exponential terms in equations (2.21) are the translation factors and these modify the stationary states $\chi_i^A(\vec{r_A})$ and $\chi_j^B(\vec{r_B})$ centred on the target and projectile respectively. The motion of the nuclei relative to each other has an effect on the electronic wave-functions, even at infinite separation.

As can be seen in equations (2.22) the total energy of the travelling state is a sum of internal energy and kinetic energy.

$$\begin{aligned} i\frac{\partial}{\partial t}\phi_i^A(\vec{r},t) &= \left\{\epsilon_i + \frac{1}{2}q^2v^2\right\}\phi_i^A(\vec{r},t) \\ i\frac{\partial}{\partial t}\phi_j^B(\vec{r},t) &= \left\{\epsilon_j + \frac{1}{2}(1-q)^2v^2\right\}\phi_j^B(\vec{r},t) \end{aligned} \tag{2.22}$$

2.2 Types of Basis Functions

The types of functions used to represent the electrons in a collision event are determined by what is expected to happen.

When the nuclear motion is slow compared to the associated speed of the electrons, the electrons have time to sample the potentials of both nuclei before a significant change in nuclear separation. Here the adiabatic approximation is valid. A quasi-molecule is formed and the use of molecular states to represent the system is appropriate. The eigenfunctions are calculated with the internuclear separation (R) fixed. R then enters the equations as a parameter.

If the speed of the nuclei is greater than (or comparable to) that associated with the electrons, the electrons do not have time to adjust adiabatically to the nuclear motion. In this case a better representation would be to use atomic basis states. The work in this thesis is concerned with the use of atomic basis states in ion-atom collision calculations.

There are various methods for representing atomic wave-functions.

2.2.1 Slater Basis Functions

A general Slater function is given in equation (2.23). The constant C ensures radial normalization (2.24) and is given in equation (2.25). The orbital exponent (ξ) is positive and k is a non-negative integer.

$$S_{k\xi}(r) = Cr^k e^{-\xi r} \tag{2.23}$$

$$\int_0^\infty S_{k\xi}(r) S_{k\xi}(r) r^2 dr = 1 \tag{2.24}$$

$$C = \frac{(2\xi)^{k+1\frac{1}{2}}}{\sqrt{(2(k+1))!}} \tag{2.25}$$

By defining the orbital exponent as in equation (2.26), where Z is the nuclear charge, and imposing the conditions in equations (2.27), small sets of Slater functions can be used to represent the radial part of a hydrogenic wave-function exactly.

$$\xi = \frac{Z}{n} \tag{2.26}$$

$$\begin{aligned} n &= 1, 2, 3... \\ 0 \leq k &\leq n-1 \end{aligned} \tag{2.27}$$

Although the Slater functions are not orthogonal it is easy to construct an orthogonal set.

2.2.2 Sturmian Basis Functions

Gallaher and Wilets used Sturmian basis functions for their calculations of proton-hydrogen scattering[18]. The basis states they used are given in equations (2.28) and (2.29).

$$\Phi_{n\ell m}^{A,B} = \psi_{n\ell m}(\vec{r}_{A,B}) \exp\left[\mp\frac{1}{2} ivz - i(\epsilon_{n\ell m} + \frac{1}{8}v^2)t\right] \tag{2.28}$$

where

$$\psi_{n\ell m}(\vec{r}_i) = \left[\frac{1}{r_i} S_{n\ell}(r_i)\right] Y_{\ell m}(\theta_i, \phi_i) \tag{2.29}$$

The Sturmian functions $S_{n\ell}(r_i)$ satisfy equation (2.30). In this equation the energy E_ℓ is a parameter and the effective charge $\alpha_{n\ell}$ is the eigenvalue.

$$\left(-\frac{1}{2}\frac{d^2}{dr^2} + \frac{\ell(\ell+1)}{2r^2} - \frac{\alpha_{n\ell}}{r}\right) S_{n\ell}(r) = E_\ell S_{n\ell}(r) \tag{2.30}$$

The simplest choice for the energy parameter is $E_\ell = -\frac{1}{2}$; the ground state of the target hydrogen atom. The functions $\psi_{n\ell m}(\vec{r})$ form an infinite and complete set. Unlike hydrogenic functions there is no continuum. Sturmian functions are discrete.

2.2.3 Gaussian Basis Functions

Gaussian functions are of the form given in equation (2.31) where α is real and positive; ℓ, m and n are non-negative integers and C is a normalization constant. It is possible to approximate the angular and radial part of hydrogenic wave-functions as linear combinations of these functions.

$$G(\alpha, \ell, m, n; r) = C_\alpha x^\ell y^m z^n e^{-\alpha r^2} \tag{2.31}$$

Gaussian functions are useful when considering multi-centre expansions. Gaussian functions are also useful for many-electron systems. The product of two Gaussians centred on different nuclei is also a Gaussian, centred at some intermediate point. Boys[5] showed that this fact could be used to evaluate stationary molecular integrals analytically. It has also been shown[10] that this method can be extended to two-centre integrals with plane-wave translation factors. Analytic evaluation of two-centre matrix elements is possible when the atomic orbitals are represented by Gaussian functions. Multiple numerical integrals are needed when a Slater basis is used. The disadvantage of Gaussians is that several functions are needed to represent a physical atomic state.

2.3 Two-electron Wave-functions

2.3.1 Introduction

The electrons in a many electron atom are indistinguishable. As fermions the wave-function used to represent them must be antisymmetric with respect to an exchange of both spatial and spin co-ordinates[6].

2.3.2 Diagonalizing a Two-Electron Basis

The two-electron wave-functions (Ψ_i) satisfy Schrödinger's equation (2.32) where the Hamiltonian is given by (2.33) and E_i are the energy levels of the two-electron atom.

$$\hat{\mathbf{H}}\Psi_i(\vec{r_1},\vec{r_2}) = E_i\Psi_i(\vec{r_1},\vec{r_2}) \tag{2.32}$$

$$\hat{\mathbf{H}} = -\frac{1}{2}\nabla_{r_1}^2 - \frac{1}{2}\nabla_{r_2}^2 - \frac{Z}{r_1} - \frac{Z}{r_2} + \frac{1}{|\vec{r_1}-\vec{r_2}|} \tag{2.33}$$

The two-electron wave-function may be represented by a linear combination of properly symmetrized pairs of wave-functions (2.34).

$$\Psi_i(\vec{r_1},\vec{r_2}) = \sum_{j=1}^{N} C_{ij}\left[\phi_{j_1}(\vec{r_1})\phi_{j_2}(\vec{r_2}) \pm \phi_{j_1}(\vec{r_2})\phi_{j_2}(\vec{r_1})\right] \tag{2.34}$$

Although this representation is not exact it is possible to demand that the Hamiltonian is diagonal within the basis i.e.

$$\left\langle \Psi_i(\vec{r_1},\vec{r_2}) \left| \hat{\mathbf{H}} \right| \Psi_j(\vec{r_1},\vec{r_2}) \right\rangle = E_i\delta_{ij} \tag{2.35}$$

The hydrogenic wave-function is a product of a spherical harmonic and a radial expansion. The radial part of equation (2.36) is a Slater type expansion.

$$\phi_i(\vec{r}) = Y_{\ell m}(\Omega)\sum_{j=1}^{N} C_{ij}r^{k_{ij}}exp(-\xi_{ij}r) \tag{2.36}$$

Here Ω is the angular part of the spherical polar co-ordinates. When the symmetric spatial combination is taken in equation (2.34) the antisymmetric spin combination must be taken for net antisymmetry; the state represented is a *singlet* state. An antisymmetric spatial and symmetric spin combination results in a *triplet* state.

The pairs of symmetrized hydrogenic wave-functions are not orthonormal. An orthonormal set needs to be created before the Hamiltonian can be diagonalized on this basis. This orthogonalization may be performed by the method of Schmidt[9].

There are two pairs of symmetrized one-electron wave-functions for both bra and ket in equation (2.35) but only half of the four terms are distinct (by co-ordinate label change); see below.

$$\left\langle \phi_{i_1}(\vec{r_1})\phi_{i_2}(\vec{r_2}) \pm \phi_{i_1}(\vec{r_2})\phi_{i_2}(\vec{r_1}) \left| \hat{\mathbf{H}} \right| \phi_{j_1}(\vec{r_1})\phi_{j_2}(\vec{r_2}) \pm \phi_{j_1}(\vec{r_2})\phi_{j_2}(\vec{r_1}) \right\rangle = 2\mathbf{H}_{ij} \pm 2\mathbf{K}_{ij} \tag{2.37}$$

where

$$\begin{aligned} \mathbf{H}_{ij} &= \left\langle \phi_{i_1}(\vec{r_1})\phi_{i_2}(\vec{r_2}) \left| \hat{\mathbf{H}} \right| \phi_{j_1}(\vec{r_1})\phi_{j_2}(\vec{r_2}) \right\rangle \\ \mathbf{K}_{ij} &= \left\langle \phi_{i_1}(\vec{r_1})\phi_{i_2}(\vec{r_2}) \left| \hat{\mathbf{H}} \right| \phi_{j_1}(\vec{r_2})\phi_{j_2}(\vec{r_1}) \right\rangle \end{aligned} \tag{2.38}$$

With the exception of the electron-electron repulsion term (to be discussed in the next section), the integrations are separable i.e.

$$\begin{aligned} \mathbf{H}_{ij} = & \int \phi_{i_1}(\vec{r_1}) \left[-\frac{1}{2}\nabla_{r_1}^2 - \frac{Z}{r_1} \right] \phi_{j_1}(\vec{r_1}) d\vec{r_1} \int \phi_{i_2}(\vec{r_2})\phi_{j_2}(\vec{r_2}) d\vec{r_2} \\ & + \int \phi_{i_1}(\vec{r_2}) \left[-\frac{1}{2}\nabla_{r_2}^2 - \frac{Z}{r_2} \right] \phi_{j_1}(\vec{r_2}) d\vec{r_2} \int \phi_{i_2}(\vec{r_1})\phi_{j_2}(\vec{r_1}) d\vec{r_1} \\ & + \int \phi_{i_1}(\vec{r_1})\phi_{i_2}(\vec{r_2}) \frac{1}{|\vec{r_1} - \vec{r_2}|} \phi_{j_1}(\vec{r_1})\phi_{j_2}(\vec{r_2}) d\vec{r_1} d\vec{r_2} \end{aligned} \tag{2.39}$$

The integrals of the type (2.40)

$$\int \phi_i(\vec{r}) \left[-\frac{1}{2}\nabla_r^2 - \frac{Z}{r} \right] \phi_j(\vec{r}) d\vec{r} \tag{2.40}$$

may be further separated into radial and angular integrals using the identity

$$\nabla_r^2 = \frac{1}{r^2}\frac{\partial}{\partial r}(r^2 \frac{\partial}{\partial r}) - \frac{1}{r^2}\hat{L}^2 \tag{2.41}$$

where $\hat{L}$ is the angular momentum operator associated with the electron at co-ordinate $\vec{r}$. The position vector $\vec{r}$ is best represented in spherical polar co-ordinates (r, θ, ϕ) since the angular momentum operator has the spherical harmonics as its eigenfunctions.

$$\hat{L}^2 Y_{\ell m}(\theta, \phi) = \ell(\ell + 1) Y_{\ell m}(\theta, \phi) \tag{2.42}$$

The angular part of the separated integral can be evaluated analytically by making use of the orthonormality of spherical harmonics.

$$\int_0^{2\pi} d\phi \int_0^{\pi} sin(\theta) d\theta \{Y^*_{\ell m} Y_{\ell' m'}\} = \delta_{\ell\ell'}\delta_{mm'} \tag{2.43}$$

The Slater-type radial integrations can also be calculated analytically by successive integration by parts.

The Electron-Electron Repulsion Term

Although the electron-electron repulsion matrix element cannot be separated into integrals over each co-ordinate it can be evaluated analytically. The multipole expansion[6] is employed for potentials of this type.

$$\frac{1}{|\vec{r_1} - \vec{r_2}|} = \sum_{L=0}^{\infty} \frac{r_<^L}{r_>^{L+1}} \frac{4\pi}{2L+1} \sum_{M=-L}^{+L} Y^*_{LM}(\theta_1, \phi_1) Y_{LM}(\theta_2, \phi_2) \tag{2.44}$$

Here θ_i and ϕ_i are the spherical polar angles of $\vec{r_i}$; $r_<$ is the smaller and $r_>$ the larger of the magnitudes of the vectors $\vec{r_1}$ and $\vec{r_2}$. Substitution of (2.44) into the last term of equation (2.39) allows the angular part of the integration to be separated out. For each term and for each electron the angular integral is a product of three spherical harmonics, one from the bra, one from the ket and one from the multipole expansion. This integration may be evaluated analytically.

$$\int Y_{\ell_1 m_1} Y_{LM} Y_{\ell_2 m_2} d\Omega = (-1)^M \left[\frac{(2\ell_1+1)(2\ell_2+1)}{4\pi(2L+1)}\right]^{\frac{1}{2}} \langle \ell_1 \ell_2 00 | L0 \rangle \langle \ell_1 \ell_2 m_1 m_2 | LM \rangle \tag{2.45}$$

The latter Clebsch-Gordan coefficient in equation (2.45) is 0 unless the following conditions apply. These conditions limit the multipole expansion to a finite number of terms.

$$|\ell_1 - \ell_2| \leq L \leq \ell_1 + \ell_2 \tag{2.46}$$

$$M = m_1 + m_2 \tag{2.47}$$

The radial integration for each term in the expansion has the form given in equation (2.48).

$$\int_0^\infty \int_0^\infty \frac{r_<^\ell}{r_>^{\ell+1}} f_1(r_1) f_2(r_2) r_1^2 dr_1 r_2^2 dr_2 \tag{2.48}$$

The inner integration is split into 2 ranges, one for the case when $r_1 > r_2$ and one for $r_2 > r_1$.

$$\int_0^\infty \left\{ \frac{1}{r_2^{\ell+1}} \int_0^{r_2} r_1^\ell f_1(r_1) r_1^2 dr_1 + r_2^\ell \int_{r_2}^\infty \frac{1}{r_1^{\ell+1}} f_1(r_1) r_1^2 dr_1 \right\} f_2(r_2) r_2^2 dr_2 \tag{2.49}$$

When the functions are of Slater type this results in a sum over integrals of the type in equation (2.50).

$$\int_0^\infty \int_0^\infty \frac{r_<^k}{r_>^{k+1}} r_1^m r_2^n e^{-ar_1} e^{-br_2} \mathrm{d}r_1 \mathrm{d}r_2 \tag{2.50}$$

These integrals may be evaluated analytically by repeated integration by parts[30].

A large number of basis functions may be needed to form a good representation of a two-electron wave-function. The diagonalization problem may be simplified by dividing the matrix into several smaller matrices; one for each total angular momentum. This is permitted because the angular integrals ensure that wave-functions with different total angular momentum are orthogonal.

2.3.3 Choice of One-Electron Functions for Diagonalization

The choice of the basis functions used to represent a two-electron system must be carefully considered. In the simplest approximation a two-electron system can be approximated by a linear combination of two hydrogenic functions. For example, consider the He($1s2s^1S$) state; the 'inner' electron may be considered to be in the $He^+(1s)$ state and the 'outer' electron in a H(2s) state. The 'outer' electron sees only one unit of charge because in this simple approximation it is assumed that the inner electron screens the nucleus with 100% efficiency. It is possible

to set up models with variable screening factors. In the ground state of helium, He($1s1s^1S$), it is not quite so clear what the screening effect each electron has on the other since they occupy almost identical quantum states (only the electron spins differ). It is possible to calculate the ground state energy for a simple trial function analytically.

The Ground State of Helium

Consider a two-electron trial wave-function (2.51). This function represents a singlet state because it is spatially symmetric. Only the radial part of the wave-function is shown; the angular part is assumed to represent an S-state. The parameter c ensures normalization; the variables a and b are non-zero and positive.

$$\psi = c^2 \left(e^{-ar_1} e^{-br_2} + e^{-ar_2} e^{-br_1} \right) \tag{2.51}$$

It can be shown that to satisfy normality c^2 is given by

$$c^2 = \sqrt{\frac{8(a+b)^4(a^2+2ab+b^2)a^3b^3}{a^6+6a^5b+15a^4b^2+84a^6b^3+15a^2b^4+6ab^5+b^6}} \tag{2.52}$$

Substituting for c^2 into (2.51), equations; (2.39), (2.41), (2.44) and (2.49) can be used to calculate the energy as follows.

$$\begin{aligned}
&\langle\psi|\hat{H}\,|\psi\rangle = \\
&-2(a+b) + \frac{ab(a^5+6a^4b+33a^3b^2+33a^2b^3+6ab^4+b^5)}{a^6+6a^5b+15a^4b^2+84a^3b^3+15a^2b^4+6ab^5+b^6} \\
&+\frac{1}{2}\frac{a^8+6a^7b+16a^6b^2+26a^5b^3+158a^4b^4+26a^3b^5+16a^2b^6+6ab^7+b^8}{a^6+6a^5b+15a^4b^2+84a^3b^3+15a^2b^4+6ab^5+b^6}
\end{aligned} \tag{2.53}$$

The right hand side of equation (2.53) can be minimized with respect to both a and b giving $a = 2.1832$ and $b = 1.1885$ (or vice versa). This yields a ground state energy of -2.876au which is within 1% of the experimental[3] value of -2.903au.

A similar procedure can be performed for the triplet ground state He($1s2s^3S$) using the following trial function.

$$\psi = c^2 \left(e^{-ar_1} e^{-br_2} - e^{-ar_2} e^{-br_1} \right) \tag{2.54}$$

This yields a minimum energy of -2.161au with $a = 1.969$ and $b = 0.321$. This is again within 1% of the experimental energy of -2.175au.

For higher lying states it may be sufficient to assume pairs of hydrogenic functions of the form $He^+(1s)$ paired with $H(n\ell)$. Better representations of the two-electron functions are achieved when several of such trial functions are diagonalized, as was outlined in section 2.3.2.

The problem with bases consisting of hydrogenic states of this type is that the continuum may not be well represented. When a general set of Slater (or other non-hydrogenic) functions is used to define the one-electron basis used in the diagonalization of the two-electron Hamiltonian, some of the resulting eigenenergies lie in the continuum. These discrete *pseudostates* lying in the continuum may be used to represent ionization.

2.4 Calculation of Matrix Elements

2.4.1 Overview

Overlap and coupling matrix elements (2.4) are used to integrate the time dependent occupation amplitudes during a collision event (see section 2.1).

$$i\sum_{k=1}^{N} O_{jk}\dot{a}_k = \sum_{k=1}^{N} H_{jk}a_k \qquad \text{for all } j \tag{2.55}$$

$$\hat{H} = -\frac{1}{2}\nabla_{r_1}^2 - \frac{1}{2}\nabla_{r_2}^2 - \frac{Z_A}{r_1} - \frac{Z_A}{r_2} - \frac{Z_B}{|\vec{R}-\vec{r_1}|} - \frac{Z_B}{|\vec{R}-\vec{r_2}|} + \frac{1}{|\vec{r_1}-\vec{r_2}|} \tag{2.56}$$

Consider a two-electron system where both electrons may be on the target nucleus or one may have been transferred to the projectile. This system is represented by a total of N channels, where M are direct (both on target) and $N - M$ are transfer channels. The overlap and coupling matrices can now each be divided

into four submatrices (2.57)

$$\mathbf{O} = \begin{pmatrix} \mathbf{S} & \mathbf{N} \\ \bar{\mathbf{N}} & \bar{\mathbf{S}} \end{pmatrix} \qquad \underline{\mathbf{H}} = \begin{pmatrix} \mathbf{M} & \mathbf{K} \\ \bar{\mathbf{K}} & \bar{\mathbf{M}} \end{pmatrix} \tag{2.57}$$

The overlap submatrix $\mathbf{S}$ is the unit matrix $\mathbf{I}$ because the two-electron target states are pre-orthonormalised (2.58).

$$S_{jk} = \left\langle \phi_j^{TT} | \phi_k^{TT} \right\rangle = \delta_{jk} \qquad \text{(where } j,k \leq M\text{)} \tag{2.58}$$

The superscript TT indicates that both electrons are attached to the target nucleus. The coupling matrix $\mathbf{M}$ can also be greatly simplified (2.60), where E_j is the eigenenergy of the two-electron state ϕ_j^{TT}.

$$M_{jk} = \left\langle \phi_j^{TT} \middle| \hat{H} \middle| \phi_k^{TT} \right\rangle \qquad \text{(where } j,k \leq M\text{)} \tag{2.59}$$

$$= E_j \delta_{jk} + \left\langle \phi_j^{TT} \middle| -\frac{Z_B}{|\vec{R} - \vec{r_1}|} - \frac{Z_B}{|\vec{R} - \vec{r_2}|} \middle| \phi_k^{TT} \right\rangle \tag{2.60}$$

The matrix elements M_{jk} can be calculated by breaking the problem down into one-electron integrals and representing the potential due to the projectile on each electron as a multipole expansion.

The calculation of the elements of the matrices $\bar{\mathbf{S}}$, $\mathbf{N}$, $\bar{\mathbf{N}}$, $\bar{\mathbf{M}}$, $\mathbf{K}$ and $\bar{\mathbf{K}}$ all involve two-centre integrals. The spatial integrals are shown below and take place over both electron co-ordinates. It is assumed that these integrals take place with the inter-nuclear vector $\vec{R}$ fixed. Here the superscript T_1P_2 indicates that one electron is on the target while the other is on the projectile. The number labels with these superscripts distinguish the two electrons. In order to evaluate the integrals a change to prolate spheroidal co-ordinates is needed; see the following

three sections.

$$\mathbf{N} = \left\langle \phi_j^{TT} \right| W(\vec{r_2}) \left| \phi_{k'}^{T_1 P_2} \right\rangle + \left\langle \phi_j^{TT} \right| W(\vec{r_1}) \left| \phi_{k'}^{T_2 P_1} \right\rangle \quad (2.61)$$

$$\bar{\mathbf{N}} = \left\langle \phi_{j'}^{T_1 P_2} \right| W^\dagger(\vec{r_2}) \left| \phi_k^{TT} \right\rangle + \left\langle \phi_{j'}^{T_2 P_1} \right| W^\dagger(\vec{r_1}) \left| \phi_k^{TT} \right\rangle \quad (2.62)$$

$$\bar{\mathbf{S}} = \left\langle \phi_{j'}^{T_1 P_2} \right| \left. \phi_{k'}^{T_1 P_2} \right\rangle + \left\langle \phi_j^{T_1 P_2} \right| W^\dagger(\vec{r_2}) W(\vec{r_1}) \left| \phi_{k'}^{T_2 P_1} \right\rangle \quad (2.63)$$

$$= \delta_{j'k'} + \left\langle \phi_j^{T_1 P_2} \right| W^\dagger(\vec{r_2}) W(\vec{r_1}) \left| \phi_{k'}^{T_2 P_1} \right\rangle \quad (2.64)$$

$$\mathbf{K} = \left\langle \phi_j^{TT} \right| \hat{H} W(\vec{r_2}) \left| \phi_{k'}^{T_1 P_2} \right\rangle + \left\langle \phi_j^{TT} \right| \hat{H} W(\vec{r_1}) \left| \phi_{k'}^{T_2 P_1} \right\rangle \quad (2.65)$$

$$\bar{\mathbf{K}} = \left\langle \phi_{j'}^{T_1 P_2} \right| W^\dagger(\vec{r_2}) \hat{H} \left| \phi_k^{TT} \right\rangle + \left\langle \phi_{j'}^{T_2 P_1} \right| W^\dagger(\vec{r_1}) \hat{H} \left| \phi_k^{TT} \right\rangle \quad (2.66)$$

$$\bar{\mathbf{M}} = \left\langle \phi_{j'}^{T_1 P_2} \right| \hat{H} \left| \phi_{k'}^{T_1 P_2} \right\rangle + \left\langle \phi_j^{T_1 P_2} \right| W^\dagger(\vec{r_2}) \hat{H} W(\vec{r_1}) \left| \phi_{k'}^{T_2 P_1} \right\rangle \quad (2.67)$$

where $\hat{H}$ is given in equation (2.56) and $W(\vec{r})$ are translation factors.

$$W(\vec{r_1}) = e^{-i(\vec{v}\cdot\vec{r_1})} \quad (2.68)$$

$$W(\vec{r_2}) = e^{-i(\vec{v}\cdot\vec{r_2})} \quad (2.69)$$

When both electrons are on the target they are not shown to be distinguishable. If all four combinations of one-electron functions used to construct the two-electron state were to be written out, it could be seen that only two terms are distinct by an electron label change. These distinct terms are the ones shown in equations (2.61) through (2.67). In these equations the co-ordinates $\vec{r_1}$ and $\vec{r_2}$ are centred on the target nucleus. In the current body-fixed co-ordinate system centred on the target a translation factor need only be applied when an electron is on the projectile nucleus. $W(\vec{r}_{1,2})$ is the part of the translation factor which is dependent on the electronic co-ordinates. As the remainder of the translation factor is independent of the electronic co-ordinates (it only has time dependency) it enters after the integration as a phase factor (2.70).

$$\tau_i(t) = e^{i(-\epsilon_i t - \frac{1}{2}v^2 t)} \quad (2.70)$$

Here ϵ_i is the internal energy of the one-electron wave-function.

2.4.2 Charge Exchange Matrix Elements

In a two-electron system with one electron on each nucleus the total wave-function representing the system is made up from a linear combination of one-electron wave-functions on each centre with the appropriate translation factors. It will become apparent that the use of prolate spheroidal co-ordinates simplifies the mathematics of charge exchange integrals; these will be introduced in the following section. The evaluation of the integrals needed for one-electron charge exchange matrix elements will follow. It will be shown that these integrals carry over directly for two-electron calculations with only a small increase in complexity. The two-electron repulsion integral will then be evaluated.

2.4.3 Prolate Spheroidal Co-ordinates

Prolate Spheroidal Co-ordinates (also called *confocal elliptic co-ordinates*) are a natural choice when calculating two-centre matrix elements. Figure 2.2 and equations (2.71) describe the co-ordinate system. The ranges for the co-ordinates are given in equations (2.72).

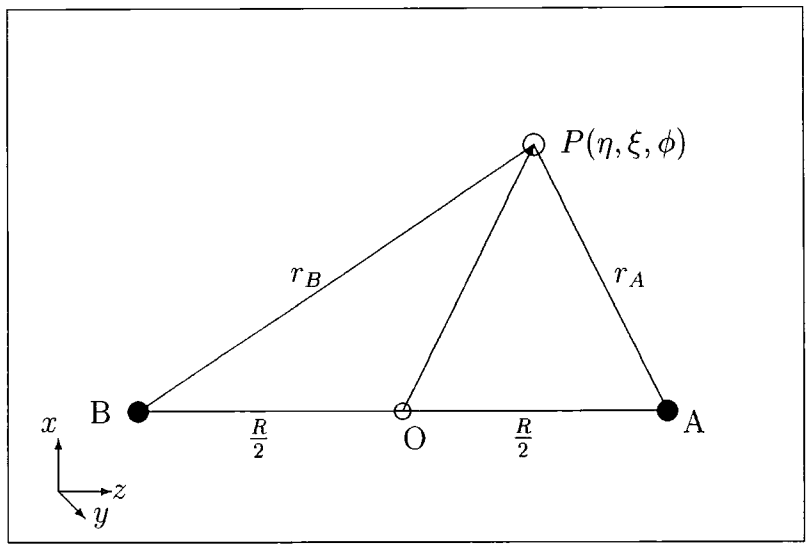

Figure 2.2: Prolate Spheroidal Co-ordinates

$$\begin{aligned}\xi &= \frac{1}{R}(r_A + r_B) \\ \eta &= \frac{1}{R}(r_A - r_B) \\ \phi &= tan^{-1}\left(\frac{y}{x}\right)\end{aligned} \tag{2.71}$$

The surface of constant ξ is an ellipsoid with foci at points **A** and **B** and axis of revolution along the line **AB**. The surfaces of constant η are hyperboloids with the same foci and revolution axis.

$$\begin{aligned}1 \leq \xi &\leq \infty \\ -1 \leq \eta &\leq +1 \\ 0 \leq \phi &\leq 2\pi\end{aligned} \tag{2.72}$$

The *body-fixed* cartesian co-ordinates (where z lies along the line **AB**) are given by equations (2.73). The volume element in prolate spheroidal co-ordinates can be derived from these and is given in equation (2.74).

$$\begin{aligned}x &= \frac{R}{2}\left[(\xi^2 - 1)(1 - \eta^2)\right]^{\frac{1}{2}} \cos(\phi) \\ y &= \frac{R}{2}\left[(\xi^2 - 1)(1 - \eta^2)\right]^{\frac{1}{2}} \sin(\phi) \\ z &= \frac{R}{2}\xi\eta\end{aligned} \tag{2.73}$$

$$d\tau = \frac{R^3}{8}(\xi^2 - \eta^2)d\xi d\eta d\phi \tag{2.74}$$

2.4.4 One-Electron Exchange

McCarroll[36] considered the simple system involving only one electron and two protons and the following charge transfer reaction.

$$H^+ + H(1s) \longrightarrow H(1s) + H^+ \tag{2.75}$$

Recalling from figure 2.1 the vector $\vec{v}$ lies along the space fixed z-axis where z is a cartesian co-ordinate for the electron. For the proton-hydrogen system the

wave-function for the electron on each centre is given respectively.

$$\Phi_i^A = \phi_i(\vec{r_A}) \exp(-\frac{1}{2}ivz - \frac{1}{8}iv^2t - i\epsilon_i t) \quad (2.76)$$

$$\Phi_j^B = \phi_j(\vec{r_B}) \exp(\frac{1}{2}ivz - \frac{1}{8}iv^2t - i\epsilon_j t) \quad (2.77)$$

The velocities of the nuclei are equal and opposite when measured from the centre of mass. The functions $\phi_i(\vec{r_A})$ and $\phi_j(\vec{r_B})$ are the stationary eigenfunctions on each isolated centre which satisfy.

$$\left[-\frac{1}{2}\nabla^2_{\vec{r_A}} - \frac{Z_A}{r_A} - \epsilon_i\right] \phi_i(\vec{r_A}) = 0 \quad (2.78)$$

$$\left[-\frac{1}{2}\nabla^2_{\vec{r_B}} - \frac{Z_B}{r_B} - \epsilon_j\right] \phi_j(\vec{r_B}) = 0 \quad (2.79)$$

At finite separation the electron is in the field of two nuclei and its wave-function Ψ must satisfy the time dependent Schrödinger equation (2.80).

$$\left[-\frac{1}{2}\left.\nabla^2_{\vec{r}}\right|_{\vec{R}} - \frac{Z_A}{r_A} - \frac{Z_B}{r_B} - i\left.\frac{d}{dt}\right|_{\vec{r}}\right] \Psi = 0 \quad (2.80)$$

Here centre of mass co-ordinates are used and $\nabla_{\vec{r}}$ is taken with $\vec{R}$, or equivalently time, fixed. Also the time derivative is taken with the electronic co-ordinate $\vec{r}$ fixed. At this stage the total derivative with respect to time is taken, this can be separated into the explicit derivative and a convective term (2.81).

$$\left.\frac{d}{dt}\right|_{\vec{r}} = \left.\frac{\partial}{\partial t}\right|_{\vec{r}} + \vec{v} \cdot \left.\nabla_{\vec{R}}\right|_{\vec{r}} \quad (2.81)$$

Using the vector identities (2.82) and (2.83) it is possible to rewrite $\nabla_{\vec{R}}$ yielding (2.84) and (2.85).

$$\vec{r_A} = \vec{r} + \frac{1}{2}\vec{R} \quad (2.82)$$

$$\vec{r_B} = \vec{r} - \frac{1}{2}\vec{R} \quad (2.83)$$

$$\left.\nabla_{\vec{R}}\right|_{\vec{r}} = \left.\nabla_{\vec{R}}\right|_{\vec{r_A}} + \frac{1}{2}\left.\nabla_{\vec{r_A}}\right|_{\vec{R}} \quad (2.84)$$

$$\left.\nabla_{\vec{R}}\right|_{\vec{r}} = \left.\nabla_{\vec{R}}\right|_{\vec{r_B}} - \frac{1}{2}\left.\nabla_{\vec{r_B}}\right|_{\vec{R}} \quad (2.85)$$

A trial wave-function representing the electron in the field of two colliding nuclei can be written as a linear combination of the stationary states with appropriate translation factors and occupation amplitudes (2.86).

$$\begin{aligned}\Psi = & a_i(t)\phi_i(\vec{r_A})\exp\left(-\frac{1}{2}ivz - \frac{1}{8}iv^2t - i\epsilon_i t\right) \\ & + b_j(t)\phi_j(\vec{r_B})\exp\left(\frac{1}{2}ivz - \frac{1}{8}iv^2t - i\epsilon_j t\right)\end{aligned} \tag{2.86}$$

Substitution of the above into the terms of the time dependent Schrödinger equation yields.

$$\begin{aligned}i\left.\frac{\partial}{\partial t}\right|_{\vec{r}}\Psi = & i\Bigg\{\dot{a}_i(t)\phi_i(\vec{r_A}) + \frac{1}{2}a_i(t)\vec{v}\cdot\left.\nabla_{\vec{r_A}}\right|_{\vec{R}}\phi_i(\vec{r_A}) + a_i(t)\phi_i(\vec{r_A}) \\ & \cdot\left[-\frac{1}{8}iv^2 - i\epsilon_i\right]\Bigg\}\exp\left(-\frac{1}{2}ivz - \frac{1}{8}iv^2t - i\epsilon_i t\right) \\ & + i\Bigg\{\dot{b}_j(t)\phi_j(\vec{r_B}) - \frac{1}{2}b_j(t)\vec{v}\cdot\left.\nabla_{\vec{r_B}}\right|_{\vec{R}}\phi_j(\vec{r_B}) + b_j(t)\phi_j(\vec{r_B}) \\ & \cdot\left[-\frac{1}{8}iv^2 - i\epsilon_j\right]\Bigg\}\exp\left(\frac{1}{2}ivz - \frac{1}{8}iv^2t - i\epsilon_j t\right)\end{aligned} \tag{2.87}$$

$$\begin{aligned}\left.\nabla^2_{\vec{r}}\right|_{\vec{R}}\Psi = & a_i(t)\left\{\left.\nabla^2_{\vec{r_A}}\right|_{\vec{R}}\phi_i(\vec{r_A}) - i\vec{v}\cdot\left.\nabla_{\vec{r_A}}\right|_{\vec{R}}\phi_i(\vec{r_A}) - \frac{1}{4}\phi_i(\vec{r_A})v^2\right\} \\ & \cdot\exp\left(-\frac{1}{2}ivz - \frac{1}{8}iv^2t - i\epsilon_i t\right) \\ & + b_j(t)\left\{\left.\nabla^2_{\vec{r_B}}\right|_{\vec{R}}\phi_j(\vec{r_B}) + i\vec{v}\cdot\left.\nabla_{\vec{r_B}}\right|_{\vec{R}}\phi_j(\vec{r_B}) - \frac{1}{4}\phi_j(\vec{r_B})v^2\right\} \\ & \cdot\exp\left(\frac{1}{2}ivz - \frac{1}{8}iv^2t - i\epsilon_j t\right)\end{aligned} \tag{2.88}$$

When the above terms are substituted into equation (2.80) after some arrangement and cancellation this yields

$$\begin{aligned}0 = & i\dot{a}_i(t)\phi_i(\vec{r_A})\exp\left(-\frac{1}{2}ivz - \frac{1}{8}iv^2t - i\epsilon_i t\right) \\ & + i\dot{b}_j(t)\phi_j(\vec{r_B})\exp\left(\frac{1}{2}ivz - \frac{1}{8}iv^2t - i\epsilon_j t\right) \\ & + \frac{Z_A}{r_A}a_i(t)\phi_i(\vec{r_A})\exp\left(-\frac{1}{2}ivz - \frac{1}{8}iv^2t - i\epsilon_i t\right) \\ & + \frac{Z_B}{r_B}b_j(t)\phi_j(\vec{r_B})\exp\left(\frac{1}{2}ivz - \frac{1}{8}iv^2t - i\epsilon_j t\right)\end{aligned} \tag{2.89}$$

Projecting out the complex conjugate of the two states Φ_i^A and Φ_j^B (given in equations (2.76) and (2.77)) yields respectively.

$$i\dot{a}_i(t) + i\dot{b}_j(t)S_{ij}\exp\left[-i(\epsilon_i - \epsilon_j)t\right] = a_i(t)C_{ii} + b_j(t)D_{ij}\exp\left[-i(\epsilon_i - \epsilon_j)t\right] \quad (2.90)$$

$$i\dot{a}_i(t)\bar{S}_{ji} + i\dot{b}_j(t)\exp\left[-i(\epsilon_i - \epsilon_j)t\right] = a_i(t)\bar{D}_{ji} + b_j(t)\bar{C}_{jj}\exp\left[-i(\epsilon_i - \epsilon_j)t\right] \quad (2.91)$$

where

$$S_{ij} = \int \phi_i^*(\vec{r_A})\phi_j(\vec{r_B})\exp\left[ivz\right]d\tau \quad (2.92)$$

$$\bar{S}_{ji} = \int \phi_j^*(\vec{r_B})\phi_i(\vec{r_A})\exp\left[-ivz\right]d\tau \quad (2.93)$$

$$C_{ii} = \int \phi_i^*(\vec{r_A})\frac{Z_B}{r_B}\phi_i(\vec{r_A})d\tau \quad (2.94)$$

$$\bar{C}_{jj} = \int \phi_j^*(\vec{r_B})\frac{Z_A}{r_A}\phi_j(\vec{r_B})d\tau \quad (2.95)$$

$$D_{ij} = \int \phi_i^*(\vec{r_A})\frac{Z_A}{r_A}\phi_j(\vec{r_B})\exp\left[ivz\right]d\tau \quad (2.96)$$

$$\bar{D}_{ji} = \int \phi_j^*(\vec{r_B})\frac{Z_B}{r_B}\phi_i(\vec{r_A})\exp\left[-ivz\right]d\tau \quad (2.97)$$

Equations (2.90) and (2.91) are coupled first order differential equations for the occupation amplitudes. These occupation amplitudes can be integrated along a trajectory provided the matrix elements (2.92-2.97) are known.

2.4.5 Two-Electron Exchange Matrix Elements

Since two-electron states are made up from linear combinations of one-electron states no further integrals are needed to evaluate similar two-electron matrix elements. The only complication arising from the extension to a two-electron system comes from the electron-electron repulsion term in the collision Hamiltonian. The evaluation of two-electron exchange matrix elements of the electron-electron repulsion term is covered in the following section.

2.4.6 Electron-Electron Repulsion Exchange Integrals

Consider the general exchange integral (2.98) where $\vec{r_1}$ and $\vec{r_2}$ represent the co-ordinates of the two electrons[45].

$$I_{iji'j'} = \int\int \psi_i(\vec{r_1})\psi_{i'}(\vec{r_2})\frac{e^{\pm i\vec{v}\cdot\vec{r_1}}e^{\pm i\vec{v}\cdot\vec{r_2}}}{|\vec{r_1}-\vec{r_2}|}\psi_j(\vec{r_1})\psi_{j'}(\vec{r_2})d\tau_1 d\tau_2 \tag{2.98}$$

Here the functions ψ are considered to be one term in the Slater expansion of a one-electron wave-function centred on either nucleus. The total matrix element will be given as a sum of such integrals over each term in the Slater expansions. If one or both electrons are not exchanged between the two nuclei then one or both exponential terms in (2.98) will be absent and the mathematics is greatly simplified. The form of ψ is as follows (when centred on nucleus A for example).

$$\psi^A = N_{\ell m} r_A^n e^{-\lambda r_A} P_\ell^m(\cos\theta_A)\cos(m\phi_A) \tag{2.99}$$

Here $N_{\ell m}$ is a normalization constant and P_ℓ^m is a normalized associated Legendre polynomial. Considering one of the electrons the total charge distribution can be written in prolate spheroidal co-ordinates.

$$\Omega_{ij}(\vec{r_1}) = \chi_i(\xi,\eta)\chi_j(\xi,\eta)\cos(m_i\phi)\cos(m_j\phi)e^{\pm i\vec{v}\cdot\vec{r_1}} \tag{2.100}$$

It is possible to expand Ω_{ij} in terms of spherical harmonics.

$$\Omega_{ij}(\vec{r_1}) = \frac{1}{\xi^2-\eta^2}\sum_{L=0}^{\infty}\sum_{M=0}^{L}\mathcal{D}_{ij}^{LM\pm}(\xi)(-1)^M P_L^M(\eta)\cos(M\phi) \tag{2.101}$$

It is possible to calculate the expansion coefficients $\mathcal{D}_{ij}^{LM\pm}(\xi)$ as follows. Consider the following identity.

$$\int_0^{2\pi}\cos(M\phi)\cos(M'\phi)d\phi = \pi(1+\delta_{M,0})\delta_{M,M'} \tag{2.102}$$

Multiplying by $\cos(M'\phi)$, integrating over ϕ and using the identity (2.102) yields

$$\begin{aligned}\int_0^{2\pi}\Omega_{ij}(\vec{r_1})\cos(M'\phi)d\phi = \\ \frac{1}{\xi^2-\eta^2}\sum_{L=0}^{\infty}\mathcal{D}_{ij}^{LM'\pm}(\xi)(-1)^{M'}P_L^{M'}(\eta)\pi(1+\delta_{M,0})\end{aligned} \tag{2.103}$$

From equation (2.100)

$$\int_0^{2\pi} \Omega_{ij}(\vec{r_1}) \cos(M'\phi) d\phi = \chi_i(\xi,\eta)\chi_j(\xi,\eta) \int_0^{2\pi} \cos(m_i\phi)\cos(m_j\phi)\cos(M'\phi) e^{\pm i\vec{v}\cdot\vec{r_1}} d\phi \tag{2.104}$$

By resolving $\vec{v}$ into directions parallel and perpendicular to the internuclear axis and invoking the identities (2.73), $\vec{v}\cdot\vec{r_1}$ can be rewritten as

$$\vec{v}\cdot\vec{r_1} = \alpha(\xi,\eta)\cos\phi - \beta\xi\eta \tag{2.105}$$

where

$$\alpha(\xi,\eta) = \frac{bv}{2}\left[(\xi^2-1)(1-\eta^2)\right]^{\frac{1}{2}} \tag{2.106}$$

$$\beta = \frac{1}{2}v^2 t \tag{2.107}$$

Now equation (2.104) becomes

$$\int_0^{2\pi} \Omega_{ij}(\vec{r_1}) \cos(M'\phi) d\phi = \chi_i(\xi,\eta)\chi_j(\xi,\eta) e^{\mp i\beta\xi\eta} \mathcal{I}_\phi^{\pm}(M', m_i, m_j) \tag{2.108}$$

where

$$\mathcal{I}_\phi^{\pm}(M', m_i, m_j) = \int_0^{2\pi} \cos(M'\phi)\cos(m_i\phi)\cos(m_j\phi) e^{\pm i\alpha(\xi,\eta)\cos(\phi)} d\phi \tag{2.109}$$

Substituting this result into equation (2.103) yields

$$\sum_{L=0}^{\infty} \mathcal{D}_{ij}^{LM'\pm}(\xi)(-1)^{M'} P_L^{M'}(\eta)\pi(1+\delta_{M',0}) = \chi_i(\xi,\eta)\chi_j(\xi,\eta)(\xi^2-\eta^2) e^{\mp i\beta\xi\eta} \mathcal{I}_\phi^{\pm}(M', m_i, m_j) \tag{2.110}$$

Multiplying by $P_{L'}^{M'}(\eta)$, integrating over η, invoking the associated Legendre orthogonality identity (2.112) and rearranging yields

$$\mathcal{D}_{ij}^{LM\pm}(\xi) = \frac{(-1)^M(2L+1)}{\pi(1+\delta_{M,0})}\frac{(L+M)!}{(L-M)!} \cdot \int_{-1}^{+1} \chi_i(\xi,\eta)\chi_j(\xi,\eta)(\xi^2-\eta^2) e^{\mp i\beta\xi\eta} P_L^M(\eta) \mathcal{I}_\phi^{\pm}(M', m_i, m_j) d\eta \tag{2.111}$$

$$\int_{-1}^{+1} P_{L'}^{M}(\eta)P_{L}^{M}(\eta)d\eta = \frac{2}{2L'+1}\frac{(L'+M)!}{(L'-M)!}\delta_{L,L'} \tag{2.112}$$

At this stage the Neumann expansion[41][42] is invoked (2.113)

$$\begin{aligned}\frac{1}{|\vec{r_1}-\vec{r_2}|} =& \frac{2}{R}\sum_{L=0}^{\infty}(2L+1)\sum_{M=0}^{L}\frac{2(-1)^M}{(1+\delta_{M,0})}\left[\frac{(L-M)!}{(L+M)!}\right]^2 \\ &\cdot P_L^M(\xi_<)Q_L^M(\xi_>)P_L^M(\eta_1)P_L^M(\eta_2)\cos\{M(\phi_1-\phi_2)\}\end{aligned} \tag{2.113}$$

Here $\xi_<$ is the smaller and $\xi_>$ the larger of the co-ordinates ξ_1 and ξ_2. Q_L^M is the associated Legendre polynomial of the second kind[1]. Substituting equations (2.74), (2.101) and (2.113) into (2.98) results in

$$\begin{aligned}I_{iji'j'} = &\iiint\iiint\sum_{L_1=0}^{\infty}\sum_{M_1=0}^{L_1}\mathcal{D}_{ij}^{L_1M_1\pm}(\xi_1)\frac{(-1)^{M_1}}{(\xi_1^2-\eta_1^2)}P_{L_1}^{M_1}(\eta_1)\cos(M_1\phi_1) \\ &\cdot\frac{2}{R}\sum_{L=0}^{\infty}\sum_{M=0}^{L}\frac{2(2L+1)(-1)^M}{1+\delta_{M,0}}\left[\frac{(L-M)!}{(L+M)!}\right]^2 \\ &\cdot P_L^M(\xi_<)Q_L^M(\xi_>)P_L^M(\eta_1)P_L^M(\eta_2)\cos(M(\phi_1-\phi_2)) \\ &\cdot\sum_{L_2=0}^{\infty}\sum_{M_2=0}^{L_2}\mathcal{D}_{ij}^{L_2M_2\pm}(\xi_2)\frac{(-1)^{M_2}}{(\xi_2^2-\eta_2^2)}P_{L_2}^{M_2}(\eta_2)\cos(M_2\phi_2) \\ &\cdot\frac{R^3}{8}(\xi_1^2-\eta_1^2)\,d\xi_1\,d\eta_1\,d\phi_1\,\frac{R^3}{8}(\xi_2^2-\eta_2^2)\,d\xi_2\,d\eta_2\,d\phi_2\end{aligned} \tag{2.114}$$

The integrals over the co-ordinates ϕ_1 and ϕ_2 are easiest to evaluate and are carried out first.

$$\begin{aligned}\int_0^{2\pi}\int_0^{2\pi}\cos(M_1\phi_1)\cos(M(\phi_1-\phi_2))\cos(M_2\phi_2)d\phi_1 d\phi_2 = \\ \pi^2(1+\delta_{M,0})^2\delta_{M,M_1}\delta_{M,M_2}\end{aligned} \tag{2.115}$$

The integrals over η_1 and η_2 can also be evaluated analytically

$$\begin{aligned}\int_{-1}^{+1}\int_{-1}^{+1}P_{L_1}^{M_1}(\eta_1)P_L^M(\eta_1)P_L^M(\eta_2)P_{L_2}^{M_2}(\eta_2)d\eta_1 d\eta_2 = \\ \left[\frac{2}{2L+1}\frac{(L+M)!}{(L-M)!}\right]^2\delta_{L,L_1}\delta_{L,L_2}\end{aligned} \tag{2.116}$$

Substitution of (2.115) and (2.116) into (2.114) yields

$$\begin{aligned}I_{iji'j'} = &\frac{\pi^2R^5}{4}\sum_{L=0}^{\infty}\sum_{M=0}^{L}\frac{(1+\delta_{M,0})(-1)^M}{(2L+1)} \\ &\cdot\int_1^{\infty}\int_1^{\infty}\mathcal{D}_{ij}^{LM\pm}(\xi_1)\mathcal{D}_{i'j'}^{LM\pm}(\xi_2)P_L^M(\xi_<)Q_L^M(\xi_>)\,d\xi_1\,d\xi_2\end{aligned} \tag{2.117}$$

Substituting the identity (2.118)

$$Q_L^M(\xi) = P_L^M(\xi) \int_\xi^\infty \frac{1}{(x^2-1)} \frac{1}{[P_L^M(x)]^2}\, dx \tag{2.118}$$

gives

$$\begin{aligned} I_{iji'j'} = & \frac{\pi^2 R^5}{4} \sum_{L=0}^{\infty} \sum_{M=0}^{L} \frac{(1+\delta_{M,0})(-1)^M}{(2L+1)} \\ & \cdot \int_1^\infty \int_1^\infty \mathcal{D}_{ij}^{LM\pm}(\xi_1) \mathcal{D}_{i'j'}^{LM\pm}(\xi_2) P_L^M(\xi_<) P_L^M(\xi_>) \\ & \cdot \int_{\xi_>}^\infty \frac{1}{(x^2-1)[(P_L^M(x)]^2}\, dx\, d\xi_1\, d\xi_2 \end{aligned} \tag{2.119}$$

One of the outer integrals needs to be split into two ranges, one where $\xi_1 > \xi_2$ and one where $\xi_1 < \xi_2$.

$$\begin{aligned} I_{iji'j'} = & \frac{\pi^2 R^5}{4} \sum_{L=0}^{\infty} \sum_{M=0}^{L} \frac{(1+\delta_{M,0})(-1)^M}{(2L+1)} \\ & \cdot \Bigg\{ \int_1^\infty \int_1^{\xi_2} \mathcal{D}_{ij}^{LM\pm}(\xi_1) \mathcal{D}_{i'j'}^{LM\pm}(\xi_2) P_L^M(\xi_1) P_L^M(\xi_2) \\ & \cdot \int_{\xi_2}^\infty \frac{1}{(x^2-1)[(P_L^M(x)]^2}\, dx\, d\xi_1\, d\xi_2 \\ & + \int_1^\infty \int_{\xi_2}^\infty \mathcal{D}_{ij}^{LM\pm}(\xi_1) \mathcal{D}_{i'j'}^{LM\pm}(\xi_2) P_L^M(\xi_1) P_L^M(\xi_2) \\ & \cdot \int_{\xi_1}^\infty \frac{1}{(x^2-1)[(P_L^M(x)]^2}\, dx\, d\xi_1\, d\xi_2 \Bigg\} \end{aligned} \tag{2.120}$$

Moving the x integration to be the outer integral in a two stage process

$$\begin{aligned} & \int_1^\infty d\xi_2 \int_1^{\xi_2} d\xi_1 \int_{\xi_2}^\infty dx + \int_1^\infty d\xi_2 \int_{\xi_2}^\infty d\xi_1 \int_{\xi_1}^\infty dx \\ = & \int_1^\infty d\xi_2 \int_{\xi_2}^\infty dx \int_1^{\xi_2} d\xi_1 + \int_1^\infty d\xi_2 \int_{\xi_2}^\infty dx \int_{\xi_2}^x d\xi_1 \\ = & \int_1^\infty dx \int_1^x d\xi_2 \int_1^{\xi_2} d\xi_1 + \int_1^\infty dx \int_1^x d\xi_2 \int_{\xi_2}^x d\xi_1 \\ = & \int_1^\infty dx \int_1^x d\xi_2 \int_1^x d\xi_1 \end{aligned} \tag{2.121}$$

results in a recombining of the two terms into one which is symmetric with respect

to the interchange of ξ_1 and ξ_2:

$$I_{iji'j'} = \frac{\pi^2 R^5}{4} \sum_{L=0}^{\infty} \sum_{M=0}^{L} \frac{(1+\delta_{M,0})(-1)^M}{(2L+1)} \int_1^{\infty} \frac{1}{(x^2-1)[P_L^M(x)]^2} \cdot \left\{ \int_1^x \mathcal{D}_{ij}^{LM\pm}(y) P_L^M(y)\, dy \int_1^x \mathcal{D}_{i'j'}^{LM\pm}(y) P_L^M(y)\, dy \right\} dx \tag{2.122}$$

Equation (2.111) shows that the coefficients $\mathcal{D}_{ij}^{LM\pm}$ are known and involve an integral over both η and ϕ. The ϕ integral (2.109) may be evaluated analytically.

$$\mathcal{I}_{\phi}^{\pm}(M', m_i, m_j) = \int_0^{2\pi} \cos(M'\phi)\cos(m_i\phi)\cos(m_j\phi) e^{\pm i\alpha\cos\phi} d\phi \tag{2.123}$$

Using the cosine rule this integral may be separated.

$$\begin{aligned} \mathcal{I}_{\phi}^{\pm}(M', m_i, m_j) = & \frac{1}{4}\left[\int_0^{2\pi} \cos\{(M'+m_i+m_j)\phi\}\, e^{\pm i\alpha\cos\phi} d\phi \right. \\ & + \int_0^{2\pi} \cos\{(M'+m_i-m_j)\phi\}\, e^{\pm i\alpha\cos\phi} d\phi \\ & + \int_0^{2\pi} \cos\{(M'-m_i+m_j)\phi\}\, e^{\pm i\alpha\cos\phi} d\phi \\ & \left. + \int_0^{2\pi} \cos\{(M'-m_i-m_j)\phi\}\, e^{\pm i\alpha\cos\phi} d\phi \right] \end{aligned} \tag{2.124}$$

These integrals are of a standard form[22] given as follows

$$\int_0^{2\pi} \cos(n\phi) e^{ix\cos\phi} d\phi = 2\pi i^n J_n(x) \tag{2.125}$$

where $J_n(x)$ is a Bessel function. The evaluation of this electron-electron repulsion exchange matrix element involves a triple numerical integral; the evaluation of this integral will be discussed in section 3.2 of chapter 3.

The other two-electron matrix elements are much simpler because they do not involve the $\frac{1}{|\vec{r_1}-\vec{r_2}|}$ term which gives rise to the Neumann expansion.

2.5 Choosing an atomic basis set

For the semiclassical close-coupling method to work the correct choice of basis functions must be made. Calculation of matrix elements is time consuming, therefore considering which matrix elements are *not needed* takes first priority.

Transfer Channels If the collision energy is high or the target charge is significantly greater than that on the projectile, charge exchange channels may be negligible. If this is the case it may be possible to perform excitation and ionization calculations by only including states bound to, or in the continuum of, the target.

Ionization Channels It may be possible to neglect states which represent the continuum in low energy collisions. Ionization channels are insignificant compared to excitation and transfer at these energies.

If two (or more) electrons are present they must in general be considered to all be active and be indistinguishable. It may be possible to treat such a system as having only one active electron. The other inner electrons are accounted for by using modified nuclear potentials.

In the close-coupling method a collision system is described at all times by a linear combination of all chosen basis states. A basis must be sufficiently large and diverse in nature to represent all physical possibilities before, during and after a collision event.

The state of the system both before and after the collision is the easiest to picture. At these times the nuclei are far apart and electrons are bound to one or the other nucleus or have been ionized. During a collision, when electrons are in the field of both nuclei, the state of the system is not so clear cut. A linear combination of final states may not be adequate to describe intermediate states; other states are needed. Basis functions used to describe the mid-collision include the so called *united atom states*: These are bound states to a hypothetical nucleus which is situated at the mid-point of the two real nuclei and has a charge equal to the sum of the two. The population of such a state after the collision represents ionization.

In a two-electron system it is necessary to consider initial and excited states of the two-electron target atom. One must also consider the possibility of ionization and both one and two-electron charge-transfer to the projectile. The calculations performed for this thesis use a two-electron basis which includes two-electron target bound states, two-electron pseudostates in the continuum of the target and one-electron transfer states but excludes two-electron transfer. The adequacy of this basis will be discussed in chapters 5 and 6.

Chapter 3

Computational Method

3.1 Parallelization

3.1.1 Introduction

A parallel computer program makes use of many processors simultaneously. In an ideal world a parallel program making use of n processors will run n-times faster than a program which makes use of only one processor. In general this is not the case for many reasons.

1. **Overheads** Communication between processors takes a finite amount of time. The more frequent and complex a communication is the larger this overhead becomes. The speed and size of the network linking the processors is also a factor to be considered.

2. **Memory** In shared memory devices a processor may have to wait for memory, used by another processor, to be made free. This constraint is in addition to the usual memory limitations.

3. **Disk Usage** If processors also share hard disk space then only one may write to it or read from it at a given time.

4. **Organization** If the way a piece of code is parallelized is not well balanced; one or more processors may at times be idle, waiting for the results of another

busy processor.

Some compilers allow for non-standard extensions to Fortran 77 for parallelization on specific architectures (e.g. Silicon Graphics). There are also various sets of library routines accessible from Fortran which can make use of a general cluster of processors, these include MPI (Message Passing Interface) and PVM (Parallel Virtual Machine). These routines allow for communication between executables across an arbitrarily large network of processors running the associated software. Although this message passing protocol is not true *fine-grained* parallelism the system works well when communication between processes is small and infrequent.

Although MPI is likely to become the standard[51], the cluster of RS6000 machines in Durham run PVM. A brief description of the capabilities of PVM are outlined in section 3.1.3. The following section covers some general parallel concepts.

3.1.2 General Parallel Concepts

The concepts to be discussed in this section are applicable to any parallel computer system. There are different ways a computational problem can be divided across multiple processors, the methods are classified as follows.

Algorithmic Distribution

The Algorithmic Distribution is often also known as the Pipeline Distribution. The processors are aligned in a linear fashion and work in a similar way to a factory production line. This method is suitable when many different operations need to be performed sequentially on each element of a large set of data. The data moves down a 'pipeline' and is operated on in turn by different processors. This method has several disadvantages. When the pipeline starts up, processors towards the end of the pipeline are idle, waiting for data to arrive. Likewise at the

end of the data stream, processors at the beginning have finished whereas those at the end are still busy. The system is only running at maximum efficiency when the pipeline is full. The pipeline operates at the speed of the slowest process. A queue of data can form before the slow processor and idle processors after, leading to a bottleneck. Communication is continuous as each data item is passed from processor to processor. The pipeline distribution is useful conceptually but not practically. If available it is usually better to use an alternative method of parallelization.

Farming Distribution

A master process distributes data to a number of identical slave processes when the farming distribution method is used. The slaves run independently without further communication until they return the finished data to a 'harvester' (or back to the master). This method is best implemented when a problem involves many similar computations which differ only by the change of a small number of parameters. The farming distribution has the advantage that it is automatically 'load balanced' i.e. if one processor runs slower than the others it will not hold up faster processors, it will simply do less work than the others. This is only the case because the slave processes are not dependent on each other.

Geometric Distribution

The geometric distribution lies somewhere between the algorithmic and farming distributions. Processors work on different areas of a problem needing occasional communication with each other, this is akin to the way a team of humans work together. Careful synchronization is important for this method to be efficient.

3.1.3 Parallel Virtual Machine

Parallel Virtual Machine[25] (PVM) is a piece of software that allows a network of UNIX computers to operate as a single parallel computer (the virtual machine). A virtual machine may consist of many computers which are not necessarily on the same local network or of the same architecture. The user can start an application on any of the computers running the PVM daemon[1]. An application can, via. subroutine calls, spawn processes on other computers, communicate with them, shut processes down, get the current virtual machine status and also add new computers to the virtual machine. The library of routines to do this is available for use with both C and FORTRAN.

Each process running on the virtual machine has a unique integer task identifier (TID) supplied by the daemon. The methods of communication are very versatile. Each message has a tag defined in the sending routine. Messages can be sent to a specific TID or broadcast to all processes on the machine. The sending process takes 3 stages. A buffer is opened, into which all the data to be sent is packed, then the data is sent. A similar 'unpacking' stage occurs on reception of a message. A message can be received from a specific TID, from any TID, with a specific tag, with any tag, or any combination of these options. Message reception can be either blocking or non-blocking. A blocking receive command will halt execution until it receives its message, a non-blocking receive command will look for a message but if it is not there execution will continue. Sychronization considerations are needed for both types of receive methods to prevent idle processors and missed messages.

[1]**D**isk **A**nd **E**xecution **MON**itor: a piece of software that runs continuously and handles system communications.

3.1.4 Close-Coupling Code Parallelization

The existing code for the calculation of charge exchange cross-sections has been adapted so that it can be run in parallel. The parallel implementation was for the cluster of 18 $\times$ IBM RS6000 machines at Durham, running PVM.

The calculation of matrix elements is the most time consuming part of a cross-section calculation. Matrix elements need to be calculated at different positions on a trajectory (z), for many impact parameters (b) and at different collision energies (E). Since the method of calculation of the matrix elements is independent of b, z and E, the farming distribution (page 40) was chosen as the parallelization method. It was possible to run calculations involving different impact parameters and collision energies concurrently. This type of parallelization satisfies the requirements for the farming distribution; the processes run independently and there is little communication.

Interface routines were written between the existing code and the PVM library routines. If the PVM library routines change or a new type of message passing software is to be installed, MPI for example, then only the interface routines need to be changed.

The implementation was as follows:

- A master program reads a subset of the input data; which impact parameters and energies are to be calculated.
- It then detects how many of the IBM's are currently available in the virtual machine and starts slave processes on each of the computers.
- When a slave starts up it receives its identifier from the master and sends a request for work.
- In response to each slave's request for work the master distributes values for the impact parameter and collision energy.

- Upon completion of the calculation the slaves request more work.
- When the master has no more work to distribute, slaves requesting work are told to self-terminate. When all slaves have finished the master exits.

The considerations and observations regarding the parallel implementation are outlined below:

- After a slave receives its task it must read all the input data for the basis functions, integration points etc. At the start all slaves would be trying to do this at approximately the same time, causing a queue of processes waiting for time to access the disk. It was decided that this method, although slightly inefficient, was superior to the alternative which was to have the master process read all of the data and then broadcast it to the slaves. The speed for each slave to read such a large amount of data from disk was much quicker than to pass it across the network with PVM.
- The matrix elements were written to very large files. These files had to be written to a disk local to the slave process to avoid excessive network usage. The local disks on the IBM's are relatively small and so these files had to be removed after each calculation. If the matrix elements were needed to be retained they were copied to a larger disk.
- Some of the matrix elements were independent of energy, these matrix elements were not deleted. The master process would distribute, *where possible,* the same impact parameters that a slave had already worked on so these matrix elements need not be re-calculated.
- If a machine was being used by another user it would run slower than the slaves with sole use of a machine. The farming distribution copes with this problem well. The slow process simply makes fewer requests for work, the

extra work being distributed evenly between faster processes, the machine as a whole being well balanced.

3.2 Numerical Evaluation of Exchange Integrals

The exchange integrals discussed in section 2.4.2 of chapter 2 cannot be evaluated analytically. Multi-dimensional numerical integrals need to be evaluated. The evaluation of the integrand is time consuming as it is over multiple sums of terms. The type of integral being considered is typically of the form

$$I = \int_1^{\infty} d\xi \int_1^{\xi} dy \int_{-1}^{+1} d\eta \, \{f(\xi, y, \eta)\} \tag{3.1}$$

The outermost integral can be difficult to perform because of the infinite upper limit; difficult to represent on a computer. It is fortunate that the integrand decays exponentially with respect to ξ and the outer integral may be transformed to the following form[36].

$$I = \int_0^{\infty} g(x) e^{-x} dx \tag{3.2}$$

This integral may be evaluated efficiently using Gauss-Laguerre quadrature, by approximating it to a sum[1]

$$I = \sum_{k=1}^{n} \omega_k g(x_k) + R_n \tag{3.3}$$

where x_k are the zeros of the n^{th} order Laguerre polynomial $L_n(x)$ and the weights ω_k are given by

$$\omega_k = \frac{(n!)^2 x_k}{(n+1)^2 \left[L_{n+1}(x_k)\right]^2} \tag{3.4}$$

The remainder R_n is given by

$$R_n = \frac{(n!)^2}{(2n)!} g^{(2n)}(x') \quad \text{where} \quad (0 < x' < \infty) \tag{3.5}$$

The approximation of this integral to a finite sum is a very good one. The remainder term rapidly becomes very small, even with highly oscillatory functions.

The integration over the y co-ordinate is needed for each evaluation of the integrand $g(x)$. The integrand for the outer integral is evaluated at ever increasing points, therefore the upper limit of the y integration is increasing. It is possible to save the last integral and only perform the new one over the additional range using the identity.

$$\int_1^{\xi_j} dy = \int_1^{\xi_{j-1}} dy + \int_{\xi_{j-1}}^{\xi_j} dy \tag{3.6}$$

The new integration over the range $[\xi_{j-1}, \xi_j]$ in equation (3.6) can be transformed onto the range $[-1, +1]$ and then integrated using Gauss-Legendre quadrature (3.7).

$$\int_{-1}^{+1} h(x)dx = \sum_{k=1}^{n} \omega_k h(x_k) + R_n \tag{3.7}$$

Here x_k is the k'th zero of the n'th order Legendre polynomial $P_n(x)$. The weights ω_k are given by

$$\omega_k = \frac{2}{(1 - x_k)^2 \left[P_n'(x_k)\right]^2} \tag{3.8}$$

and the remainder

$$R_n = \frac{2^{2n+1}(n!)^4}{(2n+1)\left[(2n)!\right]^3} h^{(2n)}(x') \quad \text{where} \quad (-1 < x' < +1) \tag{3.9}$$

The η integration is over the range $[-1, +1]$ and therefore is also performed using Gauss-Legendre quadrature.

3.3 Matrix Element Interpolation

The calculation of matrix elements is the most time consuming part of the close-coupling calculations performed for this thesis. When the matrix elements are

integrated to calculate the occupation amplitudes the integrator needs the value of the matrix elements at many points along the trajectory. An obvious time saving method is to use interpolation of the matrix elements.

The matrix elements are calculated at a number of pre-determined points and stored in files. When the integrator needs the value of a matrix element at an intermediate point it interpolates from nearby points.

When selecting a method of interpolation it is important to consider both speed and reliability. Reliable piecewise interpolations such as cubic splines are time consuming as matrix inversions are needed. Polynomial interpolation can be unpredictable if inappropriate points are chosen, leading to large oscillations at high orders.

The method of interpolation used in the code is Chebyshev interpolation.

3.3.1 Chebyshev Interpolation

Chebyshev is a polynomial method of interpolation where the absolute deviation from the expected function is minimized[24]. Using a single polynomial to fit the matrix element for an entire trajectory would not work well, the trajectory is divided up into user-defined ranges. An appropriate number of points are selected within each range for the required order of Chebyshev interpolation. A physical requirement is that the matrix elements and their first derivative are continuous with respect to time. Overlapping the ranges by one point ensured matrix element continuity since an interpolated function always passes through the fixed points. The first derivative of the matrix elements may not be continuous at these endpoints but by careful choice of the ranges this discontinuity is minimized.

The $n+1$ points at which the matrix elements are evaluated within a given range $[a, b]$ are scaled from the $n+1$ points on the range $[-1, +1]$, given by (3.10)

$$x_k = \cos\left[\frac{k\pi}{n}\right] \tag{3.10}$$

where $k = 0...n$. From the evaluations, $n+1$ coefficients are used to evaluate the interpolation function. These coefficients are

$$a_j = \frac{2}{n} \sum_{k=0}^{n} y(x_k) \cos\left[\frac{jk\pi}{n}\right] \tag{3.11}$$

and the interpolated function is given by

$$\sum_{k=0}^{n} a_k T_k(x) \tag{3.12}$$

where

$$T_k(x) = \cos(n \arccos(x)) \tag{3.13}$$

are the Chebyshev polynomials, which may be evaluated using the following recurrence relations.

$$\begin{aligned} T_0(x) &= 1 \\ T_1(x) &= x \\ T_k(x) &= 2xT_{k-1}(x) - T_{k-2}(x) \quad \text{for } k \geq 2 \end{aligned} \tag{3.14}$$

3.4 Propagation of Occupation Amplitudes

The system of coupled first order differential equations (3.15) form an initial value problem. The occupation amplitudes can be propagated to $t = +\infty$.

$$\begin{aligned} i\dot{\mathbf{a}} &= \left[\mathbf{O}^{-1}\mathbf{H}\right]\mathbf{a} \\ a_k(-\infty) &= \delta_{ik} \end{aligned} \tag{3.15}$$

Here $[\mathbf{O}^{-1}\mathbf{H}]$ is a known matrix and i is the initial channel. Infinity can be fixed at some large number beyond which the occupation amplitudes are assumed to be constant. If there are n channels in total, the problem becomes a system of $2n$ real first order coupled differential equations, since the occupation amplitudes are in general complex.

Shampine and Gordon's code 'DE' was used to solve this system[44]. This code uses a modified Adams Predictor-Corrector method.

A useful check of the progress of the integration is to check the sum of the occupation amplitudes (3.16). If this deviates too far from unity, then a so-called unitarity error has occured. A typical final unitarity value is $1.001 \pm i \times 10^{-18}$.

$$U = \sum_{k=0}^{n} a_k^2 \tag{3.16}$$

During the early stages of the calculations many unacceptable unitarity errors occured. At one time it was thought that the integrator was not able to cope with the large number of potentially stiff differential equations. Another integrator, GEAR[31], was substituted for a time. The cause of the unitarity problem was discovered elsewhere in the code. DE and GEAR subsequently both work well with unitarity errors well under 1%. These small deviations are thought to be a result of inaccuracies introduced by interpolation, not as a result of integration errors.

3.5 The Integration of Final Occupation Amplitudes

The integration of the magnitudes of the final occupation amplitudes over impact parameter yields the total cross-section for the associated channel (equation 2.7). Since the impact parameters are chosen by the user they are in general unequally spaced. Gill and Miller developed a useful algorithm for the integration of such points.

3.5.1 The Gill-Miller Algorithm

When integrating under a curve which is derived from a discrete number of points an interpolation method must be used. The trapezium rule is derived from linear interpolation. The Gill-Miller algorithm[21] derives itself from a cubic interpolation. The interpolation function between two points is a cubic which passes

through the nearest four points. This function is evaluated efficiently using divided differences, and can be integrated analytically over the range.

The only restriction of this method is that the points must be chosen in such a way that the interpolating function is well behaved. A rough-and-ready test that nothing is amiss is that the condition (3.17) is obeyed at all intermediate points for each channel i.

$$0 \leq |a_i|^2 \leq 1 \tag{3.17}$$

Chapter 4

Charge Transfer as a Fusion Diagnostic

4.1 Introduction

4.1.1 Thermonuclear Fusion

The equivalence between mass and energy (4.1) is exploited in fission reactors. When heavy nuclei split into or more smaller nuclei the mass of the products is less than the initial mass. This mass defect has been converted into energy.

$$E = mc^2 \tag{4.1}$$

Safety concerns and the production of highly radioactive waste make fission reactors an unpopular source of energy. The burning of fossil fuels contributes to the greenhouse effect and these fuels cannot meet the world's increasing demand for energy beyond the short term.

In proposed fusion reactors small nuclei combine to form a larger one, again with the release of energy. As a source of energy, fusion is virtually unlimited because of the abundance of fuel.

All energy reaching the earth from the sun is a product of fusion reactions within the Sun's core. The main energy producing reactions are those in the

proton-proton chain[46].

$$\begin{aligned} {}^{1}_{1}\mathrm{H} + {}^{1}_{1}\mathrm{H} &\longrightarrow {}^{2}_{1}\mathrm{D} + {}^{0}_{1}\bar{\mathrm{e}} + {}^{0}_{0}\nu \\ {}^{2}_{1}\mathrm{D} + {}^{1}_{1}\mathrm{H} &\longrightarrow {}^{3}_{2}\mathrm{He} + {}^{0}_{0}\gamma \\ {}^{3}_{2}\mathrm{He} + {}^{3}_{2}\mathrm{He} &\longrightarrow {}^{4}_{2}\mathrm{He} + {}^{1}_{1}\mathrm{H} + {}^{1}_{1}\mathrm{H} \end{aligned} \tag{4.2}$$

These reactions (4.2) occur with the release of approximately 27.9MeV per ^{4}He nucleus produced.

The quest for terrestrial fusion reactions has presented the following main candidates[35].

$$\mathrm{D} + \mathrm{T} \longrightarrow {}^{4}\mathrm{He} + \mathrm{n} + 17.6\mathrm{MeV} \tag{4.3}$$

$$\mathrm{D} + \mathrm{D} \longrightarrow \mathrm{T} + \mathrm{p} + 4.0\mathrm{MeV} \tag{4.4}$$

$$\longrightarrow {}^{3}\mathrm{He} + \mathrm{n} + 3.3\mathrm{MeV} \tag{4.5}$$

$$\mathrm{D} + {}^{3}\mathrm{He} \longrightarrow {}^{4}\mathrm{He} + \mathrm{p} + 18.3\mathrm{MeV} \tag{4.6}$$

Deuterium is a naturally occuring isotope of hydrogen and can be extracted from water. Tritium does not occur naturally but can be bred easily from natural and abundant lithium.

Both the D-D and D-T reactions produce neutrons. Conservation of momentum dictates that the neutron (as the lighter product) will carry away most of the kinetic energy. The neutrality of neutrons means that they cannot be magnetically confined and will therefore escape and interact with any surrounding vessels. This unfortunately leads to radiation damage and activation of materials near to the reactor. It is possible to make use of the neutrons by using them to breed more fuel. If the immediate surrounds of the vessel are lined with a lithium blanket the reactions (4.7) and (4.8) will produce more tritium fuel. The more dominant isotope of lithium is in fact ^{7}Li and its reaction produces another neutron resulting

in the tritium breeding ratio being greater than 1.

$$^{6}\mathrm{Li} + \mathrm{n} \longrightarrow {}^{4}\mathrm{He} + \mathrm{T} + 4.9\mathrm{MeV} \tag{4.7}$$

$$^{7}\mathrm{Li} + \mathrm{n} \longrightarrow {}^{4}\mathrm{He} + \mathrm{T} + \mathrm{n} - 2.5\mathrm{MeV} \tag{4.8}$$

The products of reaction (4.6) are all charged and would therefore remain in the bulk of a magnetically confined plasma. The kinetic energy would be transferred to the electrons in coulombic collisions and then bremsstrahlung radiation emitted by the accelerating electrons would travel to the surrounding heat exchangers. The disadvantages of this reaction are as follows.

1. Where there are $\mathrm{D} + {}^{3}\mathrm{He}$ reactions there are also $\mathrm{D} + \mathrm{D}$ neutron-producing reactions (4.4).

2. ${}^{3}\mathrm{He}$ does not occur naturally and therefore needs to be bred (4.5).

The deuterium-tritium reaction (4.3) *although neutron producing* is currently of high interest as the main reaction in first generation fusion devices. This is because of its *relatively* high cross-section of $5 \times 10^{-28}\mathrm{m}^2$ peaking at the deuteron collision energy of 100keV. This optimal collision energy is easily obtained in ion beam experiments but the extremely small reaction cross-section and rapid beam deterioration due to coulombic collisions makes this an impractical solution. Only a macroscopic quantity of ions with the appropriate energy will yield a large enough energy output to be of commercial use. Atoms at these high temperatures are invariably ionized and therefore fusion fuel is in the plasma state. An increasing fraction of confined plasma particles are accessing these energies as confinement techniques improve.

4.1.2 Plasmas

The plasma state of matter is the most common in the universe. Despite this fact it is the state which is least understood and most difficult to model. As an ionised

gas a plasma is an extremely good conductor. Any local net imbalance in the charge distribution sets up an electric field $\vec{E}$. The motion of charged particles causes currents which produce magnetic fields $\vec{B}$. These fields in turn cause ionic and electronic motion. The motion of a plasma is therefore very complex. The behaviour of fusion plasmas is especially complex, this can be seen by considering some aspects of plasma particle dynamics[8].

Plasma Particle Dynamics

Consider an ideal cold plasma which consists of an equal number of uniformly distributed positive and negative charged stationary particles. The negative particles are considered to be electrons. The positive particles are ions and are assumed to be sufficently massive to be unaffected by the motion of electrons. The displacement of a number of electrons leaves behind a region which has a positive charge. This net charge imbalance sets up an electric field which accelerates the electrons. The electrons now oscillate about their initial position and will do so indefinitely if collisions do not occur. The frequency of this oscillatory behaviour is known as the **electron plasma frequency** ω_{pe}.

$$\ddot{x} = -\frac{e}{m}E \tag{4.9}$$

$$\vec{E} = \frac{n_0 e}{\epsilon_0}\vec{x} \tag{4.10}$$

where n_0 is the particle density, yielding

$$\omega_{pe} = \left(\frac{n_0 e^2}{m\epsilon_0}\right)^{\frac{1}{2}} \tag{4.11}$$

A typical fusion plasma has an electron density of the order of $10^{20}\mathrm{m}^{-3}$, this gives the electron plasma frequency $\omega_{pe} = 5.6 \times 10^{11}\mathrm{rad\ s}^{-1}$.

Consider also the motion of an electron in a magnetic field. Here the Lorentz force acts on the electron.

$$\ddot{\vec{x}} = -\frac{e}{m}\dot{\vec{x}} \times \vec{B} \tag{4.12}$$

This oscillatory motion also has a characteristic frequency. The **electron cyclotron frequency** is thus given by

$$\omega_{ce} = \frac{e}{m}B \tag{4.13}$$

A typical fusion plasma has a magnetic field of up to 3T, this gives the electron cyclotron frequency $\omega_{ce} = 5.3 \times 10^{11}\text{rad s}^{-1}$.

The similarity in magnitude between the electron cyclotron frequency and the electron plasma frequency encourages the behaviour of the plasma to be chaotic in nature.

Debye Length

The Debye length is a measure of the distance at which the potential due to a charge is screened by its neighbours. When a test charge is inserted into a region of plasma, nearby charges are attracted or repelled slightly. This rearrangement screens the potential of the original test charge. Assuming all the ions remain stationary and the electrons are in thermal equilibrium adopting a Boltzmann distribution, the Debye length is given by.

$$\lambda_D = \left\{ \frac{\epsilon_0 kT}{2n_0 e^2} \right\}^{\frac{1}{2}} \tag{4.14}$$

In practice the Debye length is smaller than this because the ions can move and increase shielding.

Magnetohydrodynamics

It is possible to treat a bulk plasma as a continuous fluid. It is however a *charged* and *conducting* fluid in the presence of both magnetic and electric fields. For a plasma to be modelled macroscopically it must be collision-dominated. For this to be the case the MHD length scale must be large compared to the mean free path between collisions. A similar requirement is that a particle's distribution

function is locally Maxwellian and that the different species of particles have the same temperatures. The latter is the case when the MHD length scale is large compared to the Debye length. The mass conservation equation (4.15), the adiabatic equation of state (4.16), the resistive Ohm's law (4.17) and the momentum equation (4.18) are all fundamental to MHD theory in addition to Maxwell's equations (4.19)-(4.22).

$$\frac{\partial \rho}{\partial t} + \nabla \cdot (\rho \vec{v}) = 0 \tag{4.15}$$

$$\frac{d}{dt}\left(\frac{p}{\rho^{\gamma}}\right) = 0 \tag{4.16}$$

$$\vec{E} + \vec{v} \times \vec{B} = \eta \vec{J} \tag{4.17}$$

$$\vec{J} \times \vec{B} - \nabla p = \rho \frac{d\vec{v}}{dt} \tag{4.18}$$

$$\nabla \cdot \vec{B} = 0 \tag{4.19}$$

$$\nabla \cdot \vec{E} = \frac{\rho}{\epsilon_0} \tag{4.20}$$

$$\nabla \times \vec{B} = \mu_0 \vec{J} + \epsilon_0 \mu_0 \frac{\partial}{\partial t} \vec{E} \tag{4.21}$$

$$\nabla \times \vec{E} = -\frac{\partial}{\partial t} \vec{B} \tag{4.22}$$

Here ρ is the density, p is the pressure, γ is the ratio of specific heats, η is the resistivity and $\vec{J}$ is the current density. The permittivity and permeability are given by ϵ_0 and μ_0 respectively and c is the speed of light.

In theory it is possible to solve the complete set of equations given known boundary conditions. In practice this proves too difficult and various approximations must be applied, for example, assuming quasi-neutrality, before progress can be made.

4.1.3 Methods of Plasma Confinement

A plasma needs to be confined in a way which prevents, or at least minimises, the plasma's contact with material surfaces. Contact with a material surface cools the plasma rapidly. Material contact may also cause sputtering which results in

the plasma becoming polluted. Three methods of confining plasmas are outlined briefly below.

Magnetic Confinement It is possible to confine a plasma using an externally applied magnetic field. Currents within the plasma also contribute to this magnetic field. However, it is not possible to confine a plasma using an externally applied electric field; the field is cancelled out within the bulk of the plasma because of its very high conductivity. Typically a magnetically confined plasma has a density of $2 \times 10^{20}\mathrm{m}^{-3}$ and can be confined for a time of the order of a few tens of seconds.

Inertial Confinement An inertially confined plasma is one which is produced by high power lasers brought to a focus on a small pellet of fuel. In fusion experiments the pulse is high powered ($\gtrsim 10^{15}\mathrm{Wcm}^{-2}$) and typically lasts up to several nano-seconds, simultaneously ionising and compressing the fuel to a density of 1000 times the initial solid density. It is the fuel particle's inertia which confines the plasma long enough for fusion to take place.

Gravitational Confinement Stars are gravitationally confined plasmas. The radius ($R_\odot$) of our star is approximately 7×10^8m. The *nuclear core* is the region where hydrogen is converted into helium (4.2) and extends to a radius of about $\frac{1}{4}R_\odot$. In the nuclear core the plasma temperature is about 1.5×10^7K and the density is $1.6 \times 10^5\mathrm{kgm}^{-3}$[32]. The minimum size and mass of a gravitationally confined plasma means that we are very unlikely to see any terrestrial devices of this type.

4.1.4 Lawson Criterion

For a fusion plasma to produce more energy than used in creating and sustaining the plasma the Lawson Criterion must be satisfied[34]. The condition at an ion

temperature of $T_i \approx 20\text{keV}$ is

$$\tau_E n_i \gtrsim 6 \times 10^{19}\text{m}^{-3}\text{s} \tag{4.23}$$

where n_i is the ion density and τ_E is the confinement time. Lawson assumed that energy losses and generated power can be reapplied to the plasma with an efficiency of $\frac{1}{3}$.

4.1.5 Ignition

A fusion plasma ignites when external heating is no longer needed. In a D-T device, alpha-particles are the product of fusion reactions. When the power of the retained alpha-particles balances all power losses, ignition occurs. The criterion for D-T ignition at an ion temperature of $T_i \approx 20\text{keV}$ is given in equation (4.24). This estimate assumes the bulk plasma is a pure, equal mixture, of D-T. As helium ash is produced it dilutes the fuel, reducing the fusion power and, unless removed, ultimately quenches the burning plasma. If too much helium ash is exhausted then its kinetic energy is lost and ignition fails. If not enough helium ash is exhausted, fuel dilution prevents ignition.

$$\tau_E n_i \gtrsim 1.8 \times 10^{20}\text{m}^{-3}\text{s} \tag{4.24}$$

4.1.6 Plasma Heating

In order to reach ion temperatures high enough for fusion to be possible the plasma must be heated in some way. There are various methods for doing this.

Ohmic Heating A plasma heats up when a current passes through it; this is similar to the behaviour of a metal. However, a plasma's resistivity decreases as its temperature increases, unlike the behaviour of metals. This leads to a practical upper limit for the ohmic heating of a plasma. When the current is generated by a transformer the bulk of the current occurs at the magnetic axis, as does the heating effect.

Radio-Frequency Heating Intense radio-frequency waves at the same or at a low harmonic of the cyclotron frequency of either the electrons or ions in the plasma are resonantly absorbed. The cyclotron frequency of a species is dependent on the magnetic field and the magnetic field is spatially dependent. This means that it is possible to heat the plasma in a given location. Typical ion-cyclotron frequencies (although mass dependent) are about 50 MHz and electron-cyclotron frequencies are about 350 GHz

Neutral-Beam Heating Neutral beams are undeviated by a magnetic field and can therefore penetrate into a magnetically confined plasma. In the JET device the beams are usually hydrogen or deutrium and have energies of around 100keV. When the beam is inside the plasma it rapidly undergoes charge exchange with plasma ions or is ionized by ion or electron collisions. The charged beam is then confined to follow the magnetic field lines. Neutral beam injection has the advantage that it can be used to refuel a plasma with deuterium. Neutral beam injection with a toroidal component can drive or contribute to the toroidal current. Since the energy of a beam affects its depth of penetration into the plasma it is possible to select and adjust the heating location and current profile. Neutral beam injection as a diagnostic tool is covered in section 4.3.2.

4.2 JET Joint Undertaking

4.2.1 Tokamak Architecture

Tokamak is a Russian acronym for 'toroidal magnetic chamber'. The choice for a toroidal configuration (figure 4.1) can be argued as follows. In general plasma particles follow magnetic field lines. Better confinement is achieved when a particle can travel for a great distance along a field line before it comes into contact with a physical surface. Many early confinement configurations involved a cylin-

drical column of plasma. Problems arose at the ends of such a plasma column. Even complicated magnetic mirror configurations which bunched the field lines to encourage the particles to be reflected allowed too many particles to escape. This end effect is removed by bending such a column into a torus.

With only a toroidal field, particles of opposite charge would drift in opposite vertical directions due to the variation of the magnetic field strength as a function of R. This sets up an electric field and leads to the plasma drifting outwards due to an $\vec{E} \times \vec{B}$ force. The poloidal field gives the particles orbits that prevent such an electric field being established.

The toroidal magnetic field is generated by external field coils, in the JET device this can be up to 3T. The fact that there is a discrete number of field coils leads to slight variations in the magnetic field which can result in instablities. The poloidal field is generated by a plasma current flowing in the toroidal direction. The magnetic field is also altered by other coils which shape and position the plasma.

The aspect ratio of a torus is defined as the major axis radius divided by the minor axis radius (R_0/a). A large aspect ratio represents a thin torus with a large hole, as the aspect ratio tends to 1 the hole closes. The aspect ratio in the JET device[1] is about 2.5 and varies between about 1.3 and 4 in other devices. The advantage of a very low aspect ratio is the high fraction of trapped electrons. This increases the resistance which in turn improves ohmic heating capabilities. The disadvantage is that there is not much room in the hole of the torus for field coils and cooling pipes which means that the magnetic field cannot be as large.

A point inside a torus can be defined most naturally with the co-ordinates given in equation (4.25) where $0 \leq r \leq a$, $0 \leq \theta \leq 2\pi$ and $0 \leq \phi \leq 2\pi$ but sometimes it is useful to think in terms of the cylindrical co-ordinates given in

[1]The average minor axis radius is taken since the JET device is not circular in cross-section

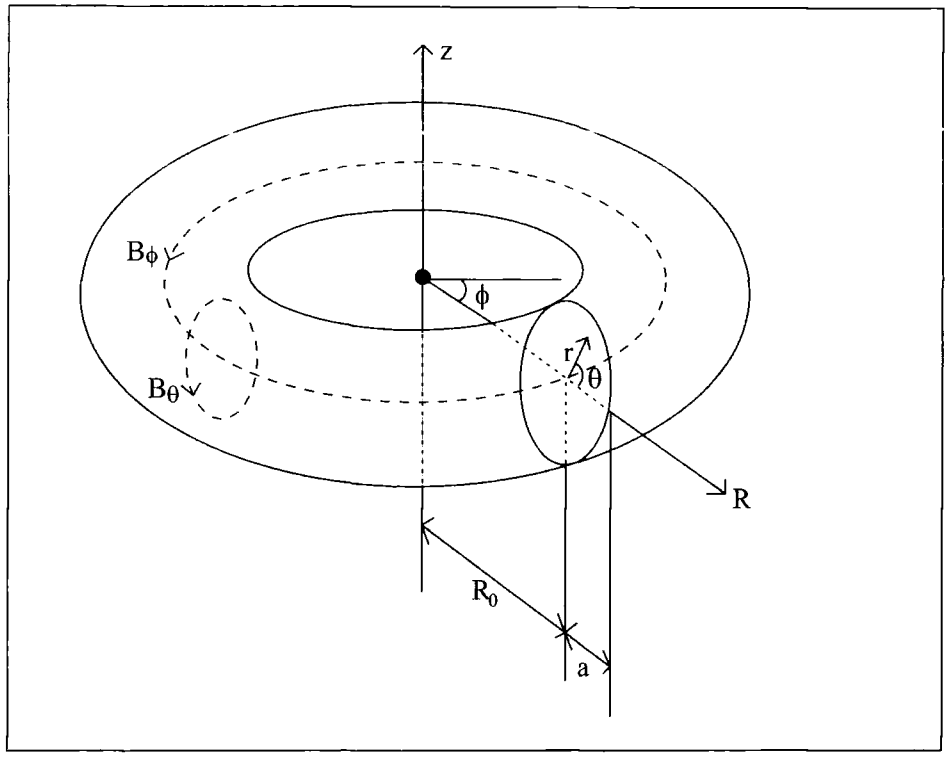

Figure 4.1: Tokamak Geometry

equation (4.26). Here ϕ measures the angle around the toroidal axis, θ is the angle around the poloidal axis, r is the radial distance from the poloidal axis, R is the distance from the central toroidal axis and z is the vertical distance from the centre of the torus.

$$\vec{r} = \vec{r}(r, \theta, \phi) \tag{4.25}$$

$$\vec{r} = \vec{r}(R, z, \phi) \tag{4.26}$$

4.2.2 The Divertor Region

Although in general plasma particles follow field lines there is also a drift effect perpendicular to the field lines. When particles drift outside the *last closed flux surface* (LCFS) they escape from the bulk of the plasma. A *limiter* is a solid surface which defines the position of the LCFS. A divertor is a region of plasma outside the LCFS. A separatrix exists between the closed flux surfaces and flux

surfaces which terminate in the divertor. Escaping particles are swept along the separatrix into the divertor.

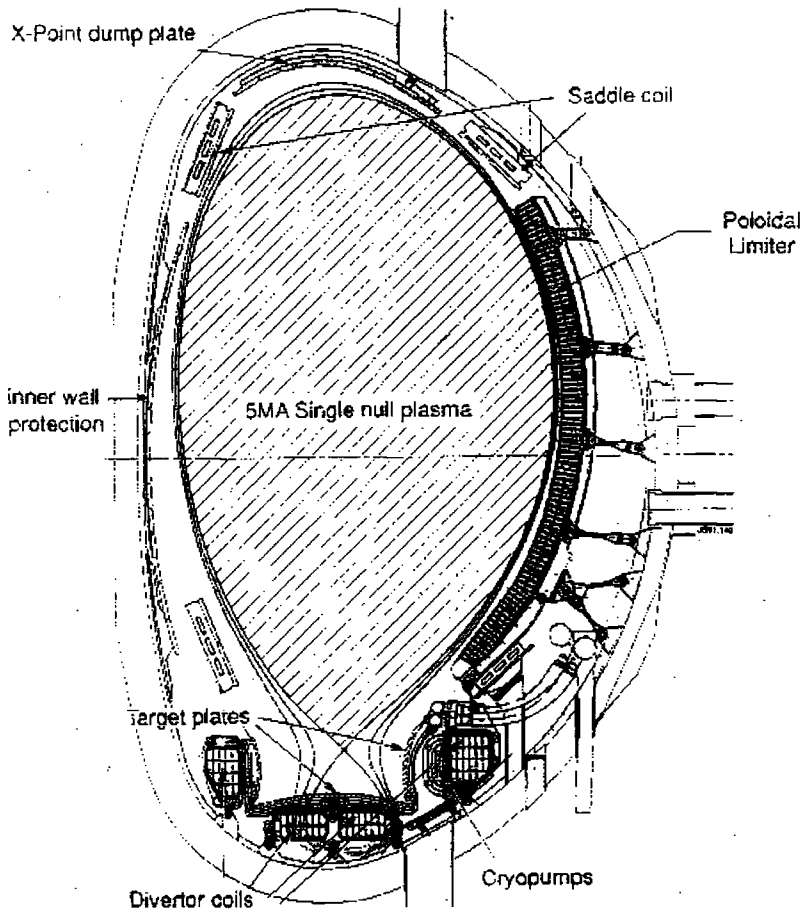

Figure 4.2: The JET Pumped Divertor[50]

The divertor region is separated from the bulk plasma by an X-point (a null in the magnetic field), see figure 4.2. The plasma in the divertor is typically cool compared to the bulk plasma and has a higher density. Particles in the divertor find it hard to re-enter the bulk plasma because of the plasma flow into the divertor. Sputtered particles and other impurites remain in the divertor, away from the hot fusion plasma. Also sputtering is reduced since it is only plasma in the divertor region which comes into contact with a solid surface. Impurites can be

expelled from the divertor using cryo-pumps. Eventually it is expected that the helium ash will be exhausted from the reactor through the divertor region. Most plasma particles enter the divertor travelling along field lines close to the seperatrix. This leads to overheating and wear at particular points on the target at the bottom the divertor. Sweeping of the position at which the main fieldlines come into contact with the target reduces localized wear. This sweeping is achieved by varying the magnetic field slightly. The most recent divertor configuration has a very high X-point and an angled target. It is expected the divertor structure used in the ITER device will be similar to the current one in JET.

4.2.3 ITER

The International Thermonuclear Experimental Reactor (ITER) is a collaboration between The European Community, USA, Russian Federation and Japan to demonstrate the technological feasibility of fusion as an energy source. Table 4.1 shows how ITER will measure up to JET (currently the world's largest operational tokamak fusion reactor)

	JET	ITER
Major Radius	3 m	7.75 m
Plasma Current	7 MA	25 MA
Plasma Volume	100 m^3	1900 m^3

Table 4.1: JET - ITER comparison

4.3 Plasma Diagnostics

4.3.1 Overview

In general a particular property of a plasma cannot be measured in isolation. Measurable quantities are affected by more than one fundamental plasma parameter. Hutchinson gives useful data (see table 4.2) showing which fundamental

parameters can be obtained from particular measurements. The quality of data is given on a scale of 1 (most reliable) to 3 (least reliable). Brief descriptions of the parameters and measurements in the table are given below. Although methods are applicable to general plasmas emphasis is given to the JET plasma.

	Parameter Diagnosed										
Property Measured	f_e	f_i	n_e	n_i	n_0	V_i	T_e	T_i	p	E	B
Magnetic measurements							2		1	1	1
Particle Flux	1	1	2	2		2	1	1		1	
Refractive index			1								1
Cyclotron Radiation	3		2				1				
Bremsstrahlung Radiation	2		2	2			1				
Čerenkov Radiation	3		3								
Line radiation			2	2	2	1	2	1			3
EM Wave Scattering	3		2	3			1	3			3
Charge Exchange		2			1			1			
Nuclear Reactions		3		2				1			
Heavy Probe Beams				2						1	3

Table 4.2: Plasma parameter measurements[33]

Distribution functions and plasma particle flux measurements

The electron and ion distribution functions are f_e and f_i respectively. These quantities are the most fundamental of plasma parameters. The distribution function is defined as the number of particles in an infinitesimal volume of phase space[2] at a given time. The spatial density $n_{e,i}(\vec{r},t)$ can be obtained by integrating the distribution function over all velocities (4.27).

$$n_{e,i}(\vec{r},t) = \int f_{e,i}(\vec{r},\vec{v},t)d\vec{v} \tag{4.27}$$

A knowledge of the distribution function of each particle species would give a complete description of the plasma. It is very difficult to measure the distribution function. The only reliable measurements for distribution functions come from plasma particle flux measurements. These measurements use probes in contact

[2]A six-dimensional space of position and velocity

with the plasma. Plasma contact with probes is limited to cool areas of plasmas where the probe will survive. In the case of fusion plasmas this restricts the use of probes to the edges of the plasma. When interpreting data from a probe one must also consider the local effect the probe has on the plasma. It is usual to operate the probe at a potential similar to that of the plasma. This is so that currents in the probe and charge build up on the probe are small, leading to little effect on the plasma.

Measurement of Electron Temperature

When an electromagnetic wave is incident on a fundamental charged particle the particle is accelerated. The accelerated charged particle emits electromagnetic radiation in all directions. This process is known as Compton Scattering. Thompson Scattering is the classical limit of this process. Since in most plasma diagnostics the electromagnetic waves used to probe the plasma are visible light or of longer wavelength ($\hbar\omega \sim 1\text{eV}$) a classical treatment is adequate.

The Doppler broadening of the emitted radiation gives a measure of the electron temperature. The difficulty arises in distinguishing this weak signal from the background radiation.

Measurement of Ion Temperature

Spectral lines characteristic to a particular species are Doppler broadened. From this broadening the temperature of the species can be calculated. Usually the Doppler broadening is more significant than Stark broadening. Assuming the ion distribution is locally Maxwellian the Doppler broadening results in a Gaussian line shape. The local ion temperature can be calculated from the width of the Gaussian.

$$T_i = \frac{1}{2} mc^2 \frac{\lambda_d^2}{\lambda_0^2} \tag{4.28}$$

where m is the mass of the radiating particle, λ_0 is the nominal (central) wavelength, λ_d is the half width of the Gaussian and c is the speed of light.

Measurement of Plasma Density

The density of a given species can be estimated from the intensity of one of its characteristic emission lines. In order to calibrate such a measurement it is important to know the proportion of ions in the upper level and the branching ratios for de-excitation.

Neutron Diagnostics

Since neutrons are produced in many of the fusion reactions they provide a good measure of the amount of fusion taking place in a reactor. The neutrality and penetrating power of neutrons means that neutron detectors can be outside the machine.

Measurement of Impurity Content

Impurities in a plasma are generally heavy species such as C, O, N and Fe. Impurities have 2 main detrimental effects on a plasma:

1. Impurities dilute fusion fuel.
2. When impurities with large Z values radiate they dissipate a large amount of energy, causing cooling of the plasma.

A measurement of impurity content can be obtained from the intensity of a spectral line characteristic to the impurity species of interest, the same way a general density measurement is taken.

4.3.2 Neutral Beam Injection

As discussed earlier, neutral-beam injection provides refuelling and an alternative plasma heating mechanism. As a beam passes into a plasma it can be used as a

probe to diagnose various plasma parameters. An overview of this technique and its implementation at JET is provided by von Hellermann[29].

The JET device is divided up into eight segments around the torus. The neutral beam injectors are in octants numbered 4 and 8 which are directly opposite each other. Both banks of injectors inject particles in a clockwise direction (when viewed from above), the same direction as plasma rotation. Each bank of injectors has eight single neutral beam injectors. In general 4 lie normal and 4 lie tangential to the magnetic flux surfaces although the angle of intersection varies from the edge to the centre of the plasma. Figure 4.3 shows the layout of the active charge exchange diagnostic during the 91/92 experiments.

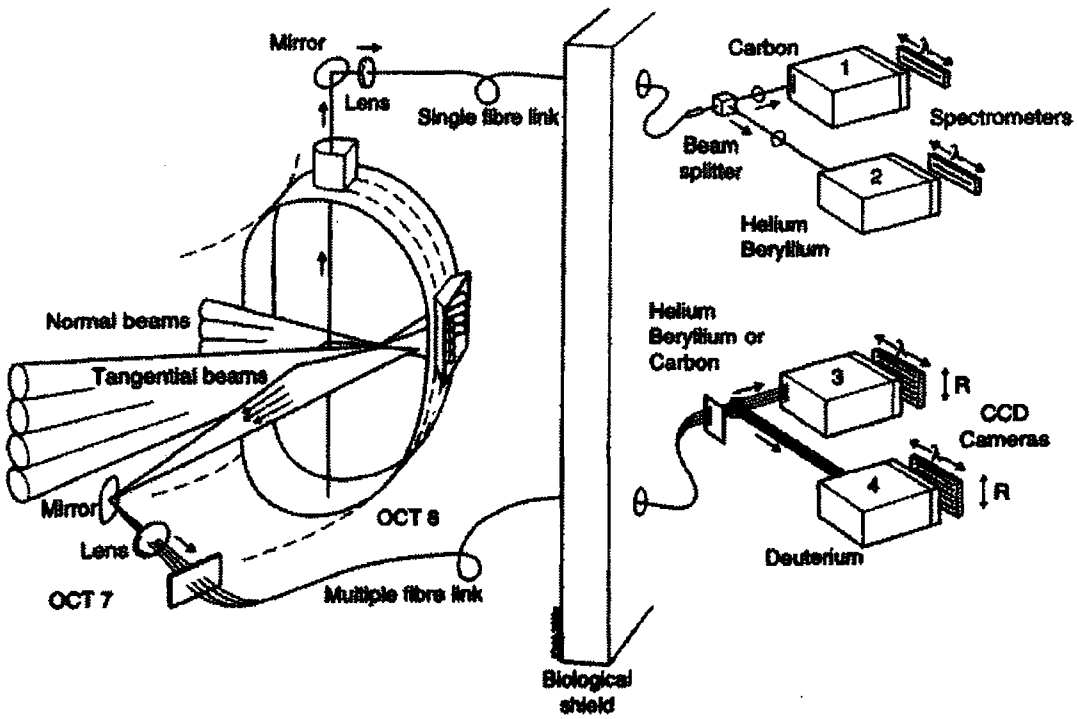

Figure 4.3: Schematic of the JET CX Diagnostic[20]

There are two main viewing lines:

- A view through the top port in octant 8 intersects the neutral beams near

the plasma axis. This viewing line is also used to see into the divertor region at the bottom of the torus.

- The second view is almost parallel with the magnetic field lines at the intersection with the neutral beams. This view can be varied slightly to give several lines of sight, able to give a radial profile from the plasma edge to the centre. These views are taken from an adjacent octant: from octant number 7 in the 91/92 campaign leading to blueshift and octant number 1 in the 94/95 campaign leading to redshift of the spectral lines.

Beam Attenuation

As a neutral beam passes into the plasma electrons are removed by charge exchange or ionization processes, the beam then attenuates as charged particles are removed from the beam by the magnetic field. It is possible to measure the density of a plasma by how rapidly the neutral beam attenuates. The intensity I of such a beam given at a point B relative to a point A is given by

$$I(B) = I(A) \exp\left[-\int_A^B \alpha(\ell) d\ell\right] \tag{4.29}$$

where $\alpha(\ell)$ is the attenuation coefficient. This attenuation coefficient is a function of all electron removing cross-sections and the densities of the particles which cause the removal of electrons. The evaluation of a particular species density is usually performed by an iterative procedure.

Active Charge-Exchange Spectroscopy

Passive observations of spectral lines resulting from charge transfer from intrinsic neutrals are only available at the plasma boundary. By *actively* introducing neutrals into the hot, normally fully ionized, central region of the plasma in a controlled way, the resulting spectral line observations give a valuable insight into the properties of this region. In general these active measurements are a more

reliable diagnostic because the original beam parameters are known and can be extrapolated deep into the plasma.

The two-stage reaction given in equation (4.30) is used in active charge exchange spectroscopy. Here X^0 is the neutral beam atom which donates an electron into an excited state of a plasma ion Y. This excited atom decays radiatively. The wavelength is characteristic of the transition and is observed by external spectrometers.

$$\begin{aligned} X^0 + Y^{Z+} &\longrightarrow X^+ + Y^{(Z-1)+}(n\ell) \\ Y^{(Z-1)+}(n\ell) &\longrightarrow Y^{(Z-1)+}(n'\ell') + h\nu \end{aligned} \tag{4.30}$$

Of special interest are the following transitions (4.31). The helium transition helps locate helium ash in the plasma. The latter two help monitor the presence of beryllium and carbon, the two main impurities which are sputtered from the inner lining tiles. All three transitions result in the emision of visible light.

$$\begin{aligned} He^+(n=4) &\longrightarrow He^+(n=3) + [\lambda \approx 468.5\text{nm}] \\ Be^{3+}(n=6) &\longrightarrow Be^{3+}(n=5) + [\lambda \approx 465.9\text{nm}] \\ C^{5+}(n=8) &\longrightarrow C^{5+}(n=7) + [\lambda \approx 529.1\text{nm}] \end{aligned} \tag{4.31}$$

The observed spectrum around wavelengths of 468.5nm comes from several distinct He^+ contributions. Here the viewing line is assumed to be towards the beams as in the 91/92 experimental setup.

Contributions to the observed spectrum around 468.5nm

Using known parameters and the expected shape of each peak it is possible to resolve the observed spectra into distinct contributions and derive useful data from them.

core contribution This contribution can be modelled by a Gaussian because it results from the thermalized helium particles in the core of the plasma. The

peak is slightly shifted from the nominal wavelength because of the bulk rotation of the plasma around the torus. The half width of this peak gives a measure of the ion temperature, see equation (4.28). The bulk rotation of the plasma core is given in (equation 4.32).

$$v_{rot}\cos(\alpha) = -\frac{\Delta\lambda}{\lambda_0}c \tag{4.32}$$

where α is the angle the viewing line makes with the toroidal direction and $\Delta\lambda$ is the shift from the nominal wavelength λ_0.

edge contribution This is caused by passive charge exchange with neutrals at the edge of the plasma. It is also approximately Gaussian and shifted due to rotation. This has a lesser or greater contribution depending on the direction of the viewing line.

fast contribution This contribution is only present when at least one of the injectors is injecting helium. This peak is strongly blue shifted (or red-shifted in the case of the 94/95 experiments). Although this peak is non-Gaussian because the beam of helium particles is not thermalized, the energy distribution of the injected particles is known.

plume contribution The plume effect[13] is a result of the following reactions.

$$\mathrm{D}^0_{beam} + \mathrm{He}^{2+}_{plasma} \longrightarrow \mathrm{D}^+_{beam} + \mathrm{He}^+_{plasma} \tag{4.33}$$

$$\mathrm{He}^0_{beam} + \mathrm{He}^{2+}_{plasma} \longrightarrow \mathrm{He}^+_{beam} + \mathrm{He}^+_{plasma} \tag{4.34}$$

Both reactions produce He^+ which are capable of following magnetic field lines for many metres before being fully ionized. In typical reactor conditions the ionization time is about 10^{-5}s and thermal velocities are about $10^5 \mathrm{ms}^{-1}$. During this time it is possible that the He^+ ions could travel back in front of the viewing line and be excited, by for example electron

impact, and then decay radiatively. This signal is weaker for the vertical viewing line because its intersection with the signal region is smaller than with the horizontal views. The plume signal is very difficult to analyse because of its non-local nature and its high dependence on the magnetic field configuration[19]. In the case of the second reaction (4.34) the two distinct contributions to the plume effect are distinguished as 'plasma plume' and 'beam plume' depending upon where the He^+ ion originated.

The spectra taken from the viewing line lying normal to the magnetic surfaces do not have shifted Gaussians because the Doppler effect is not present. Because measured intensity is an accumulation from all emissions in the line of sight a deconvolution process must be used to extract the plasma data.

Many of the neutral beam injection experiments use refuelling deuterium atoms. These beams are also used for diagnostic purposes, probing the central region of the plasma. The energy of the beam of deuterium atoms is typically 140keV in JET. Some experiments have also been carried out using helium atom injection specifically for diagnostic purposes. Helium beams are used to study the effect and transport of helium in the plasma in preparation for fusion alpha-particle detection in future D-T experiments.

$^3He^0$ beams up to energies of 150keV were injected into the JET device in 1991. This deposited a large number of helium atoms and subsequently nuclei in the centre of the plasma. The observations gave good insights into the behaviour of alpha particles at thermal and non-thermal energies in the plasma[27]. Experiments carried out in 1994/1995 using $^4He^0$ beams with energies of the order of 70keV in conjuction with deuterium heating/diagnostic beams in the opposite octant were used to study the plume effect.

Calibration of optics takes place whenever access to the torus hall is available. Although the viewports are protected by metal plates when the spectrometers are

idle the optics deteriorate over a period of usage. This is especially the case for the horizontal vacuum window which is situated close to the plasma. It is possible to calibrate measurements through this window with measurements taken along the vertical viewing line since the port at the top of the device is about 2m away from the plasma.

It is also possible to calibrate various spectroscopic measurements with each other. The aim in the spectroscopy group at JET is to achieve 'Global Data Consistency'[28]. In order to do this a database of atomic, spectroscopic and plasma data has been set up.

4.3.3 The ADAS Database

ADAS stands for Atomic Data and Analysis Structure[49]. It is both a database of atomic, spectroscopic and plasma data and an associated library of codes for the analysis of this data. ADAS is accessible interactively and allows the user to interrogate the database and perform calculations using a menu driven interface. The library of FORTRAN routines is also available for inclusion into the users own codes. Both fundamental data and data derived from them is available in the ever increasing database.

The entries in the database of interest to this thesis are those falling into the so called ADF01 category. Data in these files contain total, n and ℓ resolved charge exchange cross-sections. These files must conform strictly to the defined formatting convention since these data will by accessible by many routines across all users of the ADAS database.

The charge exchange cross-sections are used in conjunction with derived data for the respective ion populations in the interpretation of observed spectral lines. The ion population of a particular species can only be derived from spectral observations. The analysis is inherently an iterative procedure.

In order to analyse the results of helium injection, all cross-sections for processes which remove electrons from the injected atoms need to be known. Since the method of neutral beam injection introduces many helium atoms initially in metastable states, data for transitions from these states are also needed. The calculations described in chapter 5 are given in a form suitable for inclusion into the ADAS database, in Appendix A, along with a description of the ADF01 format.

4.4 Concluding Remarks

In order to confine a plasma magnetically at greater temperatures, higher densities and for longer periods requires an understanding of its macroscopic behaviour. This understanding currently relies on rules of thumb derived from experimental observations. Increasingly it will require a knowledge of the microscopic processes involved. Spectroscopy is a valuable plasma diagnostic, as it reveals how the atoms are behaving under plasma conditions. A theoretical understanding of atomic behaviour leads to a knowledge of the plasma conditions themselves. The spectral lines reveal not only the conditions in the plasma but also the location of various atomic species. Spectroscopic measurements also have the advantage of not needing contact with the plasma and leaving it unaffected.

Current interest lies mainly in the location of impurity elements which dilute the fuel and cool the plasma, hindering reactor conditions and preventing break-even. A thorough understanding of both high and low confinement modes of operation is being sought in order to achieve the correct balance of helium retention and exhaust in the quest for ignition. Divertors are used in an attempt to reduce impurites and keep any impurites that do persist away from the hot bulk plasma.

Even when the current goals of energy break-even and ignition are achieved a greater understanding of all aspects will be needed in order to construct an

economically viable and environmentally sound reactor. More consideration will need to be given to the exhaust of spent fuel and impurities as a commercial reactor would be required to run as continuously as possible.

Chapter 5

Results and Discussion

5.1 Introduction

Accurate charge-transfer cross-sections are needed in the analysis of spectroscopic data used in the diagnosis of fusion plasmas (see chapter 4). The study of helium and alpha-particles in a fusion plasma is important because alpha-particles are the product of D-T fusion reactions. Tritium is only used sparingly in the JET plasma, as a result there are not many fusion alpha-particles present. Helium atoms are injected as an alternative. The process of helium injection introduces some of the atoms in initially excited states. When inside the plasma, neutral helium atoms undergo charge exchange with many of the species present. Although cross-sections for all processes are needed, the work for this thesis was on the symmetric He^{2+} – He collision system. Cross-sections are presented and discussed for collisions where the helium atom is initially in the ground state (section 5.3.5) and when it is in the excited metastable states He($1s2s^1S$) and He($1s2s^3S$) (sections 5.3.7 and 5.3.8 respectively).

It was important to both familiarize myself with the structure and use of the code and also to test that it was working properly before embarking on a new calculation. A small calculation for charge-transfer cross-sections in H^+ – He collisions was performed first, the results are presented in section 5.2.

5.2 Charge-Transfer from He($1s1s\,^1S$) to H^+

A calculation to test both the close-coupling code and my ability to use it was devised. Excitation, ionization and charge-transfer cross-sections for collisions between protons and helium atoms have previously been calculated with this code by Slim *et al*[48]. Slim used a large basis, with a total of 51 channels, including: pseudostates in the continuum of the target, pseudostates in the continuum of the projectile (capture to the continuum) and bound states on both nuclei. His results compared well to the experimental data of Shah *et al*[43] for both ionization and single electron capture. The test calculation performed here used a much smaller basis (see Table 5.1). The number of channels used in this calculation is 14. The list of channels used only includes substates with a non-negative projection quantum number m. The symmetry of the collision system makes the cross-section independent of the sign of m. The total cross-section into a state with a particular angular momentum is given by the sum of the cross-sections into each m-substate.

Direct	**Charge-Transfer**	
	target	projectile
$He(1s1s\,^1S)$	$He^+(1s)$	H(1s)
$He(1s2s\,^1S)$	$He^+(1s)$	H(2s)
$He(1s2p\,^1P)$	$He^+(1s)$	H(2p)
	$He^+(1s)$	H(3s)
	$He^+(1s)$	H(3p)
	$He^+(1s)$	H(3d)
4 channels	10 channels	

Table 5.1: Basis functions

No attempt has been made to model ionization. The inclusion of only the $n = 2$ states on the target limits the ability to model excitation. As can be seen from Figure 5.1 even this small basis models electron capture well. Target excitation is not so well reproduced, this is due to an inadequacy of the current basis.

Although not immediately obvious on the logarithmic scale, the insufficiency of the excitation cross-section is approximately equal to the over-estimation of the electron capture cross-section. The inclusion of higher excited states on the target and continuum pseudostates would help to modify both cross-sections accordingly.

This is an important consideration when calculating cross-sections which differ by one (or several) orders of magnitude. Even if a large cross-section is accurate to within say 1%, a much smaller cross-section may be inaccurate by a large factor.

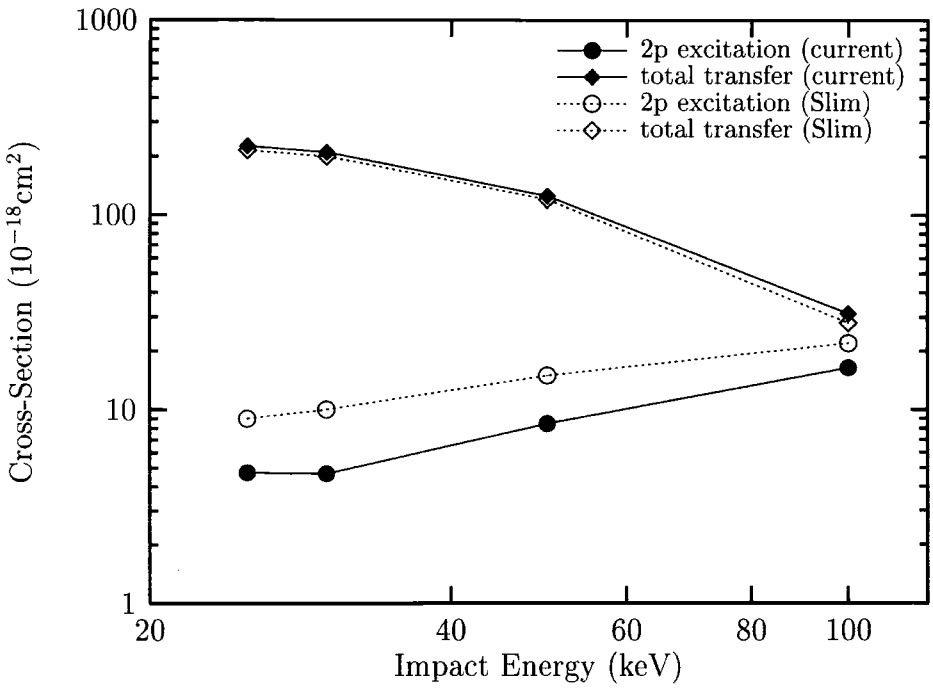

Figure 5.1: H^+ – He collision cross-sections. Comparison between the current 14 channel basis and the 51 channel calculation by Slim[48]

5.3 Charge-Transfer in the He^{2+} – He System

5.3.1 Introduction

A single electron attached to a helium nucleus in the state $He^{+}(1s)$ has a binding energy of 2au. The electrons in the ground state of a helium atom have a total binding energy of approximately 2.903au. Therefore 0.903 atomic units of energy, or equivalently 24.6eV, are needed to remove one of the electrons from the ground state of a helium atom. The metastable states $He(1s2s^{1}S)$ and $He(1s2s^{3}S)$ have binding energies of only 2.145au and 2.175au respectively. To ionize an electron from these states needs approximately one sixth of the energy needed for ionization from the ground state. Because of the proximity of these states to the continuum one expects that the cross-sections for ionization and one-electron charge-transfer are more significant from this initially excited state. Since transitions to other excited states involve crossing a smaller energy gap it is expected that excitation cross-sections will be larger too. The energy gap between the 2S and 2P states is small, leading to a very large cross-section. Coupling between these states is large even when the projectile is some distance away.

5.3.2 Basis Functions

A basis set, including up to 96 functions, was used for the calculation of one-electron charge transfer from the $He(1s1s^{1}S)$, $He(1s2s^{1}S)$ and $He(1s2s^{3}S)$ states. The two-electron singlet target states[47] are listed in table 5.2, along with their eigenenergies and, if appropriate, the experimentally measured energy. The triplet states were generated from exactly the same pairs of one-electron hydrogenic functions, with the exception of the pair optimized for the ground state (see section 2.3.3). The states are listed in table 5.3. The transfer channels are listed in table 5.4.

State	Energy(au)	Measured(au)
$He(1s1s^1S)$	-2.8765	-2.903
$He(1s2s^1S)$	-2.138	-2.145
$He(1s2p^1P)$	-2.122	-2.124
$He(1s3s^1S)$	-2.059	-2.061
$He(1s3d^1D)$	-2.056	-2.055
$He(1s3p^1P)$	-2.055	-2.055
$He(1s4s^1S)$	-2.033	-2.033
$He(1s4f^1F)$	-2.031	-2.031
$He(1s4d^1D)$	-2.031	-2.031
$He(1s4p^1P)$	-2.031	-2.031
$He(1s5g^1G)$	-2.020	-2.020
$He(1s5f^1F)$	-2.020	-2.020
$He(1s5p^1P)$	-2.018	-2.020
$He(1s5d^1D)$	-2.016	-2.020
$He(1s5s^1S)$	-2.013	-2.021
'p'-pseudostate	-1.994	n/a
'd'-pseudostate	-1.975	n/a
'p'-pseudostate	-1.944	n/a
's'-pseudostate	-1.894	n/a
'd'-pseudostate	-1.865	n/a
'p'-pseudostate	-1.841	n/a
'p'-pseudostate	-1.632	n/a
'd'-pseudostate	-1.575	n/a
's'-pseudostate	-1.226	n/a
'p'-pseudostate	-1.198	n/a
'd'-pseudostate	-0.728	n/a
'p'-pseudostate	-0.237	n/a

Table 5.2: The 61 singlet basis-states used for the target with energy levels and comparison to measured values[3]

State	Energy(au)	Measured(au)
He($1s2s^3S$)	-2.174	-2.175
He($1s2p^3P$)	-2.131	-2.133
He($1s3s^3S$)	-2.068	-2.069
He($1s3p^3P$)	-2.057	-2.058
He($1s3d^3D$)	-2.056	-2.055
He($1s4s^3S$)	-2.036	-2.036
He($1s4p^3P$)	-2.032	-2.032
He($1s4d^3D$)	-2.031	-2.031
He($1s4f^3F$)	-2.031	-2.031
He($1s5f^3F$)	-2.020	-2.020
He($1s5g^3G$)	-2.020	-
He($1s5s^3S$)	-2.019	-2.022
He($1s5p^3P$)	-2.019	-2.020
He($1s5d^3D$)	-2.016	-2.020
'p'-pseudostate	-1.997	n/a
'd'-pseudostate	-1.975	n/a
'p'-pseudostate	-1.949	n/a
's'-pseudostate	-1.937	n/a
'd'-pseudostate	-1.865	n/a
'p'-pseudostate	-1.852	n/a
'p'-pseudostate	-1.656	n/a
'd'-pseudostate	-1.578	n/a
's'-pseudostate	-1.445	n/a
'p'-pseudostate	-1.250	n/a
'd'-pseudostate	-0.748	n/a
'p'-pseudostate	-0.339	n/a
's'-pseudostate	+2.008	n/a

Table 5.3: The 61 triplet basis-states used for the target with energy levels and comparison to measured values[3]

Target State	Projectile State	Total Energy(au)
$He^+(1s)$	$He^+(1s)$	-4.000
"	$He^+(2s)$	-2.500
"	$He^+(2p)$	-2.500
"	$He^+(3s)$	-2.222
"	$He^+(3p)$	-2.222
"	$He^+(3d)$	-2.222
"	$He^+(4s)$	-2.125
"	$He^+(4p)$	-2.125
"	$He^+(4d)$	-2.125
"	$He^+(4f)$	-2.125
"	$He^+(5s)$	-2.080
"	$He^+(5p)$	-2.080
"	$He^+(5d)$	-2.080
"	$He^+(5f)$	-2.080
"	$He^+(5g)$	-2.080

Table 5.4: The 35 charge-transfer basis-states

5.3.3 Matrix Elements

The values of matrix elements as a function of internuclear separation, impact parameter and collision energy can give insight into the resulting amplitudes and cross-sections.

Direct Matrix Elements

The direct overlap matrix elements are known trivially to be of the form of a unit matrix. The two-electron states on the target have been pre-orthonormalized.

The coupling matrix elements (5.1) between the singlet states $He(1s2s\,^1S)$, and $He(1s2p_0\,^1P)$ and $He(1s2p_1\,^1P)$ are given as a function of z in figures 5.2 and 5.3 for various impact parameters b.

$$\begin{aligned} &\langle 1s2s\,^1S|\,\hat{\mathbf{H}}\,|1s2p_0\,^1P\rangle \\ &\langle 1s2s\,^1S|\,\hat{\mathbf{H}}\,|1s2p_1\,^1P\rangle \end{aligned} \tag{5.1}$$

There is no matrix element dependence on collision energy because both states are on the same centre. Collision energy dependence enters when the matrix

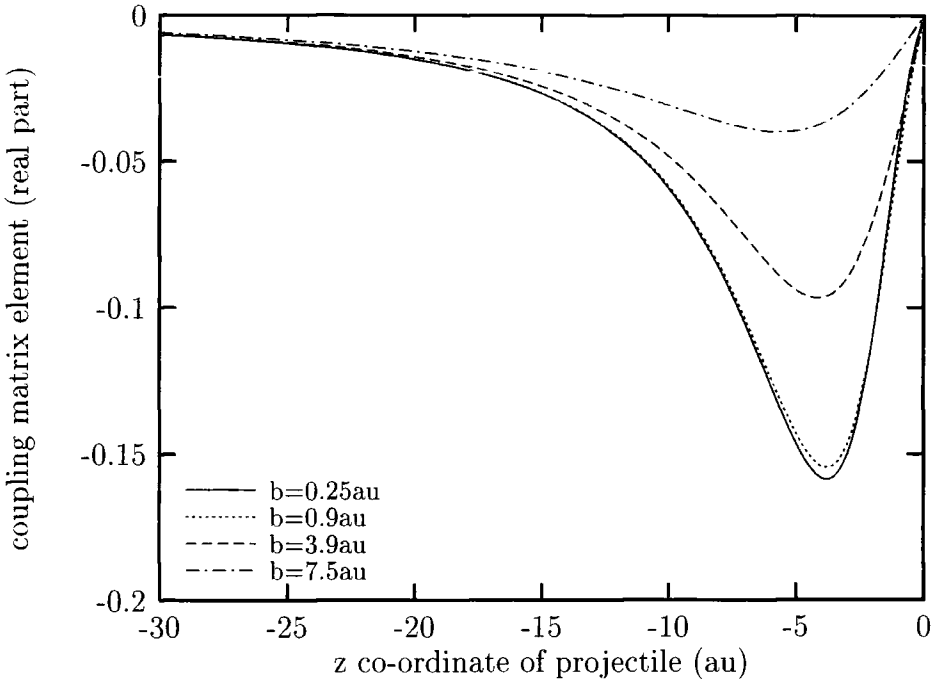

Figure 5.2: He($1s2s\,^1S$) – He($1s2p_0\,^1P$) Coupling Matrix Elements

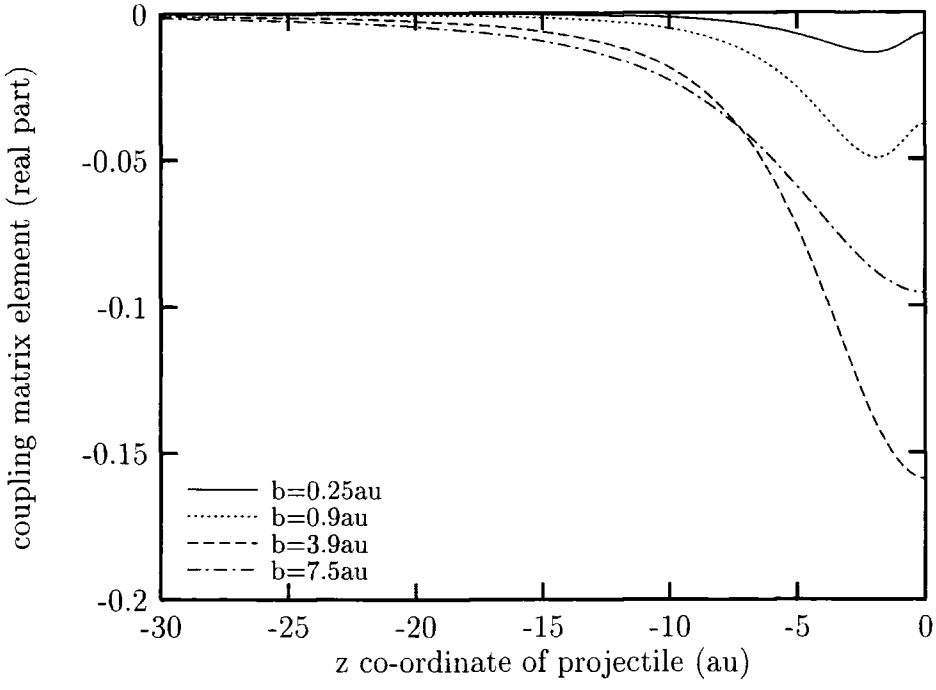

Figure 5.3: He($1s2s\,^1S$) – He($1s2p_1\,^1P$) Coupling Matrix Elements

elements are integrated. The matrix elements are real because real spherical harmonics are used for the wavefunctions and there is no translation phase factor.

There are important qualitative differences between the two figures. The curve for coupling to the He($1s2p_0\,^1P$) state passes through the origin whereas the curve for coupling to the He($1s2p_1\,^1P$) state does not. The magnitude increases as the impact parameter b tends to zero for coupling to the He($1s2p_0\,^1P$) state whereas coupling to the He($1s2p_1\,^1P$) has a maximum at a non-zero value of b. This can be explained by considering the probability distribution of p-orbitals. A p_0-orbital's probability distribution has a dumbell shape lying along the quantization axis, A $p_{\pm 1}$-orbital's probability distribution is also dumbell shaped but lies perpendicular to the quantization axis. In the space-fixed co-ordinate system in which these matrix elements are given the quantization axis coincides with the z-axis. The coupling between the two states is greatest when the probability distribution of the initial He($1s2s\,^1S$) state with a dipole induced by the incoming projectile is most like the final p-state. This is the case when ($b = 0$) and ($z \simeq \pm 4$au) for the He($1s2p_0\,^1P$) state, and when ($z = 0$) and ($b \simeq 4$au) for the He($1s2p_1\,^1P$) state.

The symmetry about the $z = 0$ axis means that matrix elements need only be calculated for negative values of z. The matrix elements for $z > 0$ are evaluated using a simple phase factor (5.2). This is a consequence of the symmetry of spherical harmonics.

$$M_{ij}(z) = (-1)^{\ell_i+\ell_j+|m_i|+|m_j|} M^*_{ij}(-z) \tag{5.2}$$

The implication is that when $\ell_i + \ell_j + |m_i| + |m_j|$ is odd the matrix element must pass through the origin, this can also be seen in figure 5.4 which shows the matrix elements for coupling between He($1s2s\,^1S$) and the He($1s3d\,^1D$) states. In this case it is the curve for $m = 1$ that passes through the origin.

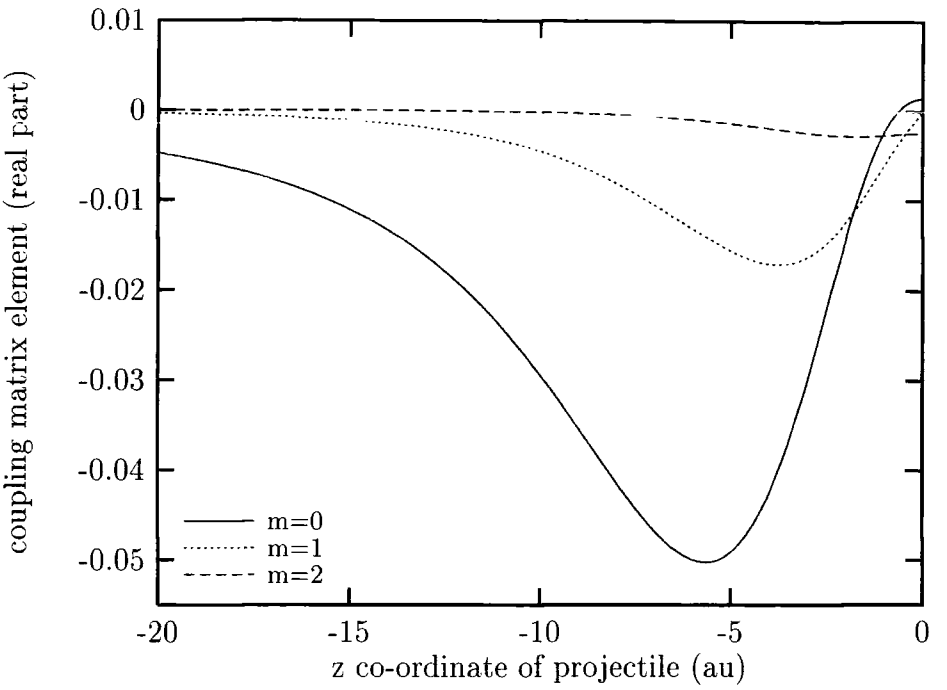

Figure 5.4: He(1s2s^{1}S) – He(1s3d^{1}D) Coupling Matrix Elements

Transfer Matrix Elements

The transfer matrix elements also respect the symmetry discussed in the previous section and therefore only need to be calculated for negative z. Figures 5.5 and 5.6 show the real and imaginary parts (respectively) of the overlap matrix element between the states He(1s2s^{1}S) and [He_t^+(1s) – He_p^+(1s)] for various collision energies. The matrix elements become more oscillatory with respect to z as the collision energy increases due to the increase in the exponential translation factor. The real and imaginary parts of the corresponding coupling matrix elements are shown in figures 5.7 and 5.8, again showing an increase in oscillatory behaviour with the collision energy. Figures 5.9 and 5.10 show the overlap and coupling matrix elements between the states He(1s2s^{1}S) and [He_t^+(1s) – He_p^+(2p)] and confirm the symmetry of the matrix elements about $z = 0$ (5.2). The real part of the $2p_0$ and the imaginary part of the $2p_1$ matrix elements pass through the origin.

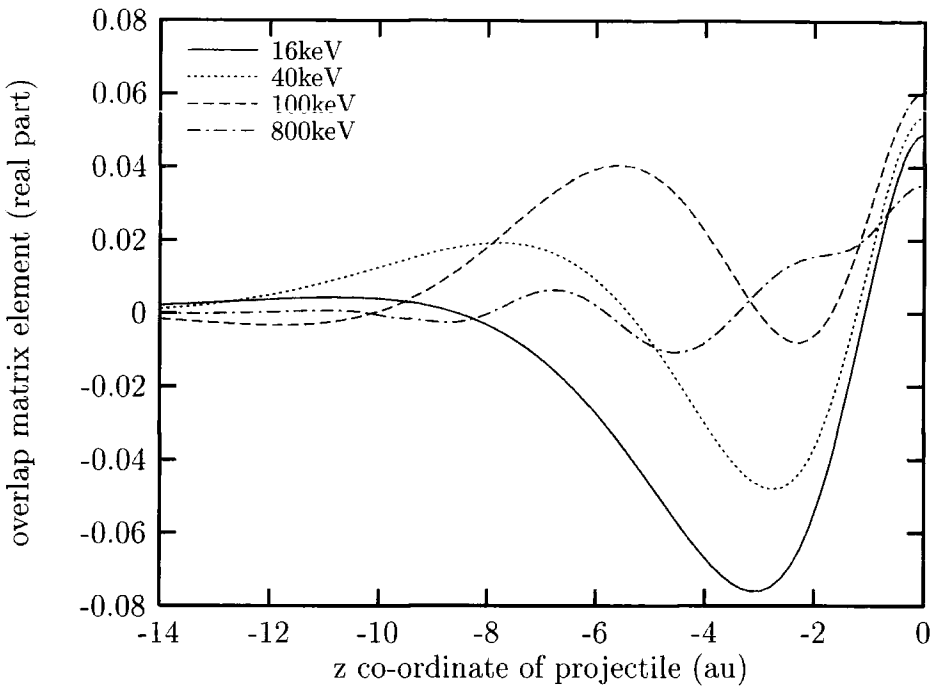

Figure 5.5: Real part of the He(1s2s^{1}S) – [He$^+$(1s) – He$^+$(1s)] Overlap Matrix Elements, for various Collision Energies (Impact Parameter=0.9au)

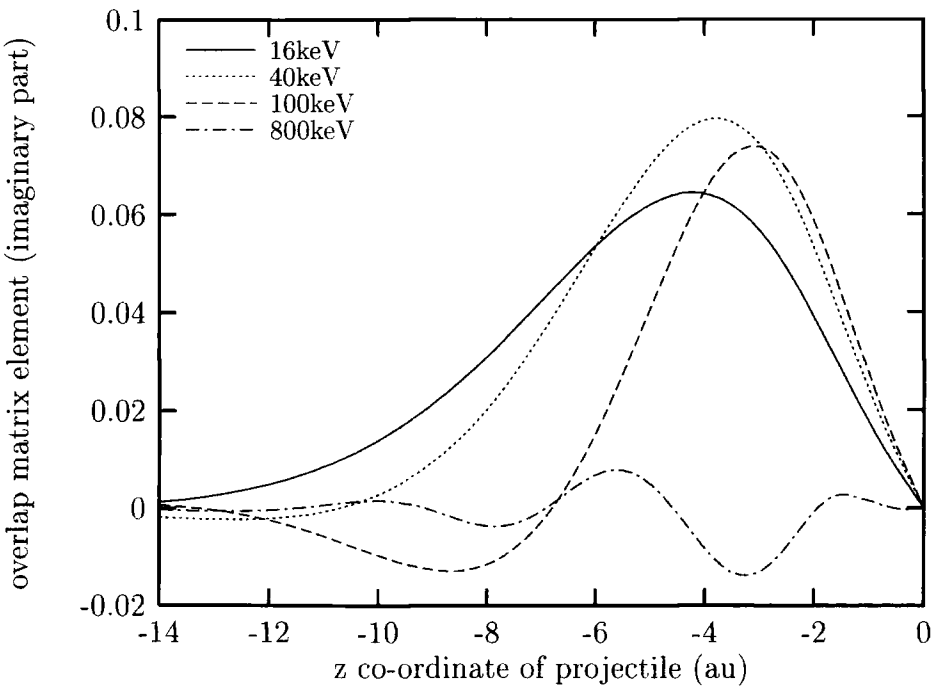

Figure 5.6: Imaginary part of the He(1s2s^{1}S)–[He$^+$(1s)–He$^+$(1s)] Overlap Matrix Elements, for various Collision Energies (Impact Parameter=0.9au)

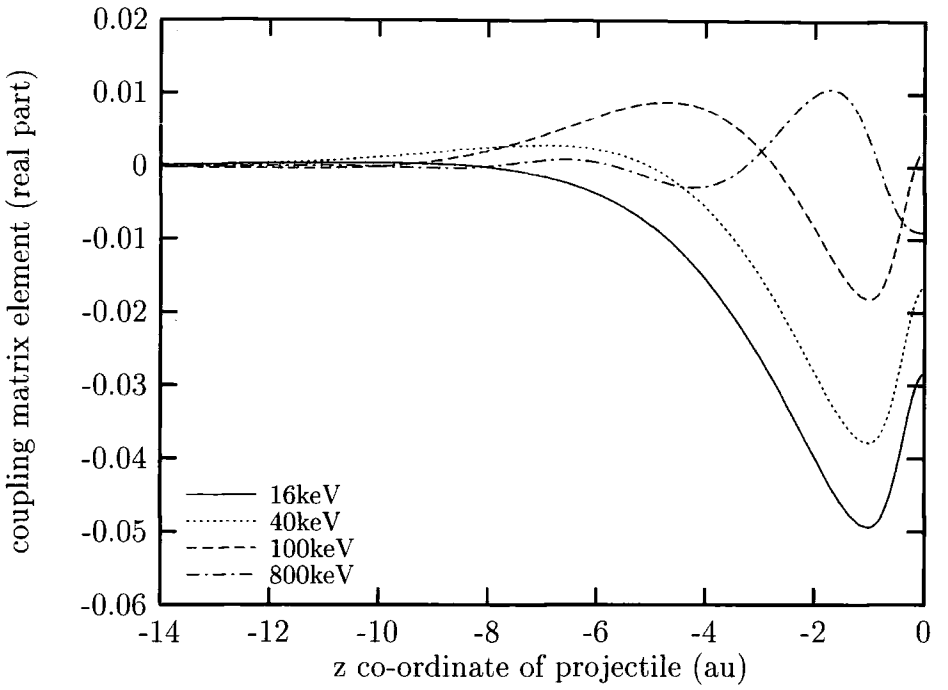

Figure 5.7: Real part of the $He(1s2s^1S) - [He^+(1s) - He^+(1s)]$ Coupling Matrix Elements, for various Collision Energies (Impact Parameter=0.9au)

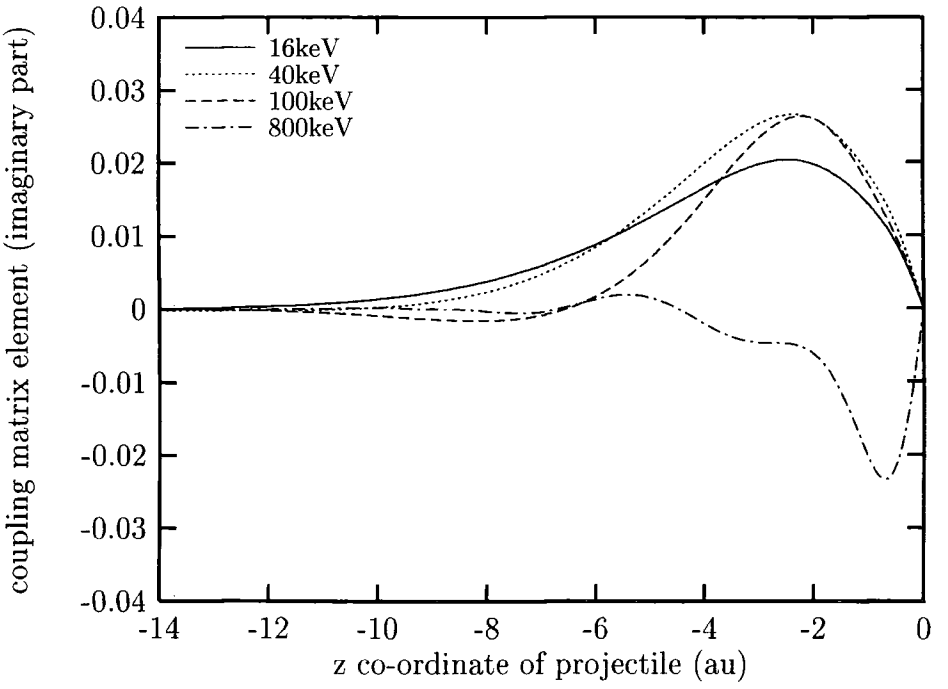

Figure 5.8: Imaginary part of the $He(1s2s^1S) - [He^+(1s) - He^+(1s)]$ Coupling Matrix Elements, for various Collision Energies (Impact Parameter=0.9au)

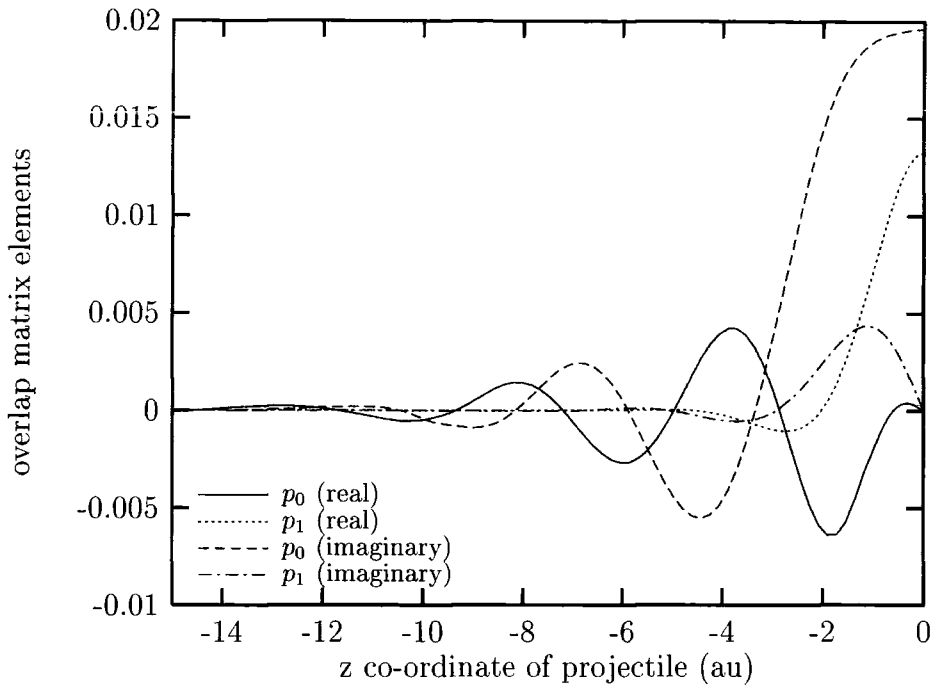

Figure 5.9: He($1s2s^1S$) – [$He_t^+(1s) - He_p^+(2p)$] Overlap Matrix Elements (Collision Energy=800keV, Impact Parameter=0.9au)

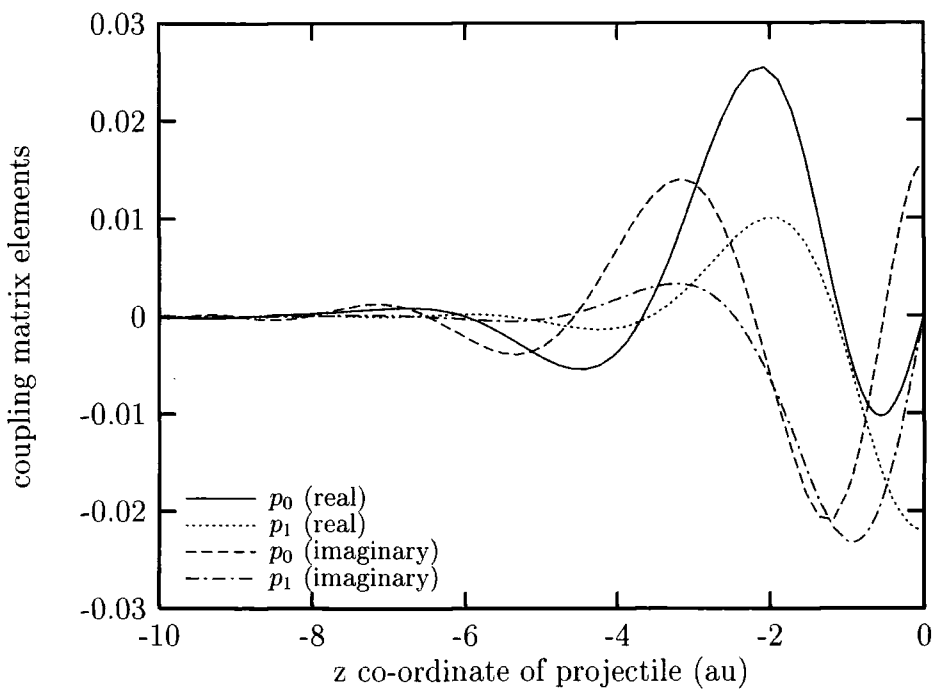

Figure 5.10: He($1s2s^1S$) – [$He_t^+(1s) - He_p^+(2p)$] Coupling Matrix Elements (Collision Energy=800keV, Impact Parameter=0.9au)

5.3.4 Convergence of Cross-Sections

It was important to confirm that the calculated cross-sections were stable with respect to the various approximations introduced in the many stages leading to the final result. The measures used to test convergence are discussed in the following sections.

Numerical Integrations for the Evaluation of Matrix Elements

The multiple integrations used to evaluate the two-centre matrix elements require a numerical solution (section 3.2). The number of integrand evaluations used may affect the integral. All of the calculations performed used 12 point Gauss-Laguerre quadrature and 16 point Gauss-Legendre quadrature. A limited number of test calculations was performed with 30 and 32 point quadrature respectively. The matrix elements were found to be unaffected (to machine single precision accuracy).

Point Separation and Interpolation

Matrix elements tend to change more rapidly with respect to z at small z. For this reason more nodes are needed at small z for a reliable interpolation. Piecewise Chebyshev interpolation was used (section 3.3) This method of interpolation does not guarantee continuity of the first derivative of the matrix elements at the endpoints of each section. These discontinuities are one of the causes of unitarity errors. In order to keep these errors to a minimum few ranges were used and hence few intersections. Relatively high order (order 9) Chebyshev interpolation was used to ensure enough points were selected. High order Chebyshev is more stable than other polynomial interpolation and copes well with slowly varying and highly oscillatory functions. Extra points were used to test the reliability of point selection.

Impact Parameter Selection

The integration of final occupation amplitudes over impact parameter theoretically takes place from $b = 0$ to $b = \infty$. By inspecting the occupation amplitudes for large values of impact parameter a practical upper limit was set (120 au), beyond which the contribution to the integral was assumed to be negligible. The reason why this upper limit needs to be so large is solely due to the large coupling between the states He(1s2s) and He(1s2p) (section 5.3.6) The numerical integration of the occupation amplitudes is performed using the Gill-Miller algorithm (section 3.5.1). The occupation amplitudes evaluated for a finite number of chosen impact parameters are interpolated using a cubic function, before integrating. The choice and number of impact parameters must be such that the interpolation, and hence the resulting cross-section is stable. Four intersecting sets of 24 impact parameters were used. More impact parameters were selected for smaller values of b since this is where the occupation amplitudes were in general more significant in magnitude and oscillatory in behaviour. Cross-sections calculated with each set or combinations of the sets could be compared. Figure 5.11 shows final cross-sections for excitation and transfer from the singlet metastable state. The labelled curves are the cross-sections evaluated by integrating over all 96 impact parameters, the other curves are for 24 and 72 impact parameters. This figure shows that the cross-sections are stable with respect to the choice and number of impact parameters used.

Trajectory Length

In the close-coupling method occupation amplitudes are integrated from initial values at time $t = -\infty$ to yield final occupation amplitudes at time $t = +\infty$. Some finite value of t (or equivalently z) must be chosen for the numerical integration, beyond which all matrix elements are negligible and occupation amplitudes are

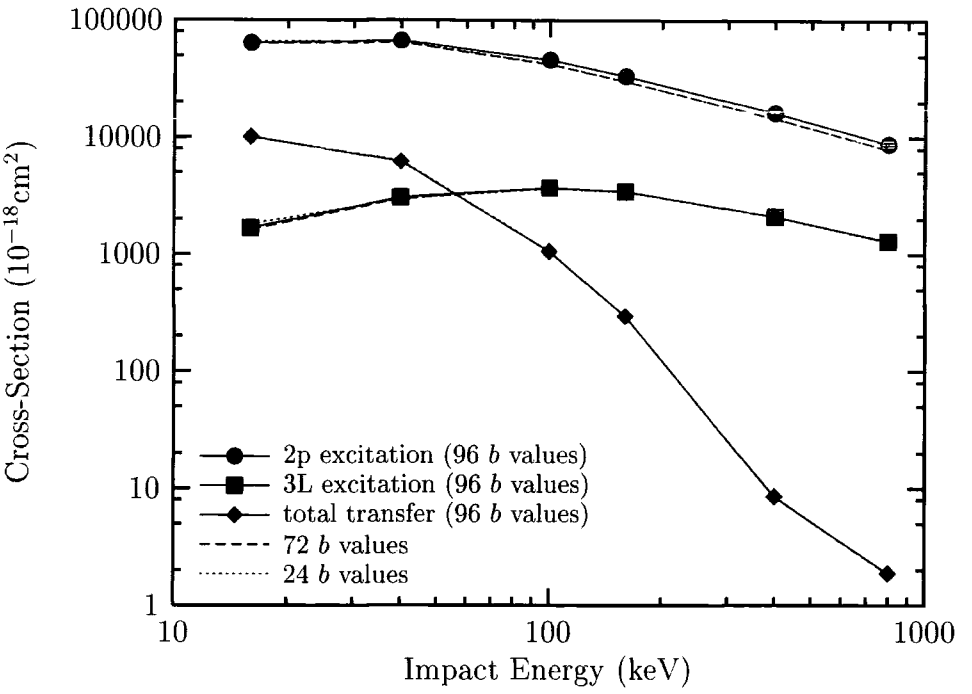

Figure 5.11: Cross-Sections for He^{2+} – He(1s2s^{1}S) collisions using 96 channels. Calculated using a total of 24, 72 and 96 impact parameters.

unchanged. The final occupation amplitudes for the state He(1s2p) are the most significant and extend out to an impact parameter of about 100au. Likewise one would expect the collision trajectory length to have an effect if it is shorter than about 100au. Figure 5.12 shows that the final occupation amplitudes for the state He(1s2p^{1}P) are unaffected when the total trajectory length is increased from 240au to 340au.

Basis Functions

Up to 96 basis functions were used, these are listed in section 5.3.2. Convergence with respect to the choice of basis is system dependent and will be discussed for each system in sections 5.3.5, 5.3.7 and 5.3.8.

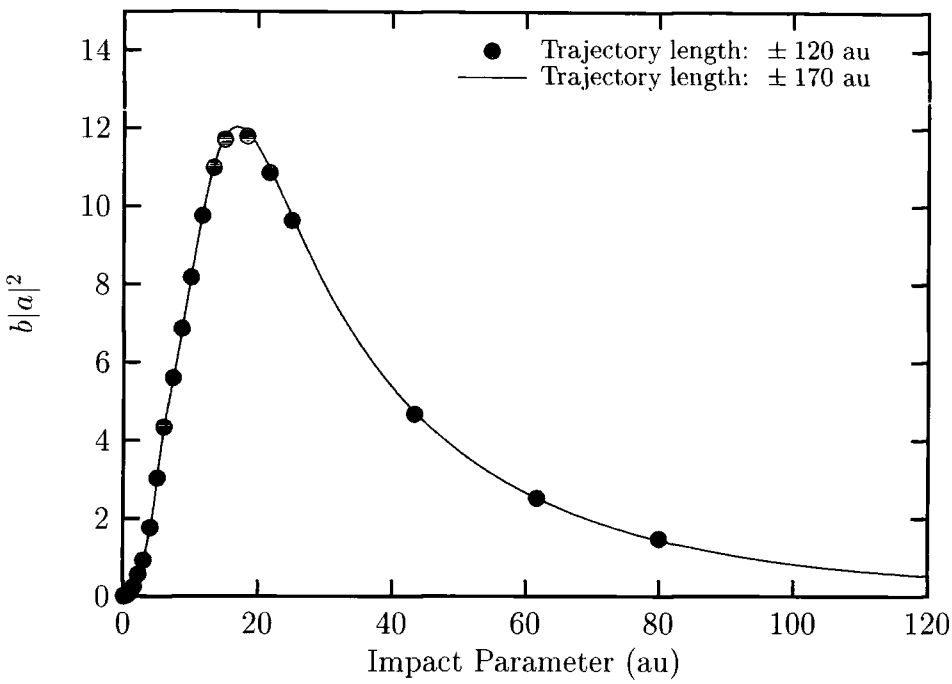

Figure 5.12: Weighted probabilities for the state He(1s2p^{1}P) using different trajectory lengths

5.3.5 Charge-Transfer from He(1s1s^{1}S) to He^{2+}

Cross-sections for excitation and one-electron charge transfer from He(1s1s^{1}S) to He^{2+} were calculated. A 96 channel basis was used for this calculation, the same as was used for the initially excited singlet state He(1s2s^{1}S) (see section 5.3.2). Cross-sections for excitation to the state He(1s2s^{1}S) and He(1s2s^{1}P) are shown in figures 5.13 and 5.14 respectively, on page 92. Total one-electron charge transfer cross-sections are shown in figure 5.15. The results are compared to those of Fritsch[16] who also used the semiclassical close-coupling method, with two-electron basis states. The maximum in the total one-electron transfer cross-section at about 150keV is observed because at this energy the projectile velocity is approximately the same as the velocity associated with the orbiting electrons.

At the lowest collision energy the current excitation cross-sections are in very poor agreement with the data of Fritsch. The other cross-sections can only be

described to be in qualitative agreement. The differences are due to an inadequacy of the current basis. Fritsch included two-electron transfer channels. The most important of these is the resonant double-transfer channel (5.3). Cross-sections to this channel are extremely large, especially at low energy (see figure 5.16 on page 93).

$$\mathrm{He_t}(1s1s^1S) + \mathrm{He_p^{2+}} \longrightarrow \mathrm{He_t^{2+}} + \mathrm{He_p}(1s1s^1S) \tag{5.3}$$

Neglecting this significant channel in the current calculation leads to this poor agreement.

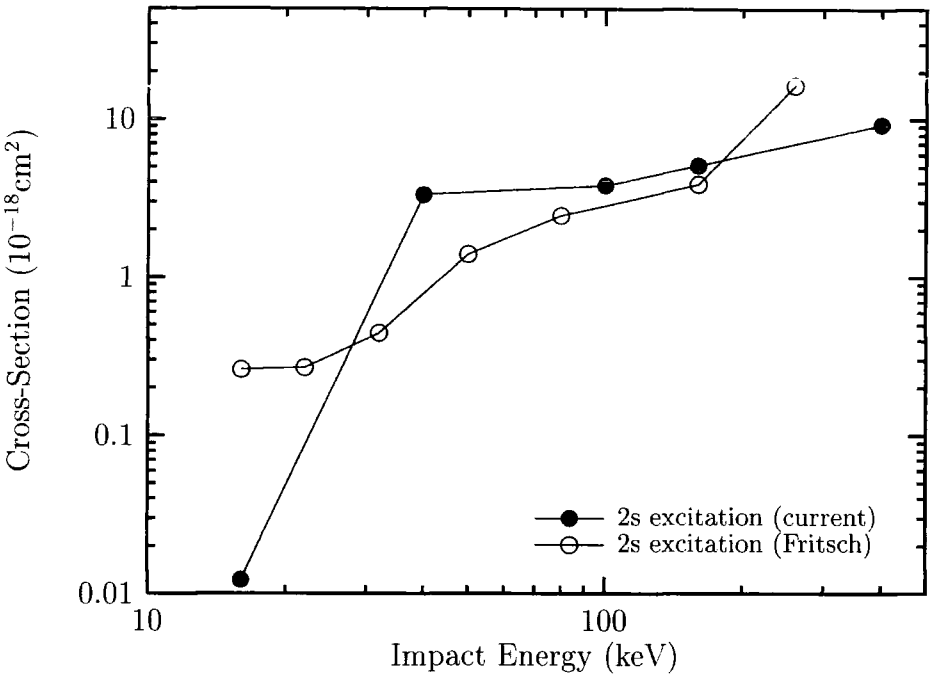

Figure 5.13: He^{2+} – He($1s1s^1S$) collision cross-sections for exitation to the state He($1s2s^1S$), current 96 channel basis, comparison to Fritsch's 59 channel basis[16]

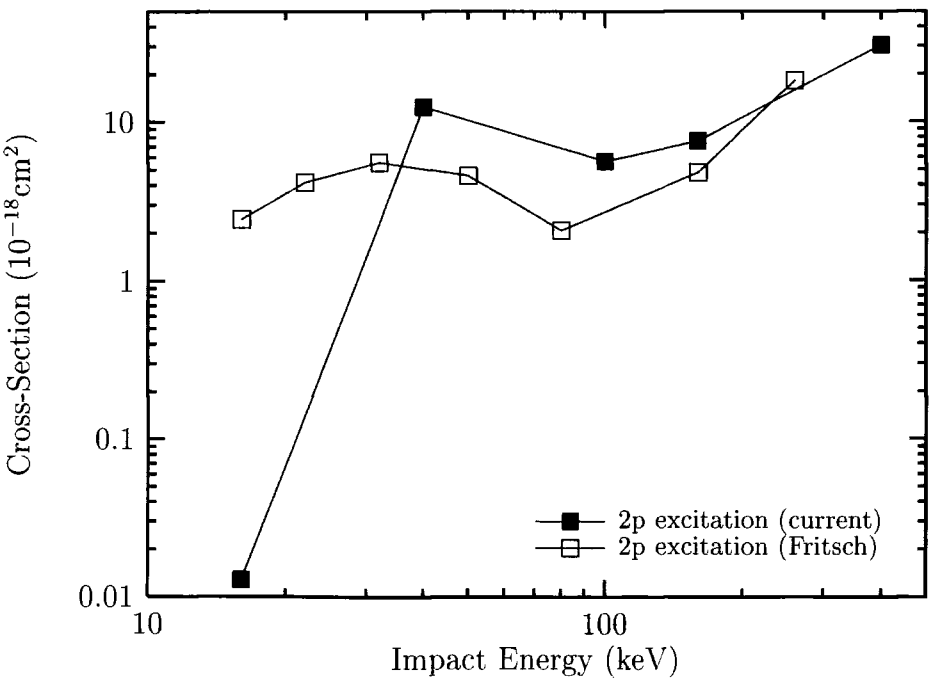

Figure 5.14: He^{2+} – He($1s1s^1S$) collision cross-sections for excitation to the state He($1s2p^1P$), current 96 channel basis, comparison to Fritsch's 59 channel basis[16]

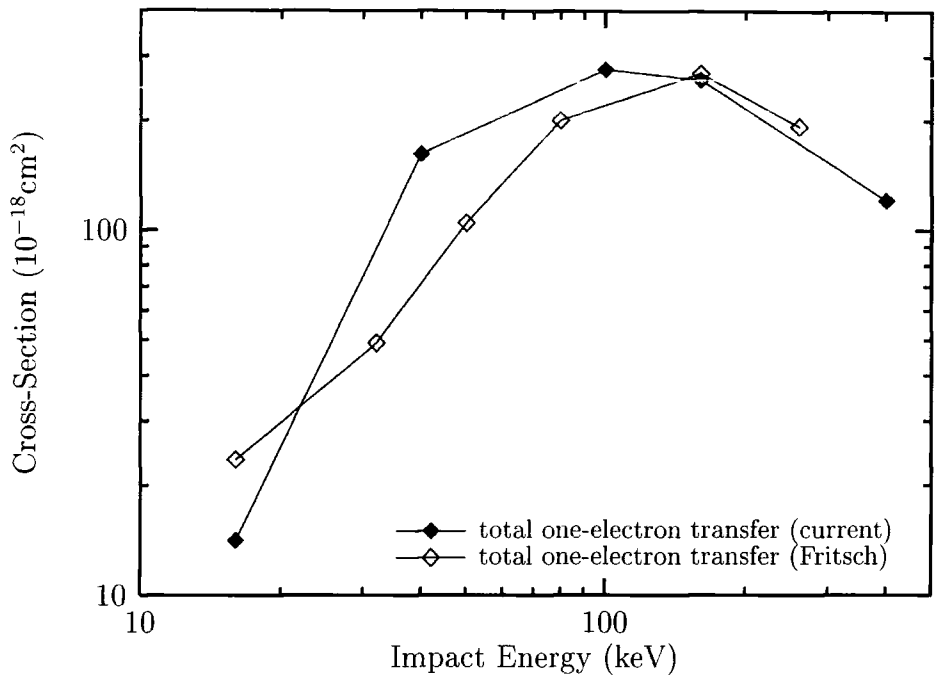

Figure 5.15: $He^{2+} - He(1s1s^1S)$ collision cross-sections for total one-electron charge transfer, current 96 channel basis, comparison to Fritsch's 59 channel basis[16]

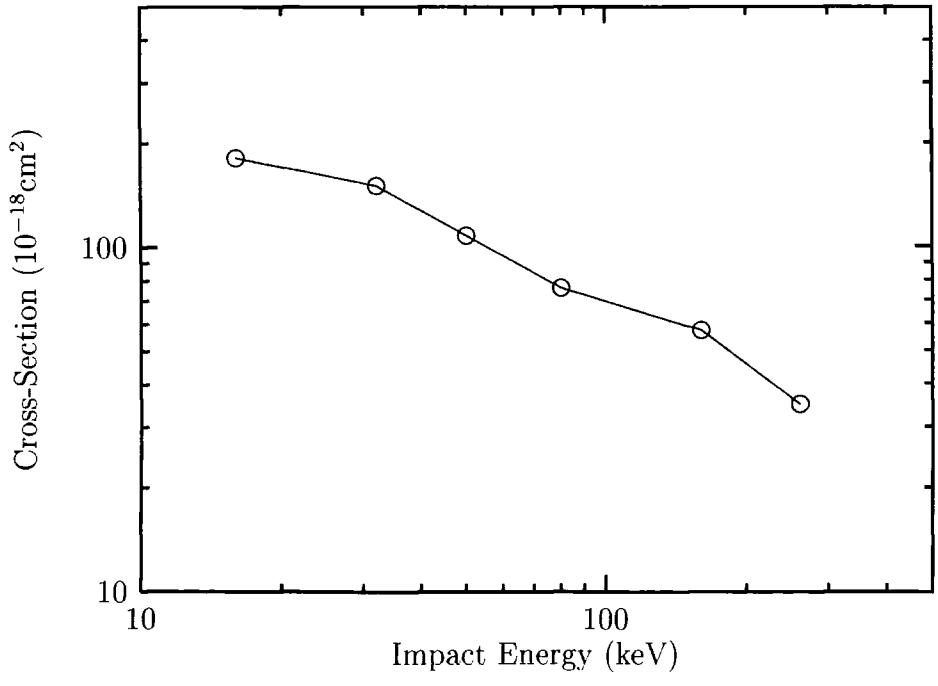

Figure 5.16: He^{2+} – $He(1s1s^1S)$ collision cross-sections for resonant two-electron charge transfer[16]

5.3.6 Occupation Amplitudes

The amplitudes in the plots in this section are scaled with the impact parameter. The area under the resulting $b|a|^2$ curve gives a true representation of the final cross-section. The cross-section in units of cm^2 is given as (5.4).

$$\sigma(\mathrm{cm}^2) = Area(\mathrm{au}^2) \times 2\pi \times 2.80 \times 10^{-17} \tag{5.4}$$

Excitation across the small energy gap from He($1s2s^3S$) to He($1s2p^3P$) results in very large occupation amplitudes (figure 5.17)

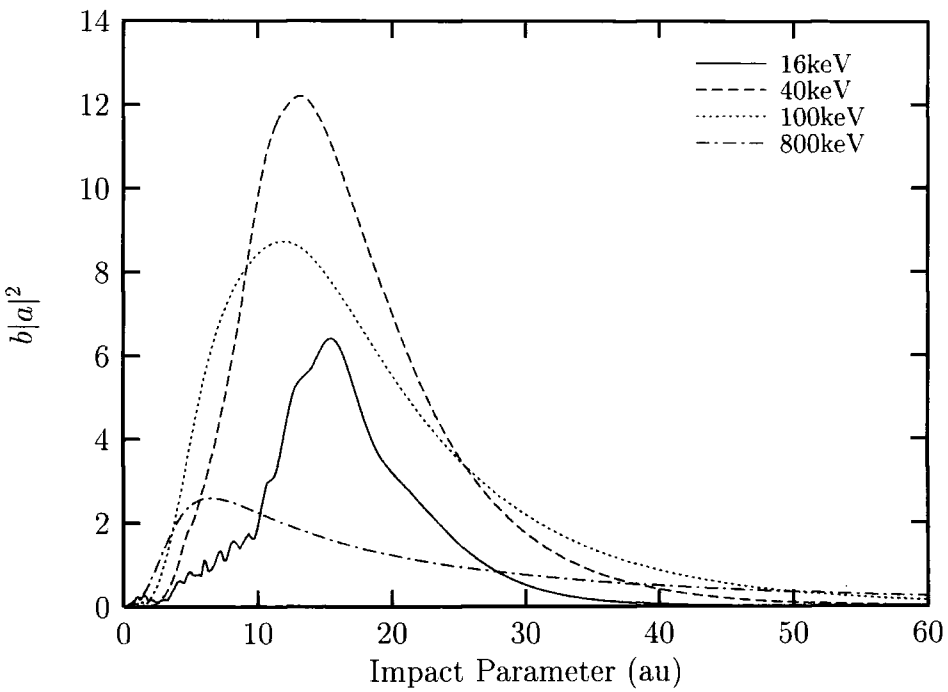

Figure 5.17: Weighted probabilities for excitation to the state He($1s2p^3P$) from He($1s2s^3S$) as a function of Impact Parameter, various Collision Energies

At low collision energy the amplitude oscillates for small impact parameters. This amplitude would not oscillate in isolation, it is in this region where there are many competing processes (namely charge transfer) leading to this behaviour. At higher energies the amplitudes follow smoother curves and extend out to impact parameters of about 100au.

The weighted probabilities for excitation to He($1s3s^3S$) are shown in figure 5.18. These are significantly smaller than those for the He($1s2p^3P$) state. The oscillatory behaviour is also much more pronounced since the amplitudes for this channel are similar in magnitude to the transfer channels, except at higher energies.

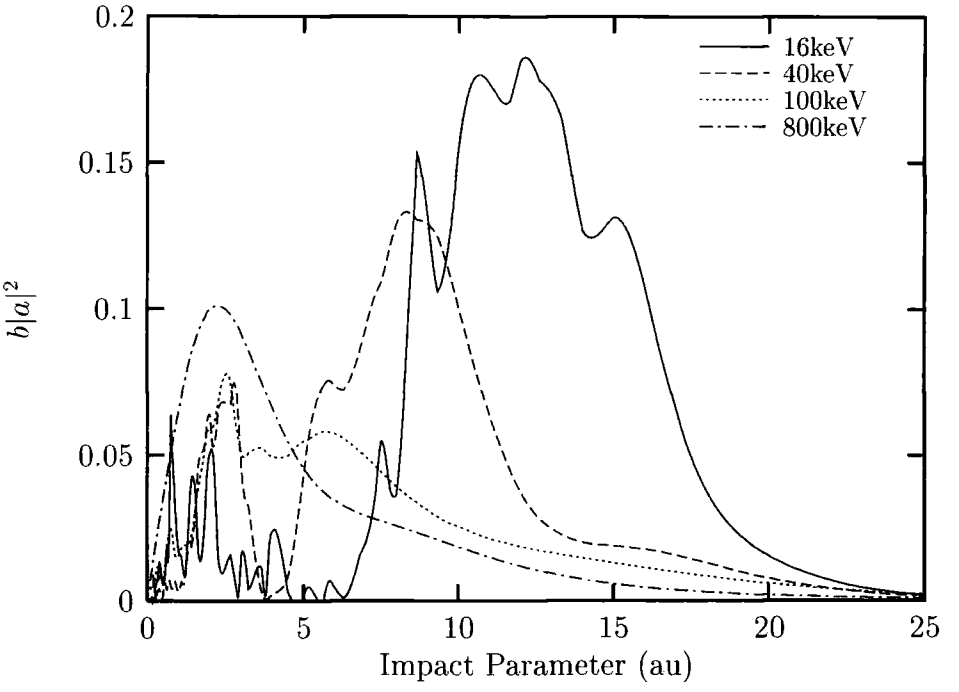

Figure 5.18: Weighted probabilities for excitation to the state He($1s3s^3S$) from He($1s2s^3S$) as a function of Impact Parameter, various Collision Energies

The weighted probabilities for transfer to the states $He_p^+(1s)$ and $He_p^+(4s)$ are shown in figures 5.19 and 5.20 respectively on page 96. These amplitudes are naturally oscillatory with respect to b because of the influence of the translation factors. The area under the final weighted probability plots for the transfer states is very much dependent on the collision energy. The charge exchange cross-sections decrease very rapidly as collision energy increases. Also the cross-section to the $He_p^+(4s)$ state is significantly larger than that to the $He_p^+(1s)$ state. This can be explained by considering the energy difference between initial and final states.

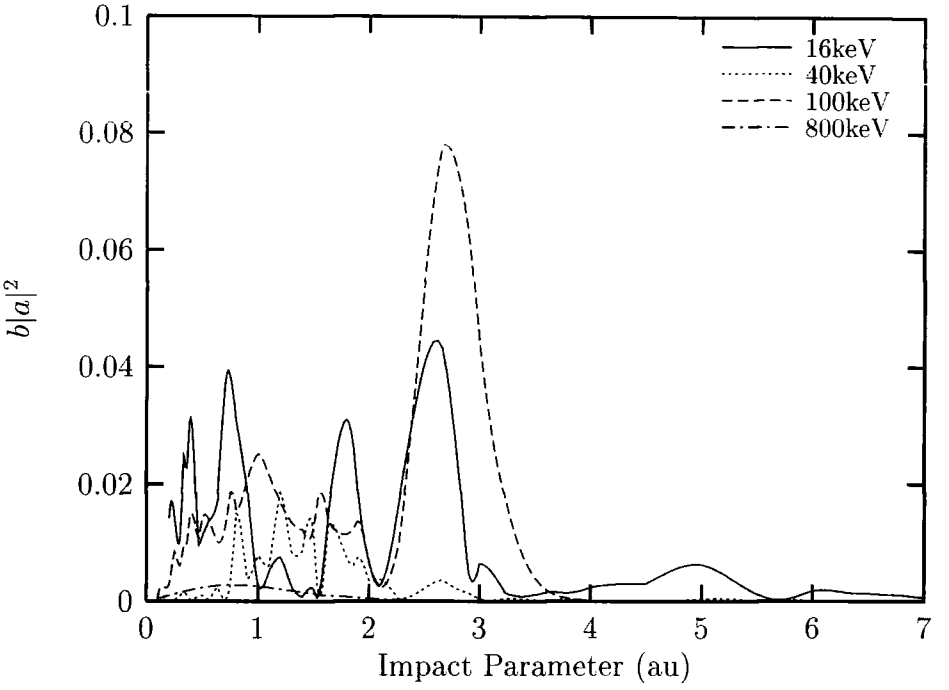

Figure 5.19: Weighted probabilities for transfer to $He^+(1s)$ from $He(1s2s^3S)$ as a function of Impact Parameter, various Collision Energies

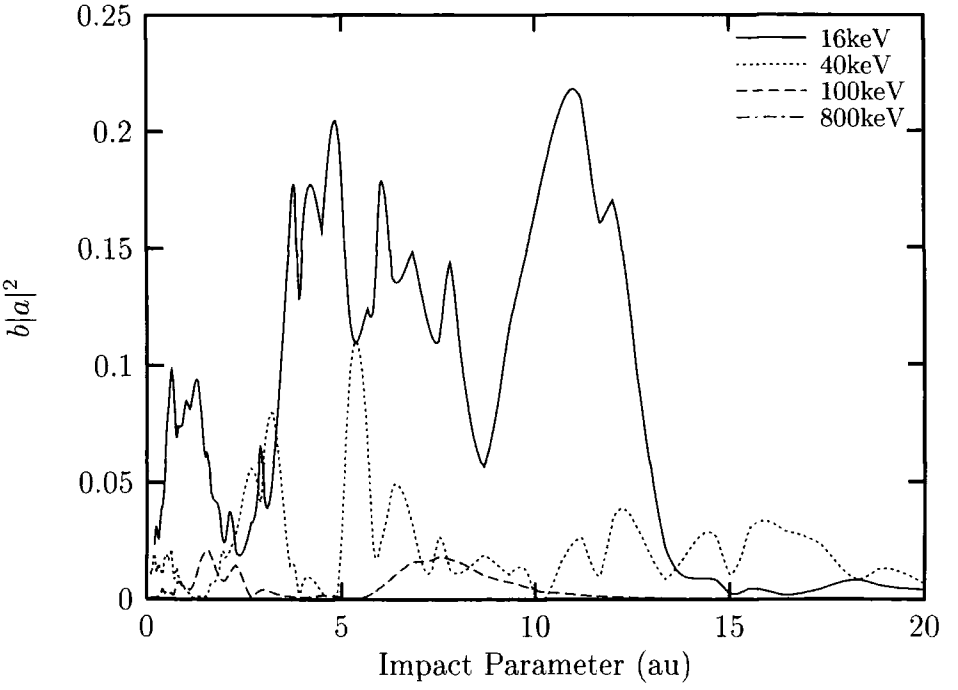

Figure 5.20: Weighted probabilities for transfer to $He^+(4s)$ from $He(1s2s^3S)$ as a function of Impact Parameter, various Collision Energies

The total binding energy of the initial He($1s2s^3S$) is -2.174au and that of the final [$He_p^+(4s) - He_t^+(1s)$] state is -2.125au. The binding energy of the [$He_p^+(1s) - He_t^+(1s)$] state is -4au, considerably further away.

5.3.7 Charge-Transfer from the Singlet-State: He($1s2s^1S$)

Fritsch performed a one-electron calculation for excitation and charge transfer from the state He($1s2s^1S$) in collision with He^{2+}[16]. The calculations presented here also use the semiclassical close-coupling method but use full two-electron basis states. A total of 96 channels were used, these are listed in section 5.3.2. Subsets of these channels were used as a test of the adequacy of the basis.

Figure 5.21 compares cross-sections calculated with 55 channels and 70 channels. The 55 channel basis includes bound two-electron target states (35 channels) and transfer states up to, and including, $He^+(n = 4)$ (20 channels). The 70 channel basis also includes transfer to $He^+(n = 5)$. Excitation cross-sections are barely affected but there is a slight increase in the total charge transfer cross-section.

Figure 5.22 shows what happens to the cross-sections when the 26 pseudostates are also included. These affect the transfer channels and the $n = 3$ excitation channels. The lower lying $2p$ channel is barely affected. The cross-sections from the 96 channel basis at a collision energy of 16keV are in fact spurious. The inclusion of the pseudostates causes serious unitarity errors at this collision energy, satisfactory final occupation amplitudes were only available for a few impact parameters. At all other energies the unitarity errors were within 1%.

Charge transfer specifically to the $He^+(n = 4)$ and $He^+(n = 5)$ are compared to the results of Fritsch in figures 5.23 and 5.24 respectively. The best agreement is found at intermediate energy. The differences at high energy may be accounted for by the fact that the cross-sections are extremely small compared to the excitation cross-sections. At low energy the current excitation cross-sections are significantly

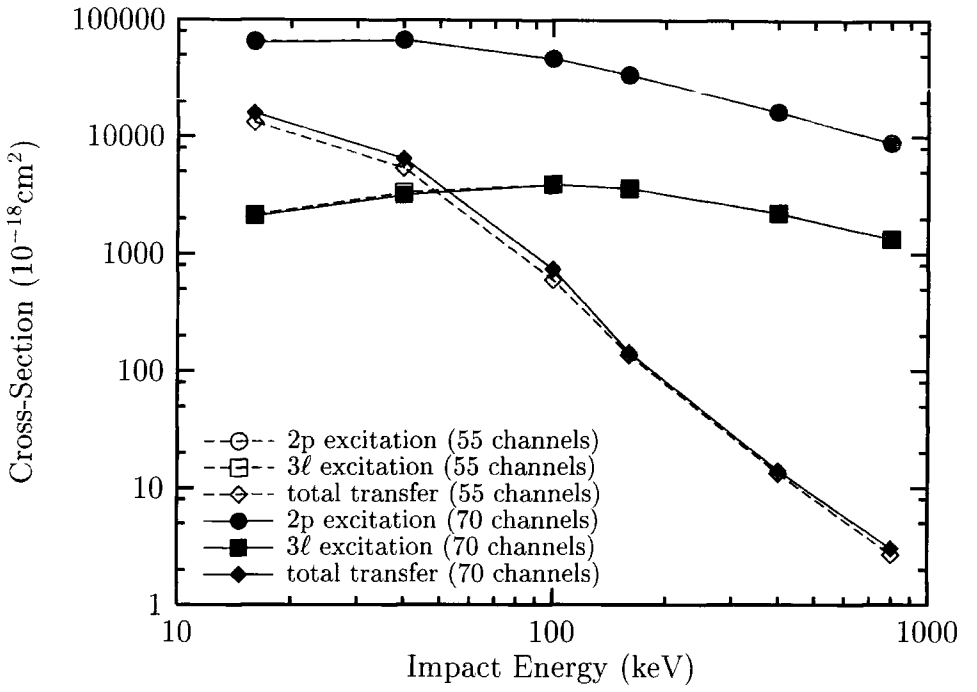

Figure 5.21: He^{2+} – He(1s2s^{1}S) collision cross-sections for excitation and one-electron charge transfer, comparison between 55 and 70 channel bases

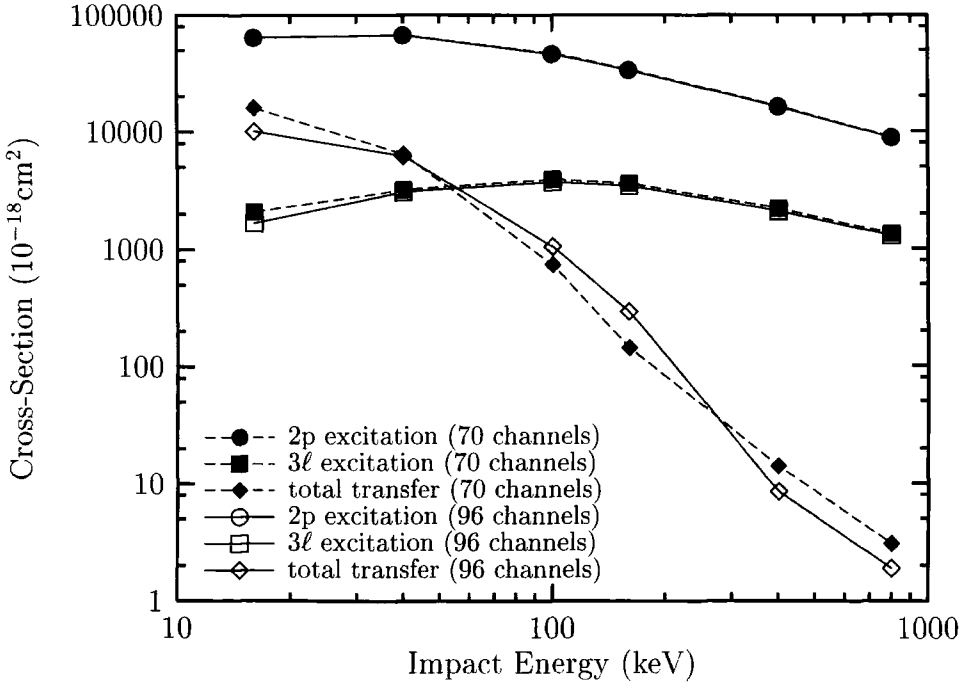

Figure 5.22: He^{2+} – He(1s2s^{1}S) collision cross-sections for excitation and one-electron charge transfer, comparison between 70 and 96 channel bases

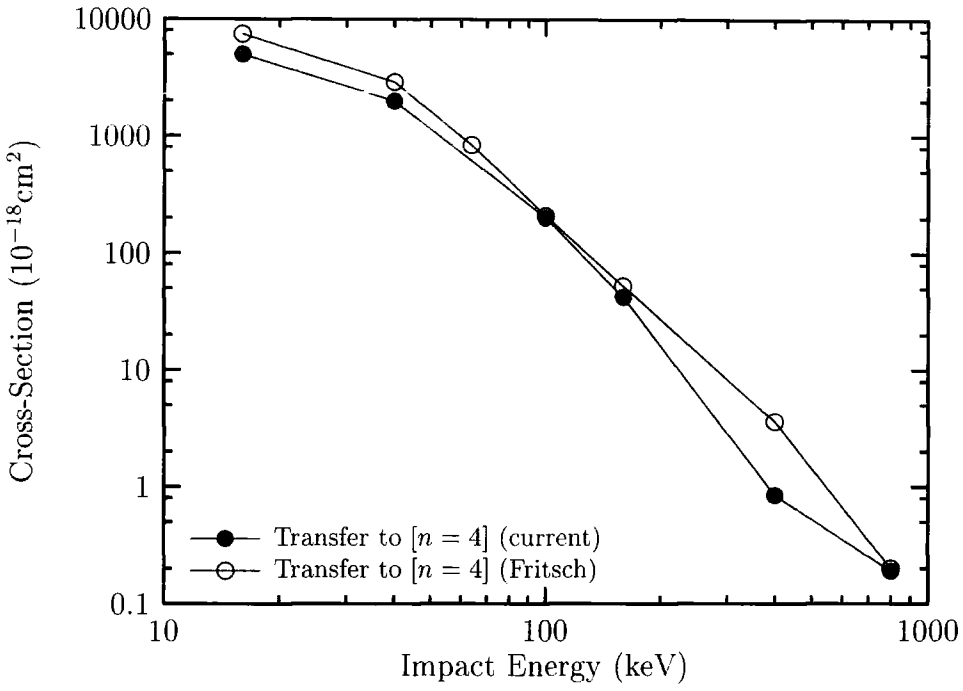

Figure 5.23: He^{2+} – He($1s2s^1S$) collision cross-sections for transfer to the states $He^+(4\ell)$, comparison to Fritsch[15]

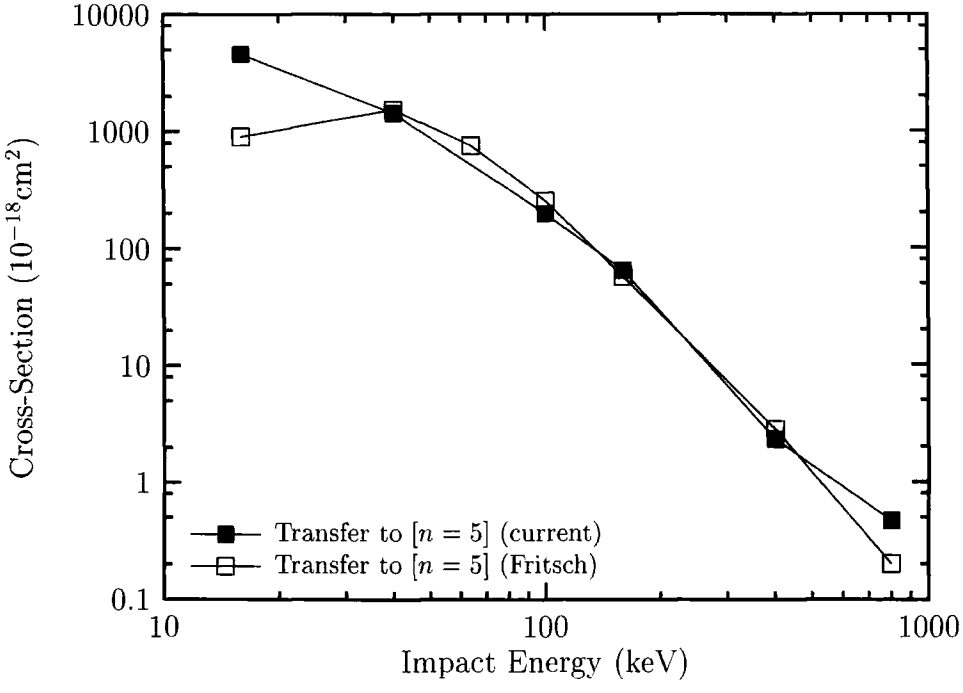

Figure 5.24: He^{2+} – He($1s2s^1S$) collision cross-sections for transfer to the states $He^+(5\ell)$, comparison to Fritsch[15]

greater than those of Fritsch. The one-electron model may be inadequate to describe these excitation channels.

Figure 5.25 shows current total charge transfer, excitation and pseudostate cross-sections compared to Fritsch's data. In this figure the cross-sections at a collision energy of 16keV are for the 70 channel basis, whereas all other cross-sections use the 96 channel basis. The pseudostate cross-section is shown to be small at the lowest energy, so their omission can justified.

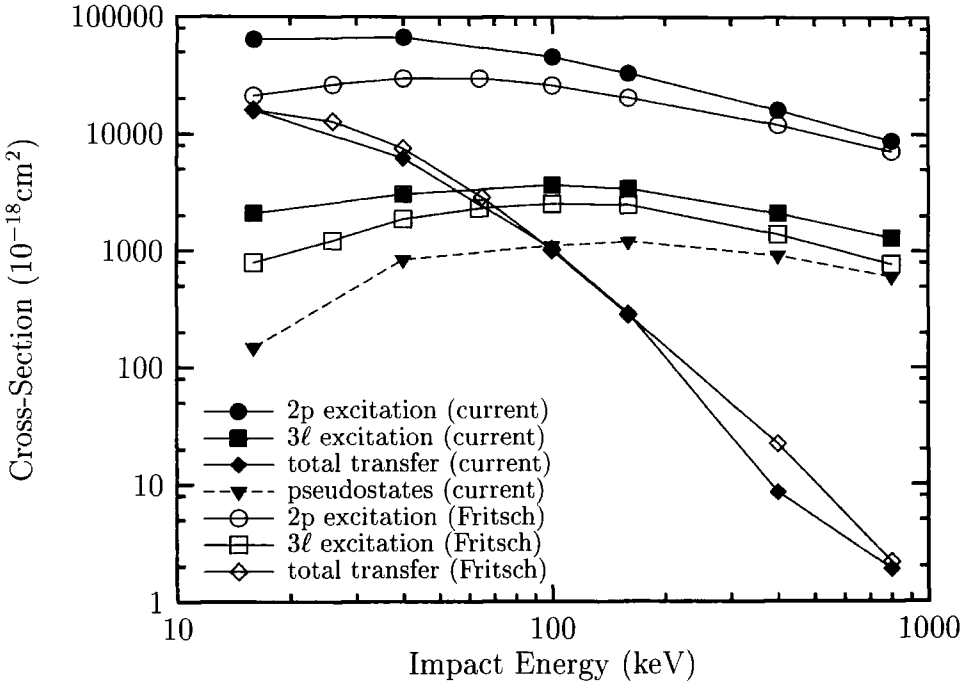

Figure 5.25: He^{2+} – He(1s2s^{1}S) collision cross-sections for total transfer and excitation, comparison to Fritsch[16]

5.3.8 Charge-Transfer from the Triplet-State He(1s2s^{3}S)

Calculations are presented for excitation and charge transfer from the initial state He(1s2s^{3}S) in collisions with He^{2+}. As with the singlet case a total of 96 basis states were used. Convergence with respect to the basis is shown in figures 5.26 and 5.27. Here there are only 34 two-electron bound states on the target, which together with the 20 channels for transfer up to $He^+(n = 4)$ makes up the 54 state

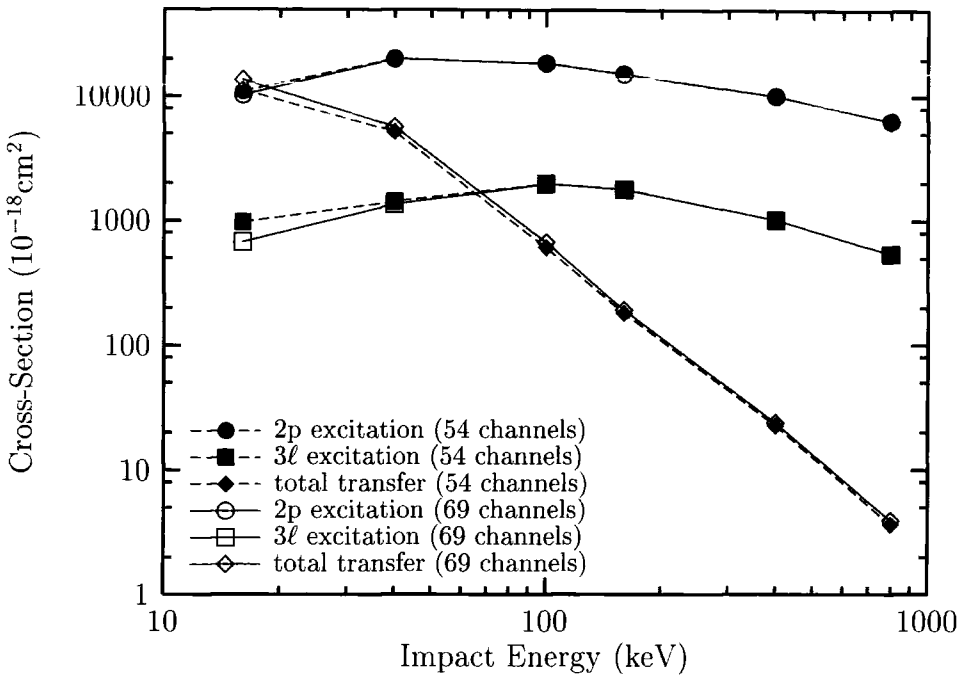

Figure 5.26: He^{2+} – He(1s2s^{3}S) collision cross-sections for excitation and one-electron charge transfer, comparison between 54 and 69 channel bases

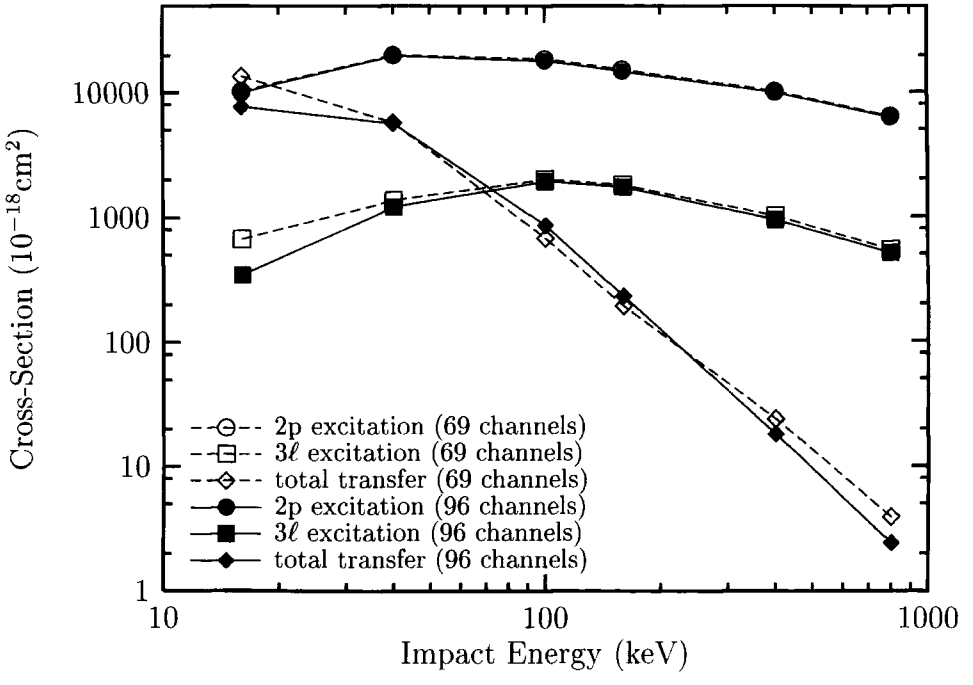

Figure 5.27: He^{2+} – He(1s2s^{3}S) collision cross-sections for excitation and one-electron charge transfer, comparison between 69 and 96 channel bases

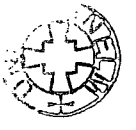

basis. The 69 channel basis also includes the $He^+(n = 5)$ transfer states. The 96 channel basis also includes the pseudostates. Again the inclusion of pseudostates caused unitarity errors at a collision energy of 16keV.

Cross-sections from the initial singlet and triplet states are compared in figure 5.28. All cross-sections from the triplet state are found to be smaller than those from the singlet. The cross-sections for excitation are especially different, and increasingly so at lower collision energies. The most likely explanation for this is simply that the $He(1s2s^3S)$ ground state is more bound than the $He(1s2s^1S)$ state, indeed the energy gap for excitation to the nearest p-state is a factor of two larger.

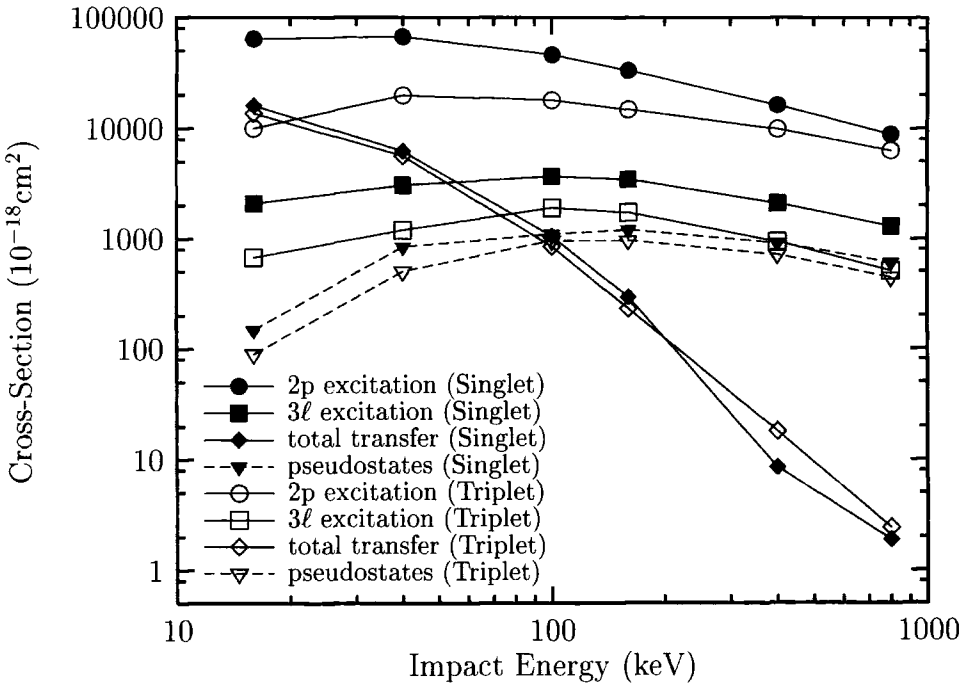

Figure 5.28: He^{2+} – He collision cross-sections for excitation and total charge transfer from the initial metastable state, comparison between singlet and triplet

5.4 468.5nm Emission

The cross-section for the emission of 468.5nm light as a result of the collisions between alpha particles and metastable helium atoms can be calculated from the

charge transfer cross-sections to the $He^+(n = 4)$ level and the branching ratios for subsequent decay (figure 5.29). [12]

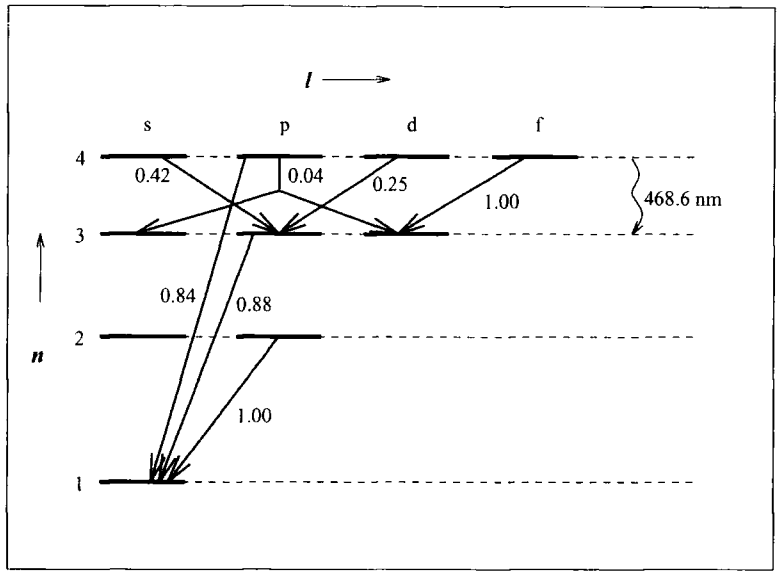

Figure 5.29: Schematic of the He^+ energy levels, with branching ratios[12]

The cross-sections for the 468.5nm emission are compared to those of Fritsch in figure 5.30 and are also shown in table 5.5. The differences between the emission cross-sections is a direct result of the differences in the state selective charge transfer cross-sections discussed in the previous two sections.

Collision energy (keV)	current calculation Triplet	Singlet	Fritsch[16] Singlet
16	1936	2453	3722
40	729.1	832.5	1148
100	44.09	80.32	45.3
160	9.063	18.88	11.6
400	0.365	0.218	0.655
800	0.073	0.099	0.046

Table 5.5: Cross-sections for charge transfer to $He^+(n = 4)$ and subsequent decay to $He^+(n = 3)$, comparison between triplet, singlet and the data of Fritsch[16]

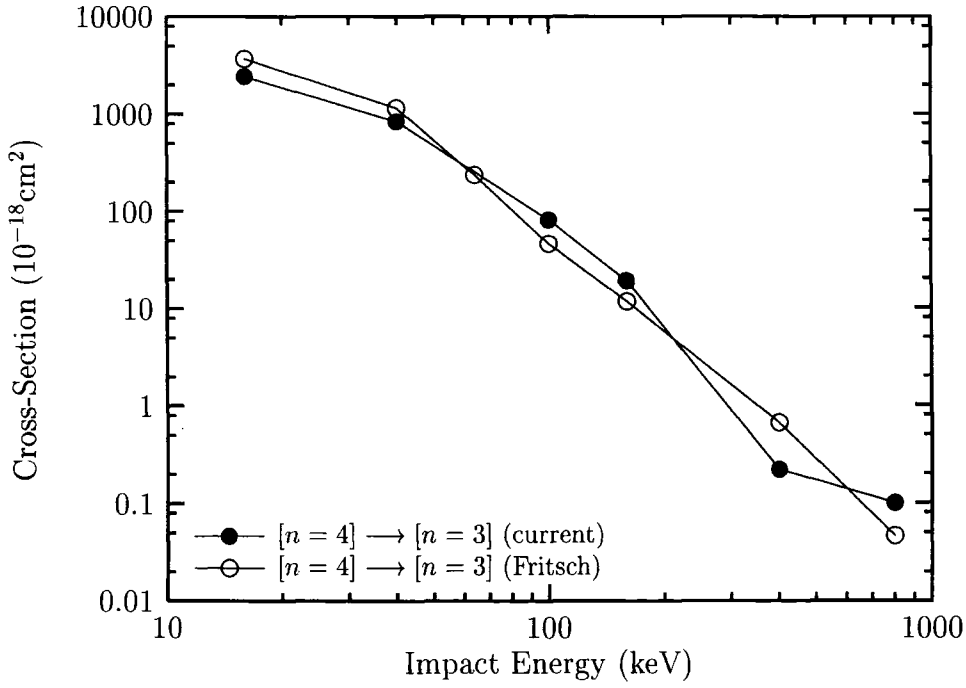

Figure 5.30: $He^{2+} - He(1s2s^1S)$ collision cross-sections for transfer to the states $He^+(4\ell)$ and subsequent decay to $[n = 3]$, comparison to Fritsch

Chapter 6

Conclusion

Charge transfer and excitation cross-sections have been calculated for collisions between alpha particles and helium atoms in initially excited states.

Atomic data of this type is needed for the analysis of spectroscopic measurements used to diagnose fusion plasmas. The $He^{2+} - He$ system is especially important. Neutral beam injection is used in the JET fusion device for both heating and as a probe of the hot central region of the plasma. Usually refuelling deuterium beams are used but occasionally helium beams are substituted. These beams place helium atoms, and subsequently nuclei, in the central region of the plasma, simulating the conditions when alpha particles are created from the fusion of deuterium and tritium. As the helium atoms enter the plasma they undergo ionization and charge exchange by collisions with the plasma particles. Collisions also occur with the previously injected alpha particles, which have become thermalized. Charge transfer to the $He^+(n = 4)$ state leads to visible radiative decay.

Charge transfer from the ground state of helium atoms has been well studied. The neutral beam in the JET device is known to contain a fraction of helium atoms in initially excited states. Charge transfer from the states $He(1s2s^1S)$ and $He(1s2s^3S)$ have not been so well studied. Fritsch[16] has addressed the singlet case with a one electron model. He found that cross-sections to $He^+(n = 4)$ are substantially larger from this state than from the ground state because of the near

resonance.

The current calculations have been performed using the semiclassical close-coupling method with two-electron atomic orbital basis functions. A total of 96 channels were used, including; two-electron bound states of the target up to the level of ($n = 5$); single electron charge transfer to states of the projectile up to $He^+(n = 5)$, with the target electron remaining in the ground state; and continuum pseudostates centred on the target. The charge transfer states included electron exchange and translation factors. The inclusion of pseudostates at the lowest energy caused unitarity errors, which were otherwise not present. Since the inclusion of pseudostates to represent the continuum is only necessary at higher energies, they were omitted.

The results of the calculations for the singlet metastable state have been compared to the one-electron calculation of Fritsch. Although the total one-electron transfer cross-sections are generally in good agreement, there are differences in the state selective transfer. These are thought to be accountable for by considering the excitation cross-sections. The excitation cross-sections for the current calculation are significantly larger than those found by Fritsch, and especially so at low collision energy. The current excitation cross-sections are shown to be very well converged. Fritsch's one-electron model may not be sufficient for the calculation of excitation cross-sections from this state. Since calculations of this type are very much basis dependent, the inaccuracies of the excitation channel can also be reflected in the charge transfer channels.

Charge transfer and excitation cross-sections from the initial triplet metastable state are systematically lower than those from the singlet state. This is because the triplet state is more deeply bound. Although the cross-sections from the triplet state are smaller than those from the singlet they may prove to be more important because the metastable triplet state is longer lived and will therefore

have an effect on the 468.5nm spectrum deeper into the plasma.

In the current calculation there were no basis functions to represent two-electron charge transfer, one-electron transfer with simultaneous excitation of the target or capture to the continuum. It would be interesting to see if the current calculations would be affected by the inclusion of these states. If higher transfer states were included the 468.5nm emission cross-section could be modified by the effect of electrons cascading down to the $(n = 4)$ level from higher levels. Calculations with the current basis but with the electron exchange terms omitted may give some insight into the differences between the current and the one-electron calculations.

Data for charge transfer from both the singlet and triplet initial states have been presented in a form suitable for direct inclusion into the analysis database at JET.

Appendix A

Results in ADF01 format

A.1 ADF01 files for the ADAS Database

ADF01 is a strict formatting convention for data files containing charge-transfer cross-sections for ion-atom collisions. The layout of the file can be seen in sections A.1.1 and A.1.2 where the data calculated for transfer from the singlet and triplet metastable states are shown respectively.

The first line gives the colliding species and charges. Characters after a slash are comments and are ignored by the reading routines. The second line gives the number of impact energies in the next block, if this is negative the reading program knows there are no more blocks. The minimum and maximum levels of the receiving system, in this case from 1 to 5 are then given. The collision energies are given in keV/amu and the parameter alpha is read in. The parameter alpha is used to extrapolate for cross-sections to higher lying states (not given here). For each collision energy a grand total, a sub-total for a given n-shell and individual angular momentum resolved charge transfer cross-sections are given.

A.1.1 ADF01 File for Transfer from He($1s2s^1S$)

```
HE+ 2     HE+ 0 (2)  / receiver, donor (donor state index) (2)=He(1s2s1S)
    6                / number of energies
    1                / nmin
    5                / nmax
          4.00D+00 1.00D+01 2.50D+01 4.00D+01 1.00D+02 2.00D+02 / (kev/amu)
          xxxxxxxx xxxxxxxx xxxxxxxx xxxxxxxx xxxxxxxx xxxxxxxx / alpha
          1.60D-14 6.20D-15 1.05D-15 2.94D-16 8.50D-18 1.88D-18 / total
  n  l  m                                                       / partial
  1        4.38D-20 4.68D-18 2.25D-18 1.01D-18 1.70D-18 7.94D-19
  1  0     4.38D-20 4.68D-18 2.25D-18 1.01D-18 1.70D-18 7.94D-19
  2        1.67D-16 2.61D-16 2.09D-16 1.14D-16 2.34D-18 2.60D-19
  2  0     5.63D-17 1.24D-16 5.01D-17 1.12D-17 5.79D-19 1.57D-19
  2  1     1.11D-16 1.37D-16 1.59D-16 1.03D-16 1.76D-18 1.03D-19
  3        6.25D-15 2.53D-15 4.42D-16 9.00D-17 1.32D-18 1.67D-19
  3  0     1.48D-15 4.29D-16 9.72D-17 2.74D-17 4.63D-19 1.05D-19
  3  1     2.71D-15 1.29D-15 2.00D-16 3.26D-17 4.39D-19 3.47D-20
  3  2     2.06D-15 8.15D-16 1.45D-16 3.00D-17 4.16D-19 2.69D-20
  4        4.99D-15 1.98D-15 2.00D-16 4.19D-17 8.41D-19 1.90D-19
  4  0     3.53D-16 1.56D-16 1.99D-17 2.24D-18 1.81D-19 4.99D-20
  4  1     1.26D-15 4.63D-16 5.87D-17 1.11D-17 3.07D-19 2.97D-20
  4  2     1.50D-15 8.22D-16 6.93D-17 1.48D-17 2.98D-19 4.46D-20
  4  3     1.88D-15 5.43D-16 5.23D-17 1.38D-17 5.54D-20 6.58D-20
  5        4.57D-15 1.42D-15 1.96D-16 4.66D-17 2.30D-18 4.66D-19
  5  0     2.76D-16 1.62D-16 1.46D-17 6.92D-18 5.24D-19 3.91D-20
  5  1     1.10D-15 3.83D-16 6.35D-17 1.41D-17 8.81D-19 1.26D-19
  5  2     1.04D-15 3.30D-16 5.90D-17 1.24D-17 5.56D-19 1.35D-19
  5  3     1.10D-15 2.37D-16 3.84D-17 6.43D-18 2.43D-19 1.06D-19
  5  4     1.06D-15 3.04D-16 2.00D-17 6.75D-18 9.96D-20 5.99D-20
 -1 -1
C---------------------------------------------------------------------
C
C ADF01 File for transfer cross-sections to He++ from He(1s2s1S).
C Data calculated by P.Davies using the SCCC method
C
C Peter Davies Dec. 1997
```

A.1.2 ADF01 File for transfer from He($1s2s^3S$)

```
HE+ 2      HE+ 0 (3) / receiver, donor (donor state index) (3)=He(1s2s3S)
    6                / number of energies
    1                / nmin
    5                / nmax
          4.00D+00 1.00D+01 2.50D+01 4.00D+01 1.00D+02 2.00D+02 / (kev/amu)
          xxxxxxxx xxxxxxxx xxxxxxxx xxxxxxxx xxxxxxxx xxxxxxxx / alpha
          1.38D-14 5.62D-15 8.48D-16 2.30D-16 1.80D-17 2.42D-18 / total
  n  l  m                                                       / partial
  1        9.34D-20 2.58D-18 1.37D-17 1.28D-17 1.54D-18 7.00D-19
  1  0     9.34D-20 2.58D-18 1.37D-17 1.28D-17 1.54D-18 7.00D-19
  2        5.47D-16 5.12D-16 2.32D-16 6.62D-17 6.19D-18 6.60D-19
  2  0     9.71D-17 6.62D-17 6.00D-17 1.96D-17 2.59D-18 3.87D-19
  2  1     4.50D-16 4.46D-16 1.72D-16 4.66D-17 3.60D-18 2.73D-19
  3        6.29D-15 2.52D-15 2.52D-16 4.67D-17 3.44D-18 3.64D-19
  3  0     3.76D-16 9.64D-17 1.57D-17 7.11D-18 9.76D-19 1.79D-19
  3  1     3.19D-15 1.38D-15 1.54D-16 2.64D-17 1.98D-18 1.49D-19
  3  2     2.72D-15 1.04D-15 8.27D-17 1.32D-17 4.87D-19 3.59D-20
  4        3.57D-15 1.58D-15 1.55D-16 2.76D-17 1.27D-18 1.89D-19
  4  0     1.95D-16 8.14D-17 1.40D-17 3.26D-18 2.62D-19 5.99D-20
  4  1     9.47D-16 5.42D-16 8.11D-17 1.29D-17 6.39D-19 5.79D-20
  4  2     8.04D-16 3.73D-16 3.38D-17 5.61D-18 1.88D-19 3.35D-20
  4  3     1.62D-15 5.80D-16 2.65D-17 5.78D-18 1.82D-19 3.75D-20
  5        3.22D-15 1.01D-15 1.95D-16 7.68D-17 5.58D-18 5.04D-19
  5  0     7.52D-17 9.19D-17 2.69D-17 1.01D-17 1.14D-18 7.43D-20
  5  1     3.28D-16 2.37D-16 7.43D-17 3.03D-17 2.41D-18 1.52D-19
  5  2     5.69D-16 1.72D-16 4.12D-17 1.97D-17 1.54D-18 1.60D-19
  5  3     1.39D-15 3.15D-16 2.65D-17 8.75D-18 3.24D-19 7.88D-20
  5  4     8.55D-16 1.94D-16 2.62D-17 7.90D-18 1.63D-19 3.92D-20
 -1 -1
C---------------------------------------------------------------
C
C ADF01 File for transfer cross-sections to He++ from He(1s2s3S).
C Data calculated by P.Davies using the SCCC method
C
C Peter Davies Dec. 1997
```

Index

ADAS, 71

angular momentum operator, 19

aspect ratio, 59

atom, 1

atomic units, 4

axis

  internuclear, 12

  of quantization, 13

basis, 15, 77

  function, 9, 35

  Gaussian, 7, 17

  Slater, 15, 18

  Sturmian, 16

binding energy, 77

body-fixed, 13

Born approximation, 4

bremsstrahlung, 6, 52

capture, 1

charge exchange, 1, 71, 74

  spectroscopy, 67

charge-transfer, 77

Chebyshev interpolation, 46

classical approximation, 3

classical trajectory, 4

Clebsch-Gordan coefficient, 20

close-coupling method, 5

co-ordinate

  centre of mass, 11

  confocal elliptic, 26

  laboratory, 11

  prolate spheroidal, 24, 26, 31

  spherical polar, 19

collision, 1

  high energy, 4

  intermediate energy, 5

  low energy, 5

  plane, 13

  proton-helium, 75

  relativistic, 5

continuum, 23

Coulomb potential, 3

cross-section, 2, 74

  convergence, 87

Debye length, 54

detailed balance, 10
deuterium, 51
diagnostic
    density, 65
    electron temperature, 64
    impurity content, 65
    ion temperature, 64
    neutron, 65
differential cross-section, 2
differential equation, 47
direct excitation, 1
divertor, 61
divided differences, 49
Doppler broadening, 64

elastic collision, 1
electron, 1
electron cyclotron frequency, 54
electron plasma frequency, 53
electron-electron repulsion, 19, 20, 31

fission, 50
fusion, 50
    plasma, 6

Gauss-Laguerre quadrature, 44
Gauss-Legendre quadrature, 45
Gill-Miller algorithm, 48

helium ground state, 22
hydrogenic function, 21

ignition, 57
impact parameter, 10
    approximation, 11
impurities, 6
independent event model, 8
interpolation, 45
ion, 1
    distribution function, 63
ionization, 1, 36
ITER, 62

JET, 58

Laguerre polynomial, 44
Lawson criterion, 56
Legendre polynomial, 31, 45
limiter, 60

magnetohydrodynamics, 54
matrix
    coupling, 10, 23, 82
    element, 23, 26, 42, 80
      interpolation, 45
    overlap, 10, 23
Maxwell's equations, 55
metastable, 7, 77, 97, 100
Monte Carlo method, 4
multipole expansion, 20, 24

Neumann expansion, 33
neutral-beam
    attenuation, 67
    heating, 58
    injection, 6, 65
numerical integral, 44

occupation amplitude, 9, 47, 94
ohmic heating, 57
orthogonalization, 18

parallel, 38
particle flux, 63
perturbed stationary state, 5
plasma, 52
    confinement, 55
    heating, 57
    ideal, 53
    impurities, 61
plume effect, 69
probability distribution, 82
projectile, 1
proton-proton chain, 51
pseudostates, 23
PVM, 39

quantization axis, 13

radio-frequency heating, 58
resonance, 2

Schrödinger, 10
semiclassical, 5
separatrix, 61
space-fixed, 13
spherical harmonic, 18, 31
    real, 13
symmetric collision system, 1

target, 1
Thompson scattering, 64
tokamak, 58
translation factor, 14, 25
tritium, 51

unitarity, 10
    error, 48
united atom, 36
units, 4

wave-function, 9
    hydrogenic, 18
    two-electron, 17

Bibliography

[1] Abramowitz, M. and Stegun, I.M. (1965) *Handbook of Mathematical functions.* Dover Publications.

[2] Anderson, C. and Aldhous, P. (1990) *Fusion's turn again?* Nature **347**, p114.

[3] Bashkin, S. and Stoner Jnr., J.O. (1975) *Atomic energy levels and grotrian diagrams.* vol. 1, North Holland Publishing.

[4] Bates, D.R. and McCarroll, R. (1958) *Electron capture in slow collisions.* Proc.Roy.Soc. **A245**, p175.

[5] Boys, S.F. (1950) *A general method of calculation for the stationary states of any molecular system.* Proc.Roy.Soc. **A200**, p542.

[6] Bransden, B.H. and Joachain, C.J. (1983) *Physics of atoms and molecules.* Longman.

[7] Bransden, B.H. and McDowell, M.R.C. (1992) *Charge exchange and the theory of ion-atom collisions.* Oxford University Press.

[8] Dendy, R.O. (1990) *Plasma Dynamics.* Oxford University Press.

[9] Dicke, R.H. and Wittke, J.P. (1963) *Introduction to quantum mechanics.* Addison-Wesley.

[10] Errea, L.F. *et al.* (1979) *Evaluation of molecular integrals in a basis of travelling orbitals.* J.Phys.B. **12**, p69.

[11] Folkerts, H.O. *et al.* (1993) *$He^{2+} - He$ collisions: one-electron capture versus electron removal and target-ion excitation.* J.Phys.B. **26**, L619.

[12] Folkerts, H.O. *et al.* (1994) *$He^{2+} - He$ collisions: one-electron capture and target-ion excitation.* J.Phys.B. **27**, p3475.

[13] Fonck, R.J. *et al.* (1984) *Determination of plasma-ion velocity distribution via charge-exchange recombination spectroscopy.* Phys.Rev. **A29**, p3288.

[14] Forster, C. *et al.* (1988) *Total and differential cross sections for charge transfer in $He^{2+} - He^{+}$ collisions: trajectory effects.* J.Phys.B. **21**, p3941.

[15] Fritsch, W. Hahn-Meitner-Institut, Berlin. *Private communication.*

[16] Fritsch, W. (1994) *Theoretical study of electron processes in slow $He^{2+} - He$ collisions.* J.Phys.B. **27**, p3461.

[17] Fritsch, W. and Lin, C.D. (1991) *The semiclassical close-coupling description of atomic collisions: Recent developments and results.* Phys.Rep. **202**, Nos. 1 & 2.

[18] Gallaher, D.F. and Wilets, L. (1968) *Coupled-state calculations of proton-hydrogen scattering in the sturmian representation.* Phys.Rev. **169**, no.1, p139.

[19] Gerstel, U. (1996) *Numerical simulation of the Helium-II charge exchange spectrum.* Ph.D. Thesis, Ruprecht-Karls-Universität, Heidelberg.

[20] Gerstel, U. *et al.* (1997) *Quantitative simulation of non-thermal charge-exchange spectra during helium neutral beam injection.* Plasma Phys. Control. Fusion **39**, p737.

[21] Gill, P.E. and Miller, G.F. (1972) *An algorithm for the integration of unequally spaced data.* The Computer Journal **vol 15**, p80.

[22] Gradshteyn, I.S. and Ryzhik, I.M. (1980) *Tables of integrals, series and products.* Academic Press.

[23] Gramlich, K. *et al.* (1989) *Coupled-channel calculations with Gauss-type orbitals for charge transfer and ionization in collisions for the $(He - He)^{2+}$ system.* J.Phys.B. **22**, p2567.

[24] Goodwin, E.T. (1961) *Modern computing methods.* 2nd edition, HMSO.

[25] Geist, A. *et al.* (1993) *PVM 3 User's guide and reference manual.* Oak Ridge National Laboratory, Tennessee. (ORNL/TM-12187).

[26] Green, T.A. (1965) *A proof of detailed balancing for the impact parameter method.* Proc.Roy.Soc. **86**, p1017.

[27] von Hellermann, M.G. *et al.* (1993) *Observation of alpha particle slowing-down spectra in JET helium beam fuelling and heating experiments.* Plasma Phys. Control. Fusion **35**, p799.

[28] von Hellerman, M.G. JET Joint Undertaking. *Private communication.*

[29] von Hellermann, M.G. and Summers, H.P. (1993) *Active beam spectroscopy at JET.* Atomic and Plasma-Material Interaction Processes in Controlled Thermonuclear Fusion, Elsevier Science Publishers B.V. p135.

[30] Hibbert, A. Queens University Belfast. *Private communication.*

[31] Hindmarsh, A.C. (1974) *GEAR: Ordinary differential equation system solver.* UCID-30001 REV. 3, Lawrence Livermore Laboratory.

[32] Hood, A. *Solar Plasmas.* in Dendy, R.O. (editor) (1993) *Plasma Physics: an Introductory Course.* Cambridge University Press.

[33] Hutchinson, I.H. (1994) *Principles of plasma diagnostics.* Cambridge University Press.

[34] Lawson, J.D. (1957) *Some criteria for a power producing thermonuclear reactor.* Proc.Phys.Soc. **B70**, p6.

[35] Joachain, C.J. and Post, D.E. (editors) (1983), *Atomic and Molecular Physics of Controlled Thermonuclear Fusion.* NATO ASI Series B:Physics, **vol 101**. Plenum Press.

[36] McCarroll R. (1961) *Resonance charge transfer between H(1s) and H^+ calculated by means of an approximation based on an expansion in atomic eigenfunctions.* Proc.Roy.Soc. **A264**, p547.

[37] Marshall, D.P. *et al.* (1993) *Ionization of helium by α particles within the independent event model.* J.Phys.B. **26**, L219.

[38] Massey, H.S.W. and Smith, R.A. (1933) *The Passage of positive ions through gases.* Proc.Roy.Soc. **A142**, p142.

[39] Messiah, A. (1961) *Quantum Mechanics.* volume 1. North-Holland Publishing Company.

[40] Mittleman, M.H. (1961) *Proton-Hydrogen scattering system.* Phys.Rev. **122**, p499.

[41] Neumann, F.E. (1878) *Vorlesungen über die Theorie des Potentials und der Kugelfunctionen.* Teubner.

[42] Rüdenberg, K. (1951) *A Study of Two-Centre Integrals Useful in Calculations on Molecular Structure.* J.Chem.Phys. **19**, p1459.

[43] Shah, M.B. *et al.* (1989) *Electron capture and ionization in collisions of slow H^+ and He^{2+} ions with helium.* J.Phys.B. **22**, p3037.

[44] Shampine, L.F. and Gordon, M.K. (1974) *Computer solution of ordinary differential equations: The initial value problem.* W.H. Freeman and Co.

[45] Shingal, R. and Bransden, B.H. Durham University. *private communication.*

[46] Shu, F.H. (1982) *The Physical Universe, an introduction to astronomy.* University Science Books.

[47] Slim, H.A. Durham University. *private communication.*

[48] Slim, H.A. *et al.* (1991) *Ionization and charge transfer in proton-helium collisions.* J.Phys.B. **24**, L421.

[49] Summers, H.P. (1994) *Atomic Data and Analysis Structure.* JET Internal Report, JET-IR(94)06.

[50] Thomas, P.R. (1995) *JET Overview.* (talk given at 'The 32nd Culham Plasma Physics Summer School').

[51] Welch, P. (1995) *An Introduction to High Performance Computing.* (talk given at the SEL-HPC meeting at the University of London Computing Centre).